# SEISMIC PERFORMANCE OF UNBONDED ELASTOMERIC BEARINGS ON BRIDGES: AN EXPERIMENTAL AND PARAMETRIC STUDY

A THESIS SUBMITTED TO
THE GRADUATE SCHOOL OF NATURAL AND APPLIED SCIENCES
OF
MIDDLE EAST TECHNICAL UNIVERSITY

BY

KEMAL ARMAN DOMANİÇ

IN PARTIAL FULFILLMENT OF THE REQUIREMENTS
FOR
THE DEGREE OF DOCTOR OF PHILOSOPHY
IN
CIVIL ENGINEERING

AUGUST 2015

Approval of the thesis:

**SEISMIC PERFORMANCE OF UNBONDED ELASTOMERIC BEARINGS ON BRIDGES: AN EXPERIMENTAL AND PARAMETRIC STUDY**

submitted by **KEMAL ARMAN DOMANİÇ** in partial fulfillment of the requirements for the degree of **Doctor of Philosophy in Civil Engineering Department, Middle East Technical University** by,

Prof. Dr. Gülbin Dural Ünver _____
Dean, Graduate School of **Natural and Applied Sciences**

Prof. Dr. Ahmet Cevdet Yalçıner _____
Head of Department, **Civil Engineering**

Assoc. Prof. Dr. Alp Caner _____
Supervisor, **Civil Engineering Dept., METU**

**Examining Committee Members:**

Prof. Dr. Uğurhan Akyüz _____
Civil Engineering Dept., METU

Assoc. Prof. Dr. Alp Caner _____
Civil Engineering Dept., METU

Prof. Dr. Ahmet Yakut _____
Civil Engineering Dept., METU

Prof. Dr. Kurtuluş Soyluk _____
Civil Engineering Dept., Gazi University

Assoc. Prof. Dr. Ayşegül Askan _____
Civil Engineering Dept., METU

Date: 20.8.2015

**I hereby declare that all information in this document has been obtained and presented in accordance with academic rules and ethical conduct. I also declare that, as required by these rules and conduct, I have fully cited and referenced all material and results that are not original to this work.**

Name, Last Name : Kemal Arman Domaniç

Signature :

## ABSTRACT

### SEISMIC PERFORMANCE OF UNBONDED ELASTOMERIC BEARINGS ON BRIDGES: AN EXPERIMENTAL AND PARAMETRIC STUDY

Domaniç, Kemal Arman
Ph.D., Department of Civil Engineering
Supervisor: Assoc. Prof. Dr. Alp Caner

August 2015, 160 Pages

Elastomeric bearings were used in a majority of bridges completed in Turkey. Usually, the connection between bearings and the structure were established only by means of friction. Vertical excitation can contribute to a significant damage in such cases, especially at bearing locations, as indeed was the case in the recent 1999 İzmit Earthquake. In Turkish seismic design practice, a common friction coefficient of 0.20 is frequently used. The aim of this study is to look into the values suggested by specifications for friction coefficient between bearings and steel girders through experiments and to explore dynamic and static shear behavior of unbonded bearings. An actual bridge, spanning 12 m with a concrete deck of 3.5 m width over 3 steel I-girders is constructed on a shake table with a hydraulic actuator capable of delivering a user supplied displacement history. Bearing responses under seismic loadings were measured. Due to a very high friction coefficient, bonded and unbonded bearings exhibited similar seismic performance. Results of shake table and static friction tests performed on unbonded bearings indicated that use of a friction coefficient of 0.20 in seismic analysis can be unconservatively low to determine substructure forces and may significantly overestimate seismic displacement demands. Such low values should not be used in seismic design unless indicated otherwise by test data. A comprehensive parametric study was performed and a conservative trendline of deck displacements as a function of acceleration coefficients is presented with a procedure to estimate maximum bearing shear forces for the investigated cases.



Keywords: bridge, seismic, bearing, unbonded, friction

# ÖZ

## BAĞSIZ ELASTOMER MESNETLERİN KÖPRÜLERDEKİ DEPREM PERFORMANSI: DENEYSEL VE PARAMETRİK BİR ÇALIŞMA

Domaniç, Kemal Arman
Doktora, İnşaat Mühendisliği Bölümü
Tez Yöneticisi: Doç. Dr. Alp Caner

Ağustos 2015, 160 Sayfa

Ülkemizde tasarımı ve yapımı tamamlanmış köprülerde sıklıkla elastomer mesnetler kullanılmıştır. Bu mesnetler genellikle sadece köprü kirişlerinin ağırlığından oluşan basınç altında sürtünme yardımıyla yerlerinde durmaktadırlar. 1999 İzmit depreminin de gösterdiği üzere, düşey deprem hareketi özellikle bu köprülerde mesnet bölgelerinde yoğunlaşan hasarları arttırabilmektedir. Ülkemizdeki deprem tasarımı pratiğinde sürtünme katsayısı genellikle 0.20 olarak dikkate alınmaktadır. Bu doktora tez çalışmasının amacı, şartnameler tarafından mesnetler ve çelik kirişler arasında önerilen sürtünme katsayısı değerlerini deneysel yöntemlerle incelemek ve bağsız mesnetlerin statik ve dinamik kesme davranışlarını araştırmaktır. Bu bağlamda, 12 m açıklığa sahip olan ve 3.5 m genişliğindeki betonarme tabliyenin altında 3 adet çelik I kirişten oluşan bir köprü ve köprüye istenilen deplasman kaydını uygulayabilecek bir hidrolik pistona sahip sarsma tablası inşa edilmiştir. Dinamik yer hareketi simülasyonu altında mesnet etkileri ölçülmüştür. Gözlenen oldukça büyük sürtünme katsayısı nedeniyle, bağlı ve bağsız mesnetlerin deprem performansı benzerlik göstermiştir. Sarsma tablası ve statik mesnet sürtünme testleri sonuçları, sismik analizde sürtünme katsayısının 0.20 olarak kullanılmasının altyapıya aktarılan yüklerin güvensiz şekilde az tahmin edilmesine ve sismik deplasman istemlerinin de oldukça güvenli şekilde fazla hesaplanmasına yol açabileceğini ortaya koymuştur. Aksini gösteren test sonuçları olmadığı sürece, sismik tasarımda bu kadar küçük sürtünme katsayıları kullanılmamalıdır. Kapsamlı bir parametrik çalışmanın sonucunda, sismik deplasman istemlerine ait ve ivme katsayısının bir fonksiyonu olan güvenli bir eğilim çizgisi oluşturulmuş ve mesnetlerdeki maksimum kesme kuvvetlerinin hesabı için basit bir yöntem sunulmuştur.

Anahtar Kelimeler: köprü, sismik, mesnet, bağsız, sürtünme

To My Lovely Wife

## ACKNOWLEDGMENTS

First and foremost, the author wishes to express his deepest gratitude to his supervisor Assoc. Prof. Dr. Alp Caner for his guidance, advice, insight and especially patience throughout the research. His encouragements and organizational help made this thesis possible.

The author would also like to address his sincere gratitude to all the jury members, whom kindly accepted to review his thesis. It was definitely their guidance, criticism and suggestions throughout the research that made this thesis complete.

The author would like to extend his deep appreciation to Nefize Şaban, whose help, support and friendliness were precious gifts that contributed greatly to this thesis.

The author would like to express his gratitude to his mother F. Serpil Domaniç, his father Yüksel Domaniç and his brother Nevzat Onur Domaniç for their invaluable support, encouragements and motivation especially during rough times.

The author would also like to sincerely thank and express his love to his parents-in-law, Mesut Atalay and Tuna Atalay as well as with his sister-in-law Elif Atalay, who expressed their confidence in him and supplied continuous motivation and joy.

The author would like to sincerely thank his colleagues in Yüksel Domaniç Eng. and all of his friends for their continuing support and help during this study.

Finally the author would like to thank and express his love to his wife Zeynep Domaniç for her irreplaceable support, motivation and endless love, and his little blonde storm Demir Domaniç for his unconditional sweetness and well behavior during his father's study.

## TABLE OF CONTENTS

## LIST OF TABLES

## LIST OF FIGURES

# CHAPTER 1

# INTRODUCTION

## 1.1 BACKGROUND AND OBJECTIVE

In terms of their connections, elastomeric bearings can simply be grouped into two; *unbonded* ones that have no connection to the girders and/or cap beams, and *bonded* bearings that are connected to both.

In typical engineering practice, vertical excitation is not considered in seismic bridge design per AASHTO specifications [2, 3, 4 and 5]. However, an approximate method for estimating seismic uplift forces is supplied by the same specifications, which can be of utmost importance when unbonded bearings are used.

Turkey, as well as U.S., Japan, Nepal and many others is an earthquake prone country with a very high seismic hazard. Containing abundant fault-zones with many of them being active, there is considerable possibility for a bridge to be exposed to a near-fault seismic event. Especially in such cases, estimation of design responses can be improved by considering the vertical component of seismic excitation in the design process [21].

The aim of this study is to investigate the importance of uplift connections between elastomeric bearings and the structure, to look into the values suggested by specifications for friction coefficient between bearings and structure through experiments and to explore dynamic and static shear behavior of unbonded bearings.

In Turkey, it is commonly seen that the elastomeric bearings are directly laid on the cap beams or piers having no means of connection besides friction. They are also seldom connected to the girders. Some of the existing bridges utilizing unbonded elastomeric bearings are now considered to be located in high seismic hazard zones due to recent updates on seismic hazard maps and related acceleration coefficients.

The motivation behind this thesis arises from the ongoing Turkish engineering practice regarding seismic bridge design, where a common value of 0.20 is frequently used for friction coefficient between bearings and the structure per widely used design specifications [4, 5, 13, 17 and 41] although its use is suggested under service loads. Thus, it became more of an issue to quantify the seismic performance of such unbonded systems, in order to develop seismic retrofitting methods and carry out new designs accordingly.

Results of a past study [28] indicated that such construction practices utilizing unbonded bearings may provide a fuse mechanism for the structure, decreasing the force transferred to the substructure and increasing the lateral bearing displacements by further isolating the bridge during an earthquake. It is also stated that unbonded rectangular fiber-reinforced elastomeric isolators can be effectively used in seismic design of masonry and reinforced concrete shear walls [33].

In such unbonded designs, a decrease in compression forces on bearings due to seismic loads (even if uplift of bearings may not occur) may significantly affect seismic performance by reducing the friction between bearings and the structure. Such behavior can originate due to solely longitudinal, transverse or vertical component of ground motions, or a combination of all [21, 29 and 30].

Moreover, past investigations [8, 34, 35 and 43] suggested that significant bridge damage could occur in case of unbonded elastomeric bearings, possibly due to the significance of vertical compound of seismic motion (Figure 1.1). In some cases, unbonded bearings could walk out of its supports [44], even due to only thermal movements (Figure 1.2).

While a numerical evaluation of current rules set by AASHTO and certain specifications regarding uplift devices and vertical component of seismic ground motion were carried out in the author's M.Sc. thesis [21], it is intended to present a more elaborated work in this Ph.D. study, which includes investigation of seismic performance of unbonded bearings through experiments and a parametric study.

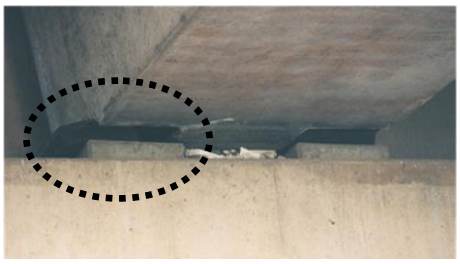

(a) Transverse movement of bearing

(b) Unseating of girder

(d) Extensive bearing damage

(c) Unseating of girder

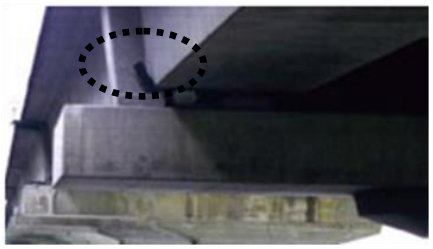

(e) Dislodging of bearing

Figure 1.1: Various damages at bearing locations observed in Sakarya Viaduct after 1999 İzmit Earthquake [8, 34, 35 and 43]

Seismic behaviors of structures are somewhat complex in nature, like seismic ground motions themselves. Simulating the effects of earthquakes on structures by static loading tests introduces many approximations to the problem itself, such as indirect representation of damping and inertial forces.

Figure 1.2: Bearing walk out due to thermal movements

Moreover, amount of nonlinearity of the structural behavior usually depends on magnitude of the exerted forces, and occasionally it can be difficult and even impossible to represent the structural behavior through modal analysis. For instance; nonlinear shear behavior of unbonded elastomeric bearings, which is dependent on both acting axial force and coefficient of friction, necessitates use of nonlinear time-history analysis methods.

These considerations led to the development of an actual bridge model with steel girders and reinforced concrete deck constructed on a shaking system capable of exerting actual ground motion records in transverse direction of the bridge. Five ground motion records were selected and scaled accordingly to stay within the limits of the actuator mechanism.

In the first part of the study, it was intended to achieve the following objectives through a detailed experimental study backed with nonlinear time-history analyses:

- To estimate the friction coefficient between rubber and steel and to verify the use of values suggested by the specifications in seismic design,
- To compare the results of shake tests and FEA (finite element analyses),
- To compare the seismic performance of unbonded and bonded bearings,

For this purpose, FEA of the bridge setup with bonded and unbonded elastomeric bearings were conducted using CSI Bridge software.

Interpretation of experimental data obtained from shake tests is presented as well with the comparison with numerical results. A discussion regarding the observed frictional behavior of elastomeric bearings at various loading rates are also included and results are compared with the suggestions of the design specifications.

In the second part of this thesis, a comprehensive parametric study consisting of approximately 800 nonlinear time-history analyses using 21 spectrum compatible ground motion records was conducted to investigate the dependence of seismic displacement demands and uplift forces on bearings to following parameters:

- Friction coefficient
- Acceleration coefficient per AASHTO
- Skew angle
- Height-to-width ratio of deck
- Fundamental frequency of the structure

Discussion of the results is presented as well as with a simple formulation describing trendline of the seismic displacement demand as a function of acceleration coefficient for the investigated cases.

## 1.2 SUMMARY, EXPLANATIONS AND FLOWCHART

Steps performed throughout this thesis are summarized and the flowchart of the study is presented in this section.

Two bridge setups were analyzed experimentally through shake table tests and numerically by FEA. A bridge setup, properties of which are explained in detail in Section 5.1, was designed and constructed at the METU Civil Engineering Department K2 Laboratory. A hydraulic actuator capable of exerting user supplied ground motion records along transverse axis of the bridge was introduced to the system.

Three different bearing types were already available for future studies and used to construct bonded and unbonded bridge setups. A set of friction tests at various loading rates on steel plates having different surface finishes were conducted using unbonded bearings, to estimate the coefficient of friction between bearings and steel. Cyclic tests are also performed on all bearings to estimate shear stiffness and damping ratios.

Total number of six bearings was used at the bridge for each setup (unbonded and bonded). Properties of test setups and bearing types are summarized on Tables 1.1 and 1.2.

Table 1.1: Explanation of test setups

| **Bridge Setup** | **Used Bearings** | **Bearing Connection** |
|---|---|---|
| Bonded | 6 x Type-1 | M12 Bolts |
| Unbonded | 2 x Type-2 (Middle) and 4 x Type-3 (Sides) | N/A |

Table 1.2: Properties of used bearings

| **Bearing Type** | **Shape** | **Dimensions (mm)** | **# of Rubber Layers** | **Thick. of an Int. Rubber Layer (mm)** | **Thick. of an Ext. Rubber Layer (mm)** | **Thick. of Steel Shim Plates (mm)** |
|---|---|---|---|---|---|---|
| Type-1 | Circular | $D_b = 150$ | 5 | 10 | N/A | 2 |
| Type-2 | Square | 150x150 | 4 | 8 | 4 | 2 |
| Type-3 | Square | 150x150 | 4 | 8 | 4 | (Fiber) |

Following bearing tests, harmonic shake table load tests were performed at various frequencies to obtain vibration characteristics of the test setups. Seismic shake table tests were then conducted using ground motion records.

Finite element models were prepared and calibrated using the results of bearing tests and harmonic shake table tests. FEA were carried out using the same ground motion records and results were compared with the experimental data.

Following shake table tests; a setup was prepared to push the bridge in longitudinal direction to estimate the coefficient of friction between bearings and steel girders, as well as to observe the static response of the bridge at low loading rates.

Last part of this thesis included a parametric study using the FEA model of the test setup and changing the following parameters accordingly:

- Friction coefficient ($\mu$=0.05, 0.10, 0.15, 0.20, 0.25, 0.30, 0.40, 0.50, 0.75 and 1.00)
- Acceleration coefficient per AASHTO (A=0.10, 0.20, 0.30 and 0.40)
- Skew angle (S=0°, 10°, 20°, 30°, 40°, 50° and 60°)
- Height-to-width ratio of deck (h/w=0.125, 0.25, 0.50, 0.75 and 1.00)
- Fundamental frequency of the bridge by changing bearing shear stiffness (f=0.607, 0.854, 1.196, 1.658 and 2.262)

Throughout this thesis;

- Bearing axial force results includes seismic contributions only, i.e. they do not include dead loads.
- The term “uplift” or “seismic uplift” implies only tensile seismic component acting on bearings. “Absolute uplift” is used where combined axial forces due to dead and seismic loads on bearings are in tension.
- “Displacement” of bearings means shear deformation of bearings.
- “Deck Displacement” means relative horizontal displacement between bottom of girders and bottom surface of bearings, i.e. total of bearing slipping and shear deformation.

Flowchart of the study is presented on Figure 1.3.

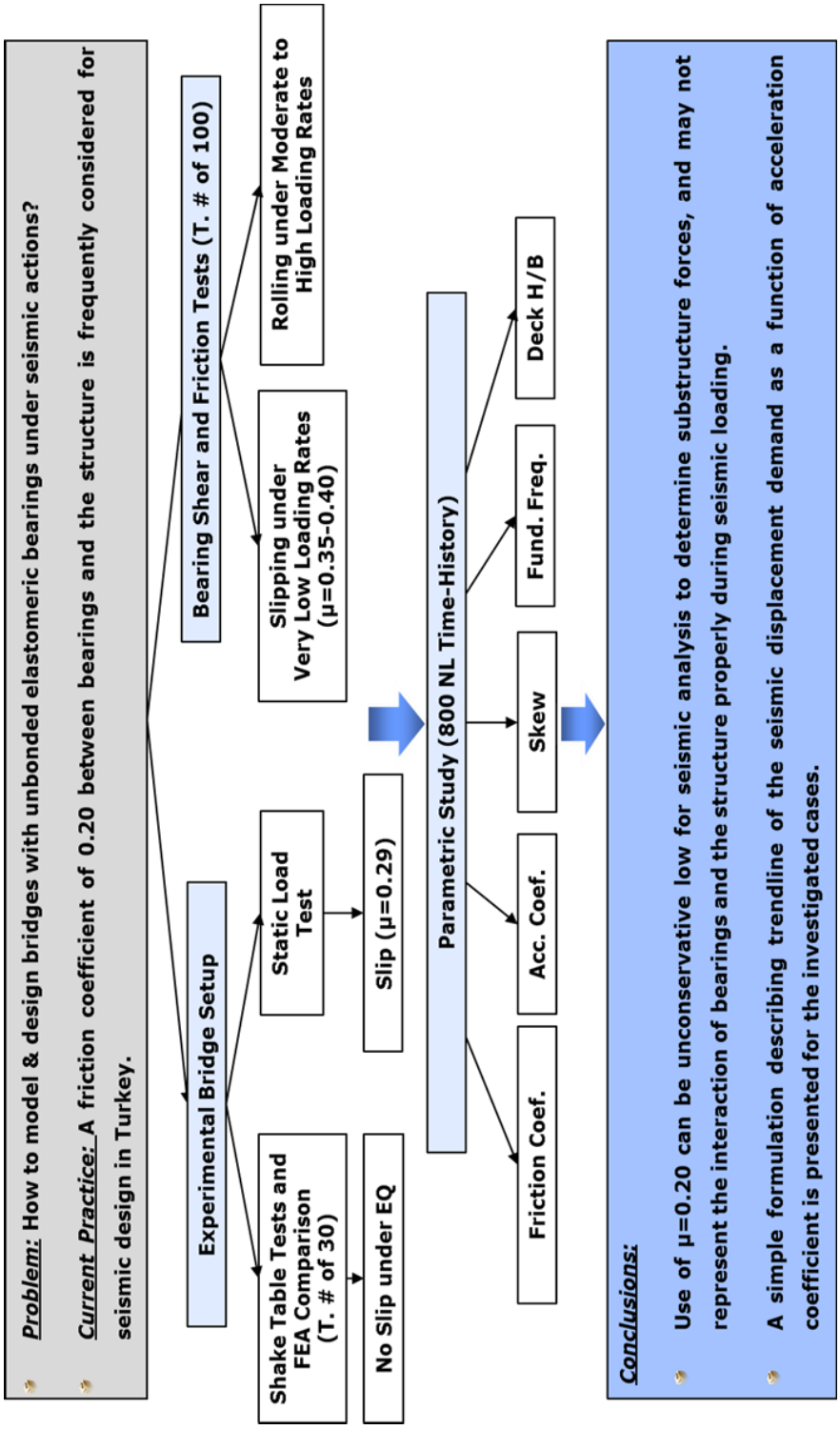


Figure 1.3: Flowchart of the study

# CHAPTER 2

# UPLIFT MECHANISM OF BEARINGS DUE TO SEISMIC LOADS

## 2.1 UPLIFT DUE TO LONGITUDINAL EXCITATION

There are two principal types of bearing layouts in longitudinal direction of a bridge. In cases where pre-stressed precast I girders are used, two lateral bearing axes are generally utilized per pier to achieve a simply supported girder design (Figure 2.1, Layout 1). This type of superstructure constitutes the majority of highway bridges in Turkey. In this design, bearing and pier axes are offset (denoted by $d$, Figure 2.2).

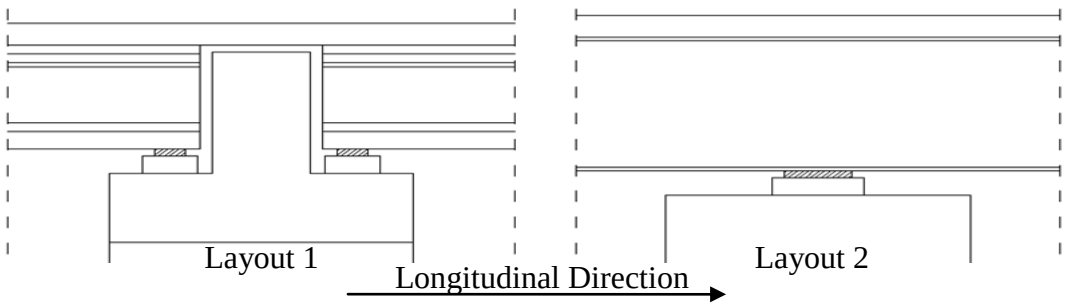


Figure 2.1: Different bearing layouts in the longitudinal direction of a bridge

On the other hand, continuous superstructure types such as steel I-girders with a concrete or steel deck, post-tensioned box sections, steel box sections and etc., usually utilizes one bearing axis over each pier (Figure 2.1, layout 2), eliminating any offset between bearing and pier axes.

Bridges utilizing bearing layout 1 (Figure 2.1) are prone to seismic uplift due to longitudinal excitations [21 and 29]. The uplift forces in bearings due to longitudinal excitations originate from upper pier moments, which are never truly zero due to resistance of bearings and superstructure to rotations along transverse axis of the bridge. Those moments yield axial force couples in bearings along opposing sides of the cap beam. Deformation of fundamental mode in longitudinal direction of such a bridge layout is presented in Figure 2.2 [21] with moment diagram of a pier as well.

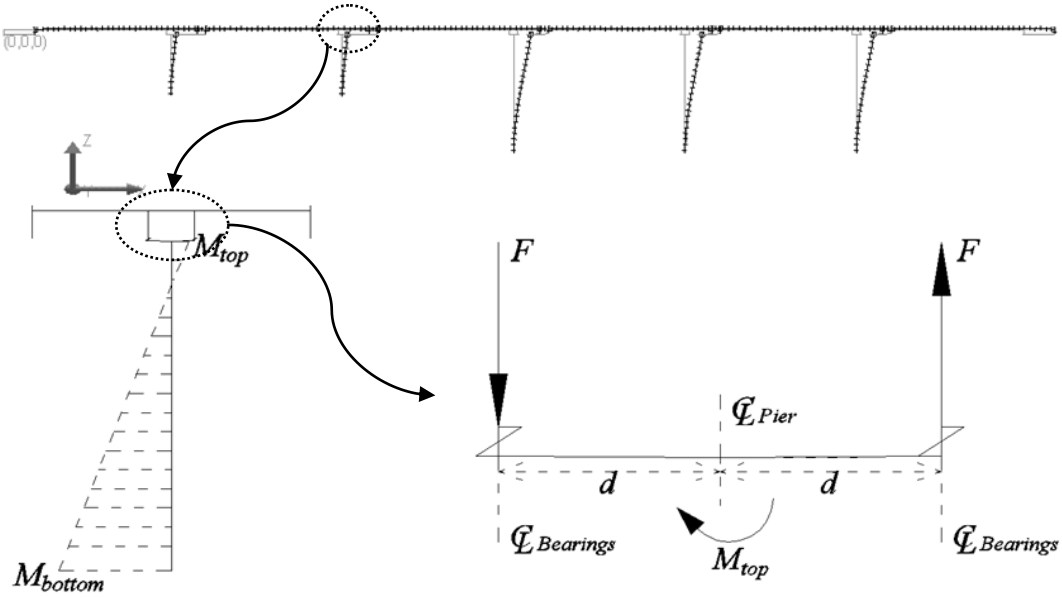


Figure 2.2: Axial force couple in bearings due to longitudinal excitation [21]

Moment at the top of the pier can be expressed as:

$$M_{top} = 2.F.d \tag{2.1}$$

Past studies also showed that, total vertical load over pier does not change significantly, leading to nearly same values at any time instant under longitudinal excitation [21].

This means, total vertical load over bearings ($F_1 + F_2$, Figure 2.3) remains equal to total dead load during seismic ground motion conforming to the fact that vertical excitation is absent.

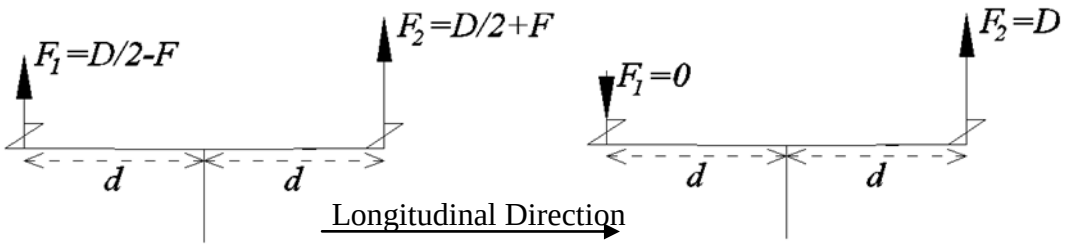


(a) Bearings are in compression

(b) One line of bearings are in tension

Figure 2.3: Axial forces in bearings under longitudinal excitation ($D$ denotes dead load carried by a bearing) [21]

It should be noted that, $F$ denotes only seismic axial force component and sum of dead and seismic axial forces on the bearings, $F_1$ and $F_2$, need not to be tensile. Such an absolute uplift of a bearing during an earthquake requires seismic contribution of bearing axial loads to be greater than dead loads. Detailed formulation of alteration of axial loads during seismic loading can be found in the author's M.Sc. thesis [21].

Past studies also indicated that rotation of the foundations during seismic loading can also contribute to the seismic uplift forces. Within a bridge, bearings over shorter piers may be likely to exhibit greater uplift forces during longitudinal excitation, due to higher foundation rotations in soft soils. It is also stated in the same study that uplift forces seems to increase in case of higher deck stiffness [29].

Moreover, it was stated in the author's M.Sc. thesis that bearings over longer piers yielded higher uplift forces in case foundation rotations are prevented, and an analytical verification was also included [21].

## 2.2 UPLIFT DUE TO TRANSVERSE EXCITATION

A simple approach was developed to describe the origination of bearing forces under transverse excitation in the author's M.Sc. thesis [21] and summarized here for convenience.

Bearing layout of a bridge with an odd number of bearings over piers $(2n + 1)$ is shown in Figure 2.4. Top pier moment will be resisted by seismic bearing force $(F_1 \dots F_n)$ couples where $d$ is the transverse spacing of bearings;

$$M_{top} = 2.(F_1.d + F_2.d + \cdots + F_n.d) \tag{2.2}$$

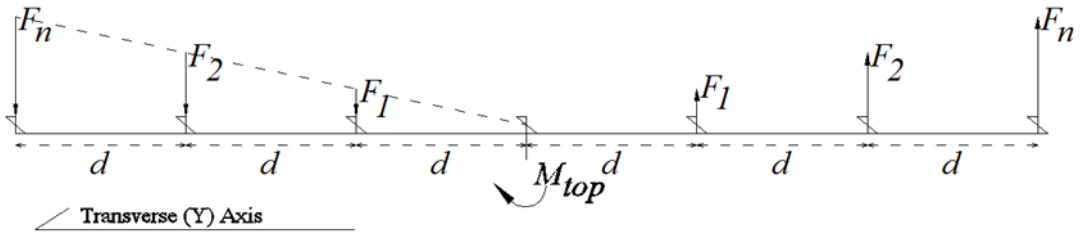


Figure 2.4: Axial bearing forces due to transverse excitation

Assuming superstructure and cap beam to behave rigid under bending about longitudinal axis, Equation 2.2 becomes;

$$M_{top} = 2.F_1.d.\sum_{i=1}^{i=n} i^2 \tag{2.3}$$

Considering the test bridge setup where total number of bearings are equal to 3 $(n = 1)$, $M_{top}$ will be equal to the moment originating due to lateral inertial force of superstructure $(F_L)$ during seismic loading (Figure 2.5);

$$M_{top} = F_L.H_S \tag{2.4}$$

where $H_S$ is the center of mass of deck measured from bottom. Rearranging Equation 2.3 for three bearings ($n = 1$) and substituting into Equation 2.4 gives;

$$F_L.H = 2.F_1.d \tag{2.5}$$

Solving Equation 2.5 for $F_1$ yields the axial forces in bearings as;

$$F_1 = F_L.H/(2.d) \tag{2.6}$$

Detailed formulation of axial bearing loads during seismic loading can be found in the author's M.Sc. thesis [21].

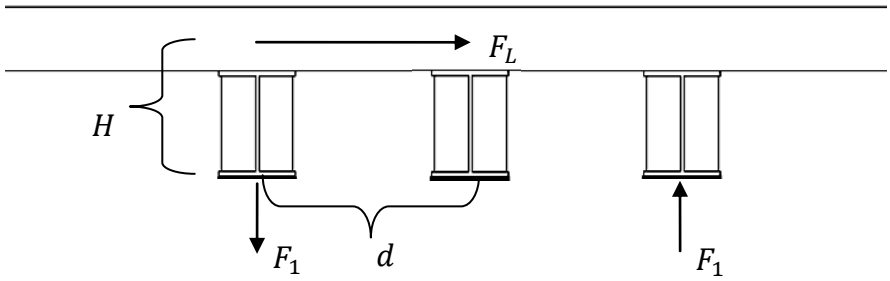


Figure 2.5: Bearing uplift forces in test bridge setup due to transverse excitations

Applying Equation (2.6) to bridge test setup where;

$F_L$ : 50kN (i.e. 0.5g lateral relative acceleration acting on superstructure)
$H$ : 0.45m
$d$ : 1.00m

Uplift forces on bearings were calculated as;

$$F_1 = 50 * 0.45/(2 * 1) = 11.25\text{kN}$$

Moreover, P-Δ effect also contributes to uplift. Considering lateral displacement of superstructure as shown in Figure 2.6, the secondary moment will be;

$$M_s = W.d_b \tag{2.7}$$

where;

$W$ : Weight of superstructure carried by the bearings over a pier

$d_b$ : Lateral displacement of bearings

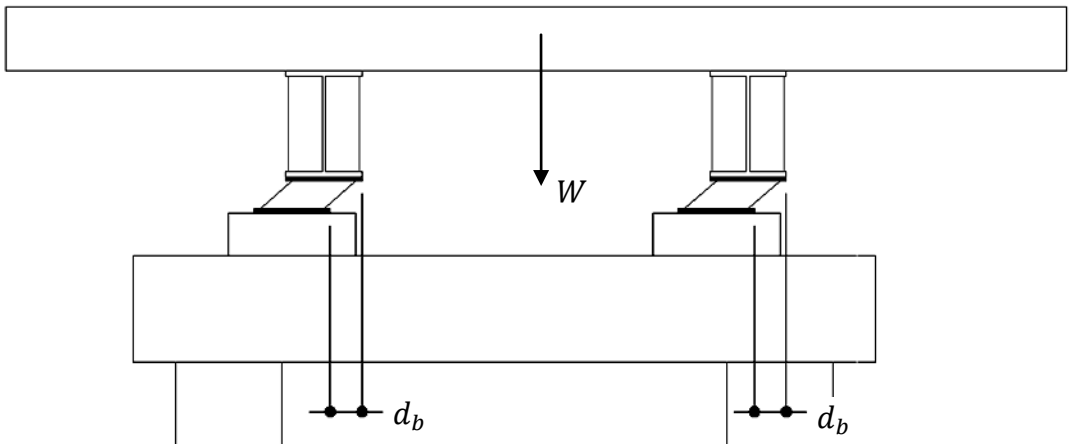


Figure 2.6: Contribution of P-Δ effect to uplift forces

Using a simple approach, secondary moment due to P-Δ effect can be distributed to bearings as axial forces by substituting $M_s$ to equation (2.3) as;

$$W.d_b = 2.F_1.d.\sum_{i=1}^{i=n} i^2 \tag{2.8}$$

Applying Equations (2.8) to the test bridge setup, properties of which are explained in Section 5.1, and assuming a lateral bearing displacement of 3.5cm, uplift forces originating from P- Δ effect were calculated as;

$$F_1 = W.d_b/(2.d) = 100 * 0.035/(2 * 1) = 1.75kN$$

Noting the dead loads on bearings are approximately 33kN (Section 5.1), the uplift force due to P-Δ effect was found to be 5% of the dead load.

## 2.3 UPLIFT DUE TO VERTICAL EXCITATION

Creating perhaps the most intuitive effect among orthogonal components of a seismic ground motion, vertical component of an earthquake directly alters axial bearing forces by reducing or increasing vertical acceleration of the superstructure.

## 2.4 COMBINED EFFECTS OF GROUND MOTION COMPONENTS ON BRIDGE TYPES

Past studies indicated that longitudinal excitations are likely to develop higher axial bearing forces of bridges with simply supported girders [21 and 29]. Moreover, bridges having fewer bearings with closer spacing along lateral direction are more likely to develop higher axial bearing forces due to transverse component of an earthquake [21].

A past study [23] also indicated that interior bearings at the end become vulnerable to uplift in bridges having tight horizontal radius, and calculated axial forces showed significant dependence on curvature.

While vertical excitation component can yield significant seismic forces in bearings of different bridge types, time of peak responses does not necessarily coincides with the responses due to longitudinal and transverse components [21].

# CHAPTER 3

# BEHAVIOUR OF UNBONDED ELASTOMERIC BEARINGS

## 3.1 GENERAL

Elastomeric bearings can simply be classified according to their connections to the structure as unbonded (no connection to the girders and/or cap beams) and bonded (connected to both). Bonded and unbonded bearings used in this study are shown in Figure 3.1.

(a) Bonded bearings (b) Unbonded bearings

Figure 3.1: Bonded and unbonded elastomeric bearings used in the test setup

Elastomeric bearings are usually directly laid on the cap beams or piers in Turkey, being only restrained by the friction force between themselves and structure. They are also seldom connected to the girders. Some of those existing bridges are now deemed to be in high seismic hazard zones, considering recent updates on seismic hazard maps and acceleration coefficients.

Use of such unbonded bearings without steel connection plates may reduce costs by eliminating the need for heavier lifting equipment, which also eases their replacement and accelerates the construction process of the bridge.

Moreover, it is stated that use of stable unbonded fiber reinforced elastomeric isolators (SU-FREI) can significantly reduce seismic demand [22] and can also help to further reduce weight and decrease costs [33].

Past studies also indicated that, elastomeric bearings may perform exceptionally even under seismic loading even if they are not designed as seismic isolators, resisting up to shear strains well beyond 50% [27 and 38], suggesting that there is a possibility that they may provide a cheaper alternative where conventional seismic isolators are not affordable [25].

Thus it became more of an issue to understand the seismic behavior of unbonded bearings in order to quantify the performance, develop seismic retrofitting methods and carry out new designs accordingly.

### 3.2 FRICTIONAL BEHAVIOUR

Bridge design specifications and past studies suggested use of following friction coefficient values between steel girders and rubber:

- $\mu$= 0.20 (AASHTO Standart Specifications [2], C14.6.10, for service loads)
- $\mu$= 0.20 (AASHTO LRFD [3, 4 and 5], C14.8.3.1, for service loads)
- $\mu$= 0.20 (CALTRANS [17], Section 7.1, for service loads)
- $\mu$= 0.35 (CALTRANS [17], Section 7.1, for seismic loads)
- $\mu$= 0.20 (Steel Bridge Design Handbook [41], Section 2.1.2)
- $\mu$= 0.20 (EN 1337-3 [13], for service loads, at 1.5 MPa compression)

An experimental study [31] conducted at University of Texas at Austin yielded coefficient of friction values of 0.288-0.339 for service loads, tested at a loading rate of 1.6mm/min.

It is also noted that [31] application of antiozonant waxes to the surfaces of elastomeric bearings can reduce friction coefficients significantly. A relaxation of the relevant provisions regarding effect of ozone on bearings was suggested to eliminate use of wax [31].

Results of another study [27] indicated that the coefficient of friction may exceed 0.35 for pressures less than 1.38MPa (200 psi) at loading rates up to 800mm/s, simulating seismic loading.

CALTRANS Memo to Designers [17] includes a commentary noting that; use of $\mu = 0.2$ can be unconservatively low to use in seismic analysis to determine substructure forces, and may not reflect the interaction of bearings and the structure properly during seismic loading. Such an analysis also may produce unrealistically large seismic displacement demands.

A past study [38] also indicated that, actual friction of coefficient values during a seismic ground motion could be significantly higher than the values suggested by specifications, and is significantly dependent on loading rate and compressive load level as also stated in AASHTO specifications [2, 3, 4 and 5].

Results of friction tests performed on unbonded bearings in this study pointed out that friction coefficient is highly dependent to loading rate, conforming past findings [38]. Detailed explanations are included in Sections 5.4.4 and 5.4.5. To summarize, static coefficient of friction for long term service loads are obtained to be greater than 0.35. Static push test applied to the bridge setup output a static friction coefficient of 0.29 (Section 5.6). Results indicated that for seismic loading (e.g. rates higher than 3000mm/min) bearings would not slip before rolling occurs under any compressive force level tested.

### 3.3 NUMERICAL SIMULATION

A plane-strain 2D FEA model was prepared using ADINA software (Figure 3.2). Type-2 bearings were modeled using elastic material properties for steel shim plates and The Mooney-Rivlin hyperelastic material model for rubber. 2D plane strain solid elements were used exclusively.

Following material properties were used to represent steel shim plates and steel shear plates of the machine:

$E$ = 200000MPa

$\vartheta$ = 0.3

$\gamma$ = 7.85ton/m$^3$

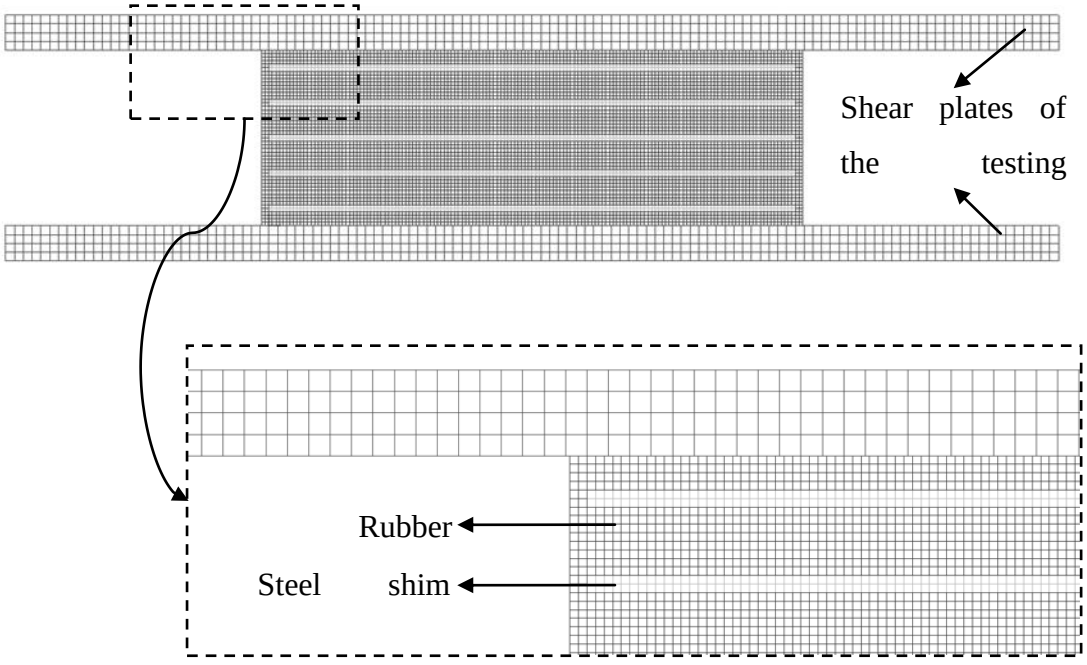


Figure 3.2: FEA model of the bearing and shear plates.

Frictional contact conditions were simulated between shear plates and top and bottom surfaces of bearings using Coulomb friction model. First, coefficients of friction over unity are used for both top and bottom interfaces to prevent slipping and to observe rolling and shear deformation behavior.

A constraint equation is applied to top shear plate, to prevent it from rotating. This reflects the case in the actual test setup explained in Section 5.4, where two bearings have to be tested simultaneously and middle plate where shear load is applied is only translates horizontally because of symmetry.

Rubber is known to be a nearly incompressible material, usually having a bulk modulus approximately thousand times of shear modulus. Mooney-Rivlin Material model is widely used to represent behavior of rubber in FEA. Formulation of the model is based on the following expression of deviatoric strain energy [6]:

$$W_D = C_1(I_1 - 3) + C_2(I_2 - 3) + C_3(I_1 - 3)^2 + C_4(I_1 - 3)(I_2 - 3) + C_5(I_2 - 3)^2 + C_6(I_1 - 3)^3 + C_7(I_1 - 3)^2(I_2 - 3) + C_8(I_1 - 3)(I_2 - 3)^2 + C_9(I_1 - 3)^3 + D_1(\exp\big(D_2(I_1 - 3)\big) - 1) \quad (3.1)$$

where $C_1$ to $C_9$ and $D_1$, $D_2$ are material constants and $I_1$, $I_2$ and $I_3$ are the principal invariants of the Cauchy-Green deformation tensor. Parameters $D_1$ and $D_2$ are usually omitted except modeling certain biological materials. For plane strain conditions, volumetric strain energy density can be written as:

$$W_V = 0.5K(J_3 + 1)^2 \quad (3.2)$$

where $K$ is the bulk modulus and $J_3$ is the reduced invariant [6].

Using Hooke's law, shear modulus and bulk modulus can be written in terms of young modulus and Poisson's ratio as:

$$G = E/2(1 + \vartheta) \quad (3.3)$$

$$K = E/3(1 - 2\vartheta) \quad (3.4)$$

The material constants $C_1$ to $C_9$ have no direct physical meanings and are usually determined from uniaxial, equal biaxial and planar tensions tests.

No practical values are available in the literature. However, in case one parameter ($C_1 \neq 0$) Mooney-Rivlin model is used (i.e. Neo-Hookean model), the material constant can be calculated as [6, 24 and 36]:

$$C_1 = G/2 \quad (3.5)$$

By selecting an appropriate Poisson's ratio ($\vartheta \approx 0.5$), Young modulus can be calculated from experimentally determined shear modulus and bulk modulus can be obtained subsequently. For example, choosing $\vartheta = 0.4995$ and using $G = 720$KPa (calculated in Section 5.4.2) yields:

$K$ = 720MPa

$C_1$ = 0.360

However, it is also known that FEA of such hyperelastic nearly incompressible elements utilizing large displacements and/or strains usually yields a negative Jacobian near interfaces due to highly distorted element meshes [42]. Even though this usually occurs only at the interface, it leads to termination of the analysis.

With the chosen parameters, analysis terminated at a lateral bearing displacement of 48mm, with a negative Jacobian at a highly distorted rubber element near boundary (Figure 3.3).

Convergence did not improved by lowering Poisson's ratio to $\vartheta = 0.495$ and using $K = 72$MPa. Analysis again terminated at 45mm lateral displacement.

However, using a two parameter Mooney-Rivlin model ($C_1 \neq 0$ and $C_2 \neq 0$) with $\vartheta = 0.4995$ led to the convergence at 55mm lateral displacement. In this case, material constants are related to shear modulus as [6, 24 and 36]:

$$C_1 + C_2 = G/2 \tag{3.6}$$

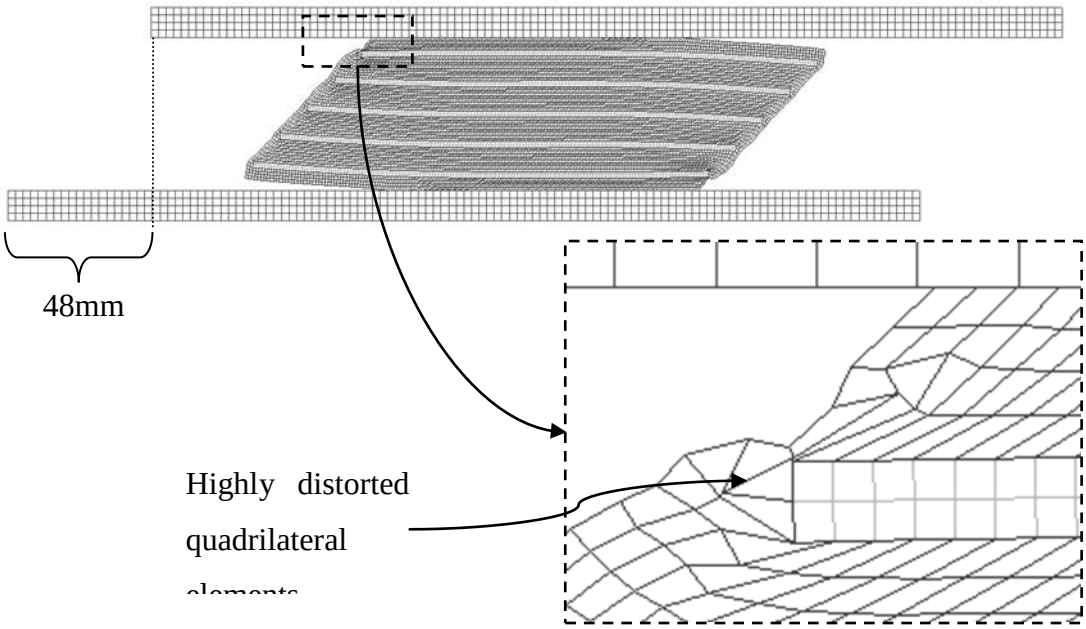


Figure 3.3: Deformed shape at the termination load step (48mm shear deformation)

Ratio of constants $C_1 = 0.224$ and $C_2 = 0.136$ are chosen to be 1.65 in conformity with a past study [15]. Furthermore adjustments using $\vartheta = 0.49975$ and $\vartheta = 0.495$ did not improve converge neither.

Shear force vs lateral bearing displacement are presented on the same graph for FEA and experimental data (Section 5.4.2) on Figure 3.4.

Both experimental and numerical results indicated that evident rolling behavior initiated after approximately 20mm shear deformation provided that slipping does not occur (Figure 3.5).

However, shear behavior was almost linear up to 50mm displacement, indicating that rolling did not have a significant effect on the shear stiffness of the bearings (Figure 3.4) conforming to the findings of a past study [27] regarding stocky bearings where height-to-width ratio is small.

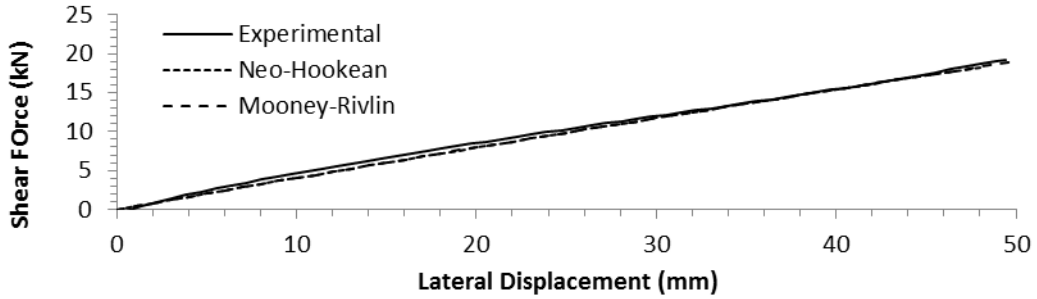


Figure 3.4: Shear force vs shear deformation obtained from FEA and experiments

Results of analyses using varying friction of coefficients between top surface of the bearing and top shear plate are shown on Figure 3.6. Maximum shear force values were equal to the multiplication of friction coefficients and the applied constant compressive load of 33kN.

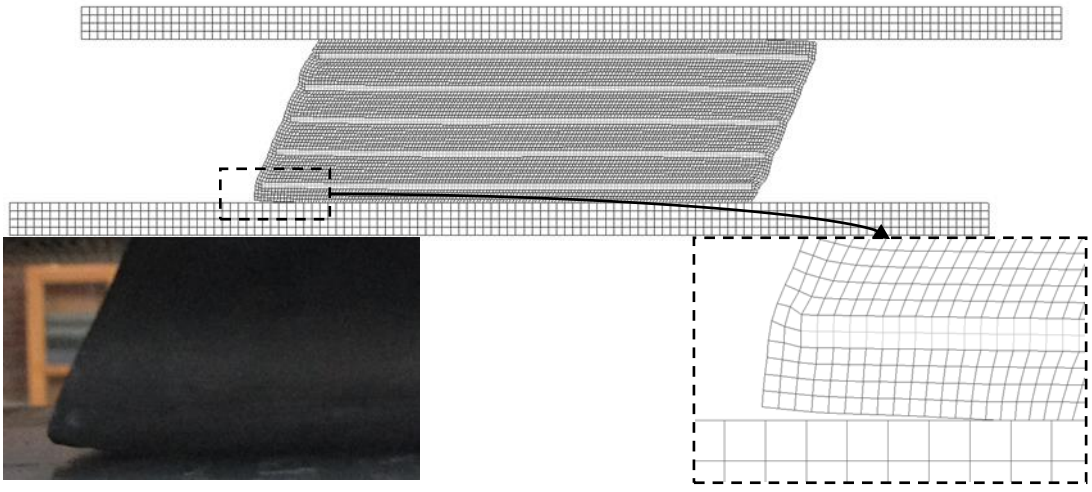

Figure 3.5: Initiation of evident rolling at 20mm lateral bearing displacement

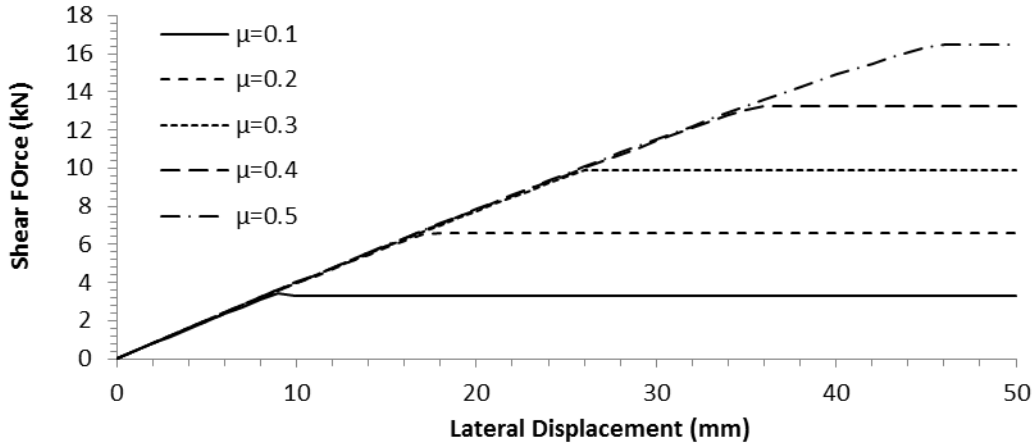


Figure 3.6: Shear force vs shear deformation for varying friction coefficient values

Deformed mesh and slipping of top friction plate in case of a friction coefficient value of 0.5 is also presented in Figure 3.7.

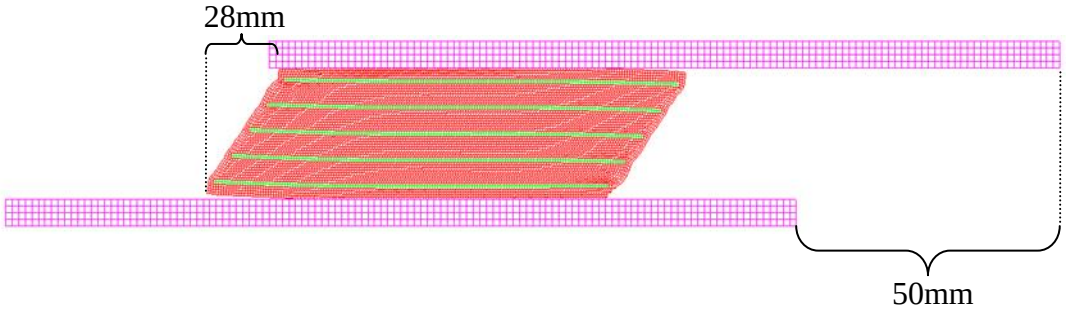


Figure 3.7: Deformed mesh at 50mm shear deformation using a friction coefficient of 0.5

# CHAPTER 4

# SEISMIC PROVISION OF CODES

## 4.1 HORIZONTAL DESIGN RESPONSE SPECTRUM

*Elastic Seismic Response Coefficient* ($C_s$) is calculated by the formula per AASHTO Bridge Specifications [2 and 3];

$$C_s = \frac{1.2 * A * S}{T^{2/3}} \tag{4.1}$$

where;

$A$ = Acceleration coefficient
$S$ = Soil site coefficient
$T$ = Period

and $C_s$ need not exceed $2.5A$. For soil profiles III or IV where $A \geq 0.30$, $C_s \leq 2.0A$. Where $T$ exceeds 4.0s;

$$C_s = \frac{3 * A * S}{T^{4/3}} \tag{4.2}$$

A plot of elastic seismic coefficient $C_s$ vs period $T$ forms design response spectrum for horizontal earthquake motion. Return period of this design earthquake motion is approximately 475 years, which corresponds to 10% probability of exceedance in 50 years.

## 4.2 VERTICAL DESIGN SPECTRUM

Although current bridge specifications and guidelines do not supply any recommendations and/or provisions about construction of a vertical design spectrum, past studies and commentary sections of these specifications contains some comments.

In commentary sections of AASHTO, it is stated that a vertical design spectrum can be constructed by multiplying the ordinates of the spectrum of horizontal motion by 2/3 [2 and 3].

Applied Technology Council also recommends the same in absence of site specific information [10]. Same approach is suggested also by New York State Department of Transportation (NYCDOT) [32]. On the contrary, a ratio of 1/2 is suggested in commentary section of American Petroleum Institute (API) Recommended Practice [7].

California Department of Transportation (CALTRANS) Seismic Design Criteria does not include a detailed discussion. It is suggested that an equivalent static vertical load shall be used for ordinary bridges where rock peak acceleration is equal to 0.6 g or greater [18].

Past studies pointed out that, horizontal/vertical peak acceleration ratio greatly depends on distance to fault and fundamental period of the structure. Same studies underlines that the common ratio of 2/3 tends to underestimate the effects of vertical component in lower period range ($T \leq 0.2 - 0.3\,sec$), especially at near fault, but being usually conservative for a higher period range [11 and 16].

Many attenuation relationships offer equations to develop empirical site-specific vertical response spectra, and an approximate procedure for distance-dependent one is supplied in [12].

## 4.3 COMBINATION OF ORTHOGONAL EXCITATIONS

No suggestion is included in AASHTO Bridge Specifications for simultaneous application of neither orthogonal horizontal nor vertical excitations. Use of two combinations of maximum horizontal responses in each direction is recommended to account for directional uncertainty of earthquakes and simultaneous occurrences of directional components [2 and 3].

The same combinations are supplied also by CALTRANS Seismic Design Criteria and ATC-6 Seismic Design Guide Lines as [9 and 18];

Load combination 1: 1.0X + 0.3Y
Load Combination 2: 0.3X + 1.0Y

where X denotes maximum specific response due to longitudinal excitation and Y does the same for transverse component.

ATC-32 Seismic Design Criteria also includes the effects of vertical excitation as well [10];

Load combination 1: 0.4X + 1.0Y + 0.4Z
Load Combination 2: 1.0X + 0.4Y + 0.4Z
Load Combination 3: 0.4X + 0.4Y + 1.0Z

NYCDOT recommends the same but with a vertical load factor of 0.3 [32]. In addition, it is pointed out at a recent study [16] that SRSS of orthogonal peak responses increased the accuracy of results.

AASHTO Guide Specifications for Seismic Isolation Design [1] includes some recommendation for simultaneous application of horizontal earthquake motions.

A scaling of ensemble horizontal SRSS spectrum of horizontal components is suggested so that the ordinates do not fall below 1.3 times the design spectrum in the period range of $T_1$ to $T_2$, which are respectively 0.5 and 1.5 times the fundamental period of vibration in the direction under consideration.

Consideration of vertical ground motion components in the load combinations supplied by AASHTO, as done by NYCDOT [32], seemed to improve the accuracy of estimation of pier axial forces and cap beam moments under combined vertical and horizontal excitations [21].

### 4.4 HOLD-DOWN DEVICE REQUIREMENTS

It is stated in AASHTO Standard Specifications and ATC-6 that; hold-down devices shall be utilized at all supports or hinges in continuous bridges of seismic performance category (SPC) C and D, where the vertical seismic force due to the longitudinal horizontal seismic component opposes and exceeds 50% but is less than 100% of the dead load reaction.

In this case, the minimum net design uplift force for hold-down device shall be 10% of the dead load that would be exerted if the span were simply supported. If the vertical force (Q) due to the longitudinal horizontal seismic load opposes and exceeds the dead load reaction (DR), the design force for the hold-down device shall be 1.2(Q-DR) but it shall not be less than 0.1DR [2]. AASHTO LRFD Specifications includes identical provisions [3, 4 and 5].

Uplift can also result in stability loss or damage. But vertical motion restrainers are usually not considered to be feasible unless other bearing retrofits are being performed [40].

The findings of the author's M.Sc. study [21] confirmed that the provisions of AASHTO governing hold-down devices are reasonably accurate, if effects of lateral horizontal component are also taken into account in addition to longitudinal component. In that case, bearings that are vulnerable to uplift could be successfully identified but bearing axial forces the associated hold-down design forces could be underestimated by 10%.

# CHAPTER 5

# EXPERIMENTAL STUDIES

## 5.1 DESCRIPTION OF THE BRIDGE SETUP

A single span bridge having 12m girder length and 3.5m width was constructed at the METU Civil Engineering Department K2 Laboratory.

Superstructure consists of a concrete slab over three IPE400 steel girders spaced 1m apart, connected with K-shaped cross-frames constructed with single angle steel profiles at every 1,3m along the length (Figure 5.1 to Figure 5.4).

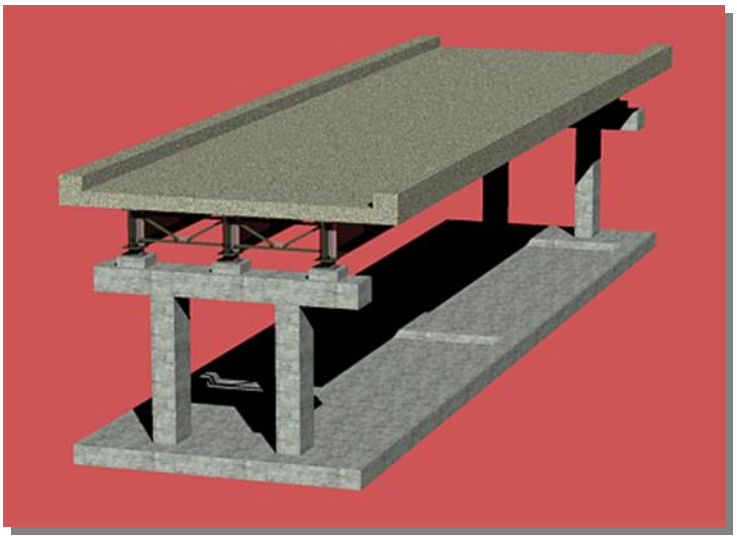

Figure 5.1: Rendered view of the bridge setup

(c) Longitudinal Layout

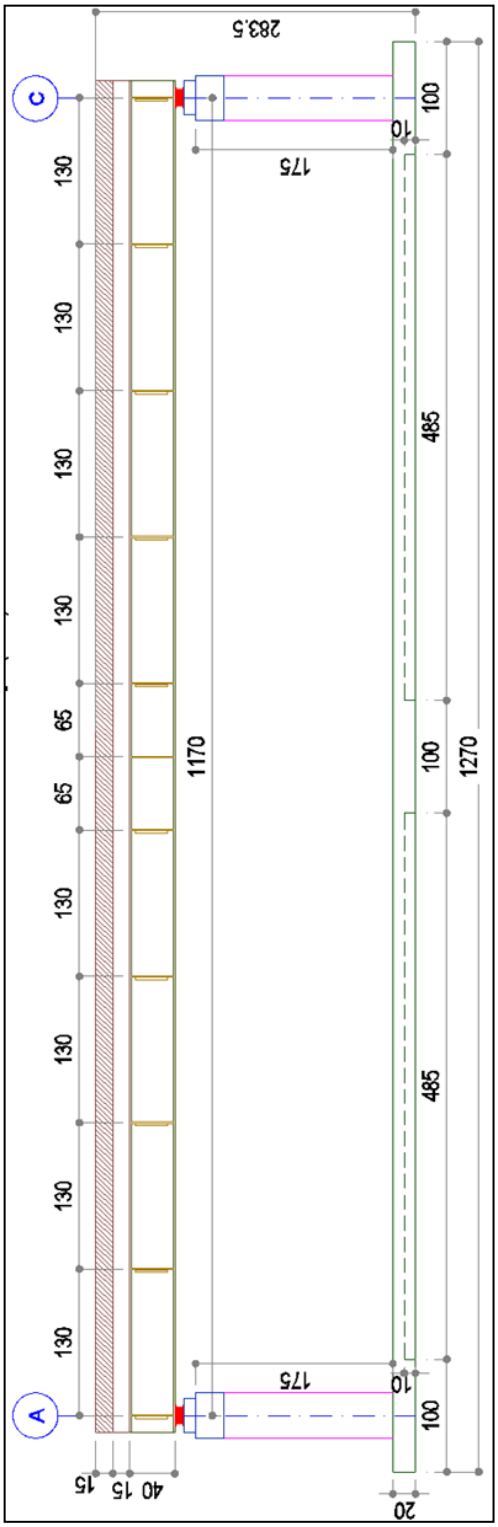


(b) Superstructure Section

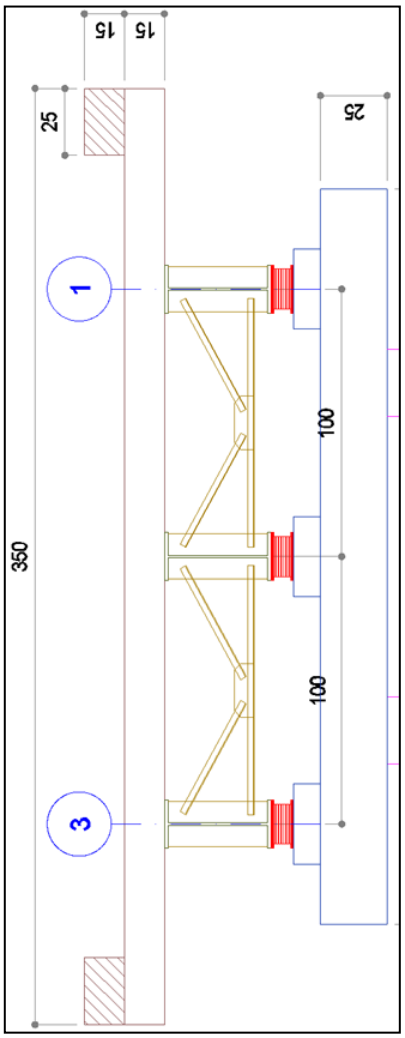


(a) Superstructure Details

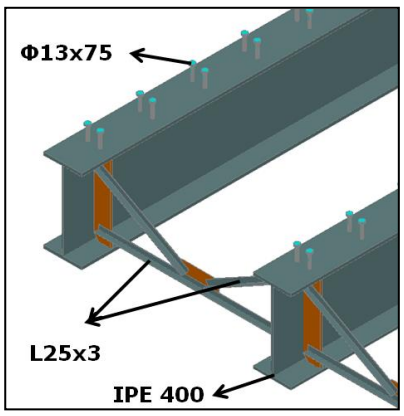


Figure 5.2: Superstructure of the bridge setup with bearing and pier axes labels

(a) Slab Rebar Details

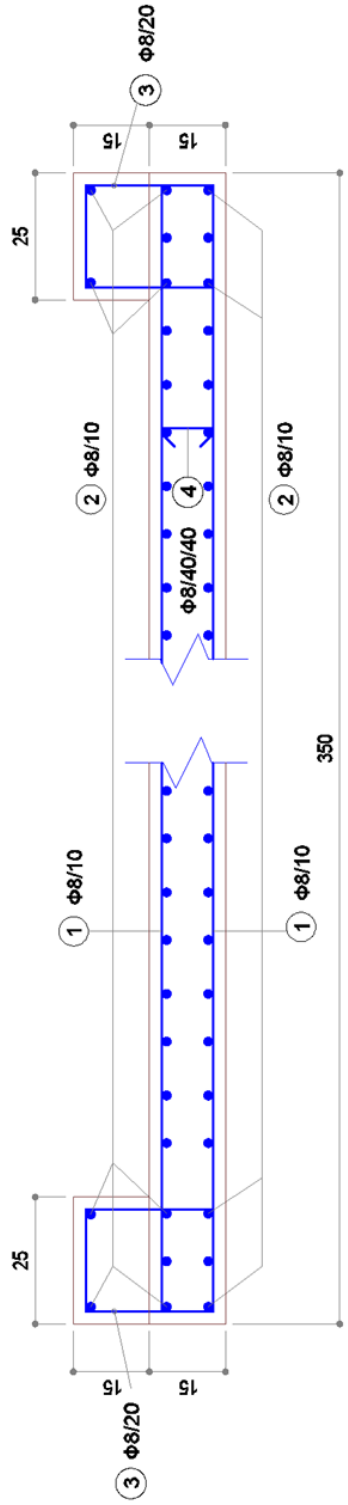


(b) Column Rebar Details

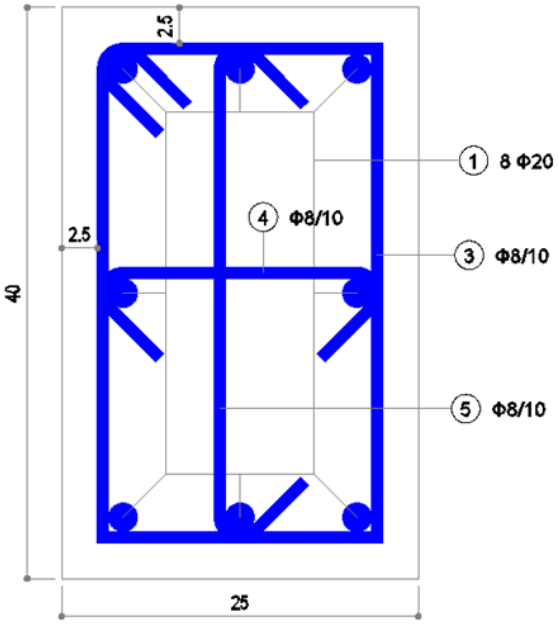


(c) Cap Beam Rebar Details

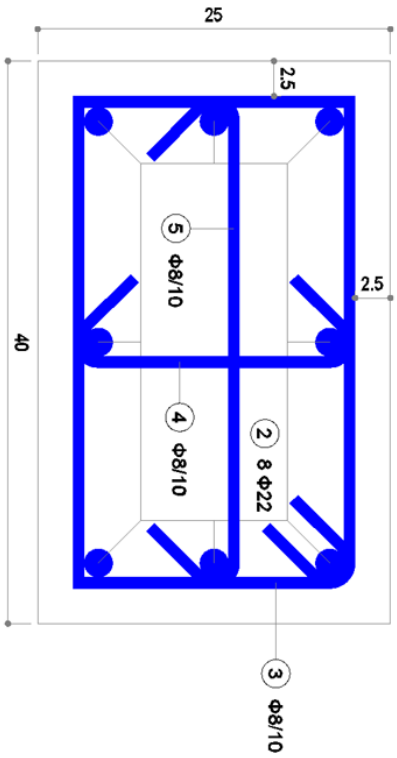


Figure 5.3: Slab, column and cap beam reinforcement details

(a) Construction Phase

(b) Finished Bridge


(c) Hydraulic Actuator

Figure 5.4: Constructed bridge setup

Clear span length of girders is 11.7m and thickness of 3.5m wide slab is 15cm. Concrete used in both substructure and deck had achieved an average strength of 25MPa at 28 days. Structural steel used for steel girders has minimum yield strength of 275MPa. All reinforcements were manufactured from S420 grade steel.

Two different bridge setups (Table 5.1) were tested, using three types of bearings (Table 5.2).

Table 5.1: Explanation of test setups

| **Bridge Setup** | **Used Bearings** | **Bearing Connection** |
|---|---|---|
| Bonded | 6 x Type-1 | M12 Bolts |
| Unbonded | 2 x Type-2 (Middle) and 4 x Type-3 (Sides) | N/A |

Table 5.2: Properties of used bearings

| **Bearing Type** | **Shape** | **Dimensions (mm)** | **# of Rubber Layers** | **Thick. of an Int. Rubber Layer (mm)** | **Thick. of an Ext. Rubber Layer (mm)** | **Thick. of Steel Shim Plates (mm)** |
|---|---|---|---|---|---|---|
| Type-1 | Circular | $D_b = 150$ | 5 | 10 | N/A | 2 |
| Type-2 | Square | 150x150 | 4 | 8 | 4 | 2 |
| Type-3 | Square | 150x150 | 4 | 8 | 4 | (Fiber) |

Bonded setup was constructed using elastomeric bearings of 150mm diameter (Type-1), which were connected to the cap beams and steel girders via anchorage bolts (Figures 3.1 and 5.5).

Square bearings of 150mm width (Type-2 for the exterior bearings and Type-3 for middle ones) were used in unbonded setup (Figure 3.1).

Total weight of superstructure is 200kN. Deck is carried by six bearings, making axial dead load on each bearing approximately 33kN. Total weight of the structure is 369kN. Weights of the components are given on Table 5.3.

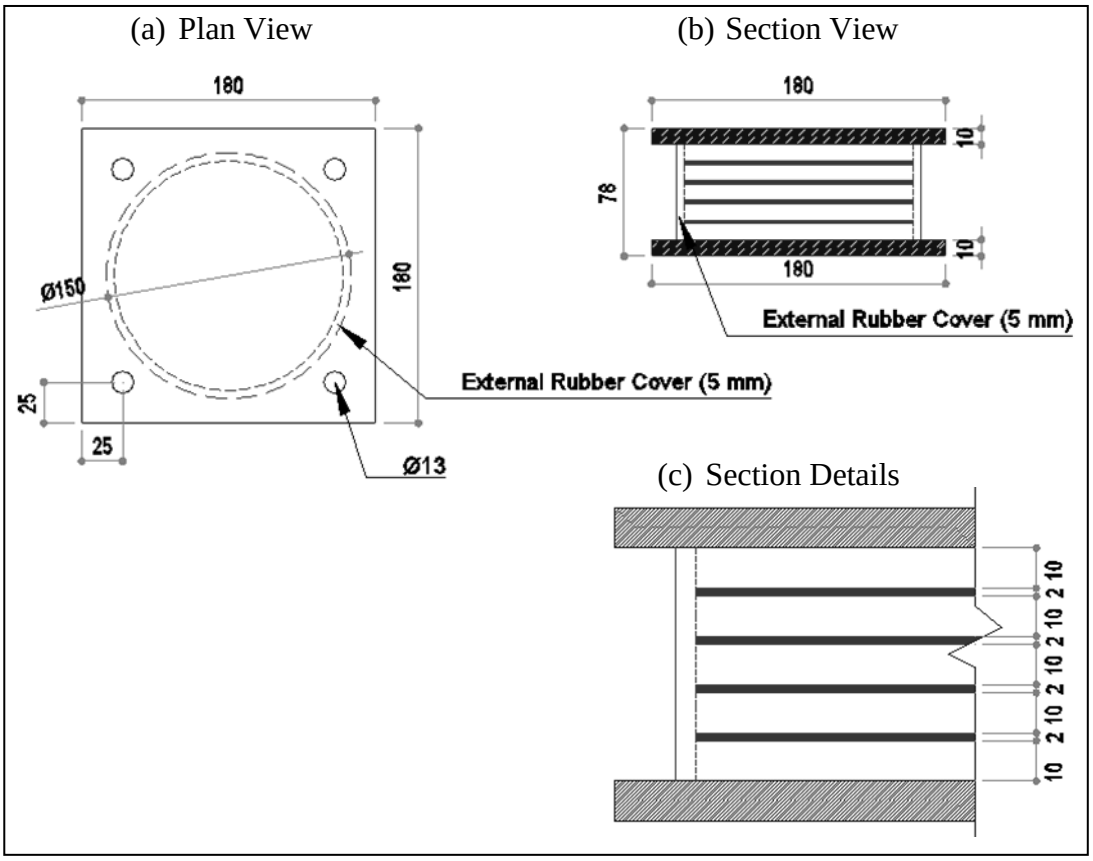


Figure 5.5: Dimensional properties of bonded bearings

Design was made per AASHTO LRFD 2007 specifications. Live load class HL-93 was modified to meet Turkish regulations, considering H30-S24 loading. Permit vehicle load of 360kN was also considered in design.

Containing 2.5% longitudinal reinforcements by area, piers were designed to withstand ultimate moments of approximately 200kN and 100kN about X and Y axis respectively. Yield moments were estimated as 175kN and 90kN about the same axes (Figure 5.7).

Table 5.3: Properties of bridge components

| Component | Material | Weight (kN) |
|---|---|---|
| Foundation Slab | Concrete (C25) | 139.3 |
| Piers | Concrete (C25) | 14.7 |
| Cap Beams | Concrete (C25) | 14.8 |
| Girders, Braces and Connections | Structural Steel (St37) | 23.4 |
| Deck Slab | Concrete (C25) | 176.6 |

Foundation slab was placed on six Teflon bearings, one under each pier and two at the mid-span. Bearings were lubricated by industrial grease. Kinetic internal friction coefficients of the Teflon bearings, designed per AASHTO [3], were estimated to be between 0.9% - 1.3% by laboratory tests, while static coefficient of friction was measured to be 1.5%.

Tests were performed under approximately 60kN (weight per Teflon bearing is $369/6 \approx 61.5kN$) axial forces for 5 cycles up to lateral ±30mm displacements. Hysteresis loop and friction coefficient graphs are presented in Figure 5.6.

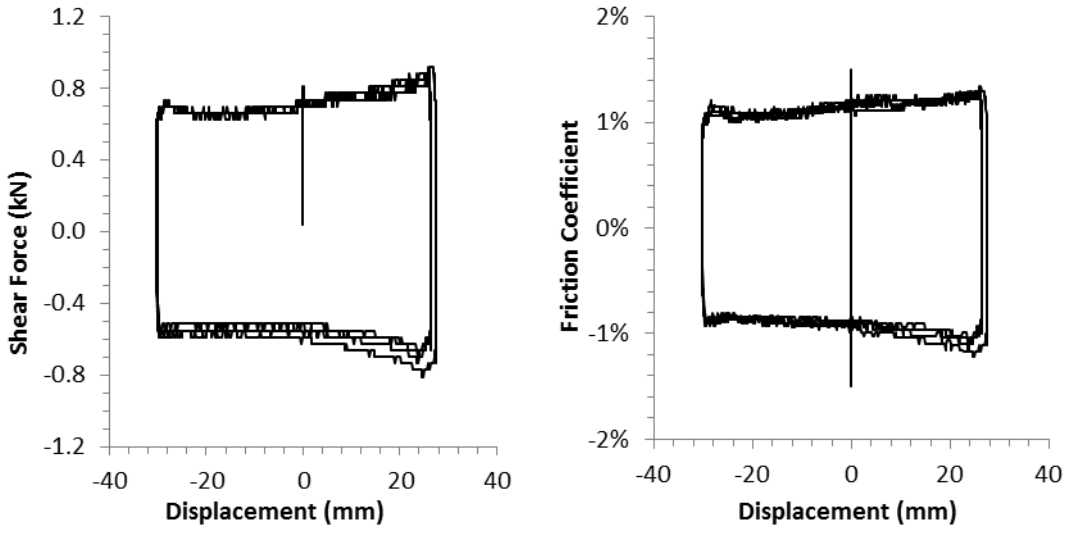


Figure 5.6: Hysteresis loop and friction coefficient vs lateral displacement graphs of Teflon bearings under 60kN axial forces

Static pushover analysis pointed out that, a lateral load of approximately 90kN applied to deck yielded 100% bearing deformations (5cm shear deformations in bearings). Maximum 600kN can be applied to superstructure before piers yield. Moment-curvature diagrams and static pushover curve is presented in Figures 5.7 and 5.8 respectively.

Result can be verified using the calculated design stiffness of a bearing, and considering total number of 6 bearings will exhibit a lateral displacement of 5cm;

$$K_d * 6 * 0.05 = 304 * 6 * 0.05 = 91.2kN$$

Recalling the weight of superstructure being $200kN$ from Table 5.3, it can be estimated that a top slab acceleration equal to $90/200 = 0.45g$ will yield 100% shear deformations in bearings.

Most sophisticated part of the setup consists of an hydraulic actuator designed and produced BESMAK (Figure 5.4), capable of exerting time-displacement functions composed of a frequency content between 1.0 – 8.0Hz with a maximum stroke of ±150mm. Maximum speed and force of the actuator are 800mm/s and 150kN respectively.

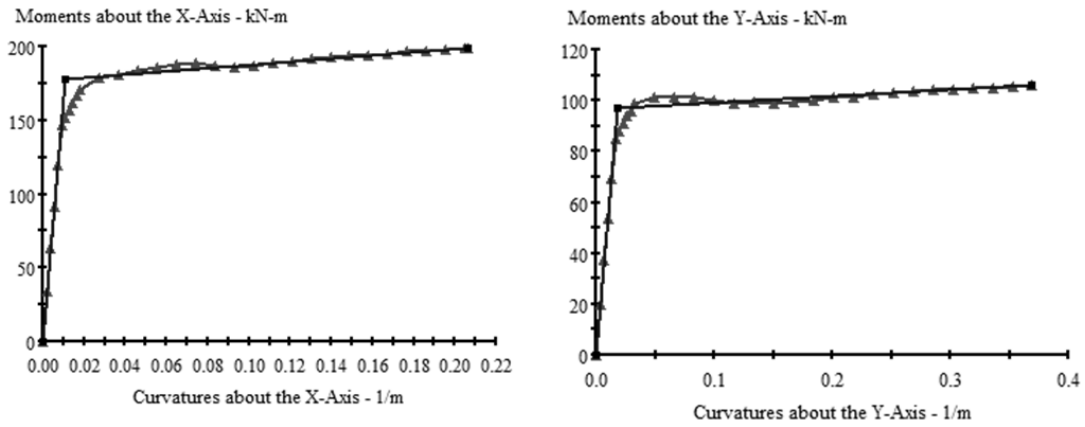


Figure 5.7: Moment-curvature diagrams of piers, calculated by XTRACT software

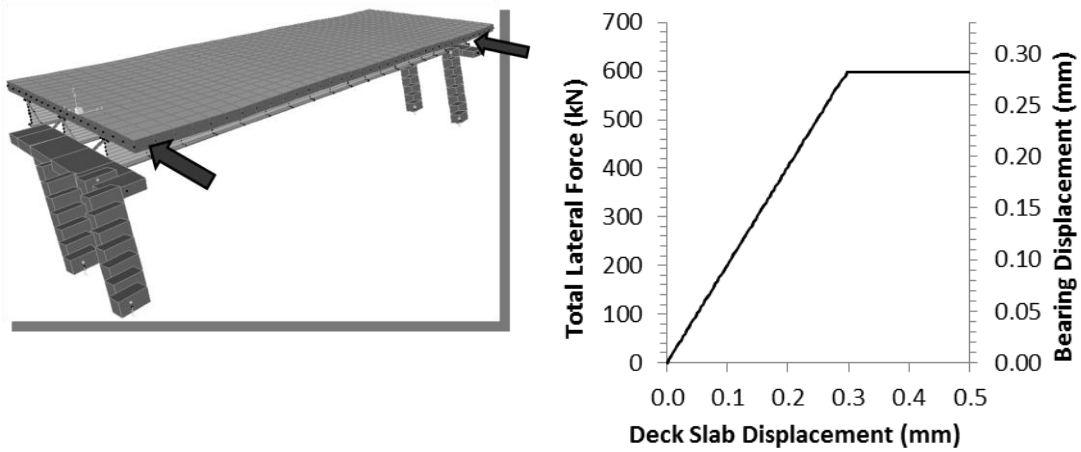


Figure 5.8: Results of lateral pushover analysis

## 5.2 APPLICATION AND INTERPRETATION OF SEISMIC LOADING

Two types of ground motions were applied to the bridge. First group consists of sinusoidal time-displacement harmonic motions. The equation of a sinusoidal motion is:

$$A(t) = A * \sin(t * f) \tag{5.1}$$

where,

t : Time (seconds)
A : Amplitude (g)
f : Frequency of the motion (Hz)
A(t) : Acceleration (g)

Response spectra of harmonic motions between frequency range of 0.5Hz and 3.0Hz having amplitude of 0.5g are presented Figure 5.9. Results indicate that, regardless of its frequency, each motion produces same pseudo acceleration on a SDOF (single degree of freedom) system having identical frequency with the motion.

This is the expected result indeed, considering that frequency content of a sine wave includes only one particular frequency.

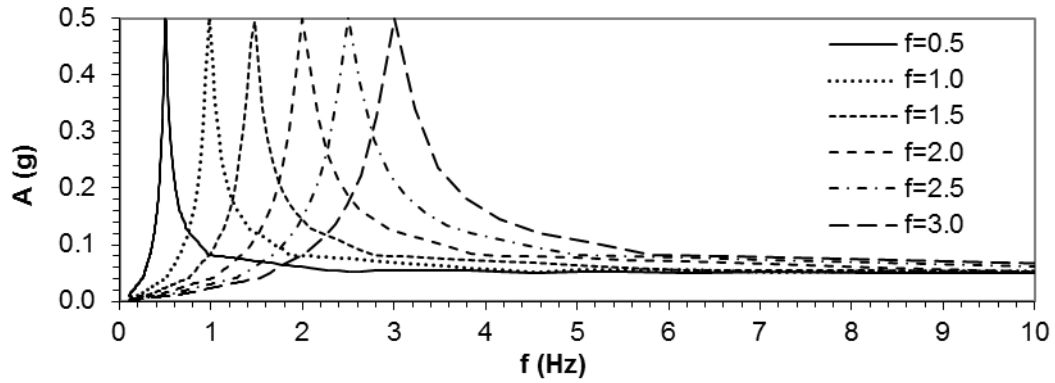


Figure 5.9: Response spectra of harmonic motions (5% damped)

Data obtained from those harmonic motions were used to estimate fundamental period and damping ratio of the bridge setup. Two methods were applied for this purpose.

*Resonant amplification method* requires the construction of a curve by plotting the same selected harmonic response amplitude against loading frequency for a system (Figure 5.10). Damped fundamental frequency is estimated from the curve by picking up the value that produces the maximum response, $p_{max}$. Natural fundamental frequency is then calculated as [14];

$$f_n = \sqrt{1-\beta^2}/f_D \tag{5.2}$$

where;

$f_D$ : Damped fundamental frequency

$\beta$ : Equivalent viscous damping ratio

Equivalent viscous damping of the system is calculated [14];

$$\beta = \frac{p_0}{2p_{max}} \tag{5.3}$$

where $p_0$ is the maximum harmonic response and $p_{max}$ is the response at zero frequency.

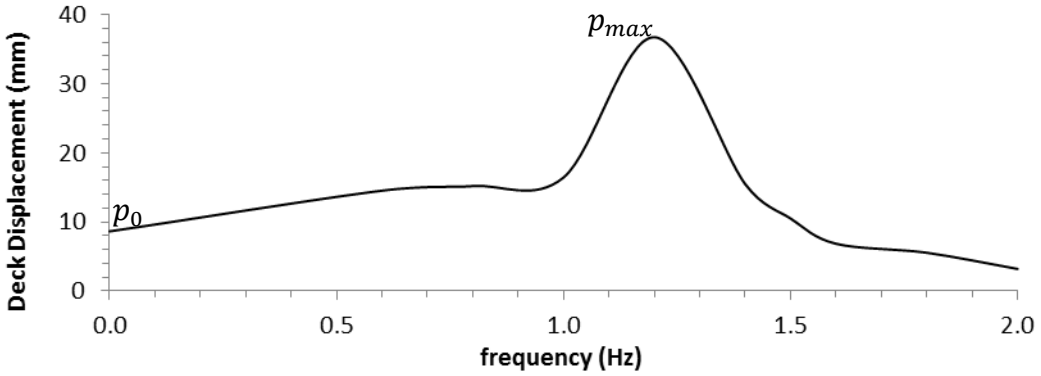


Figure 5.10: Sample frequency response curve

Second method uses the damped free vibration history of the system (Figure 5.11).

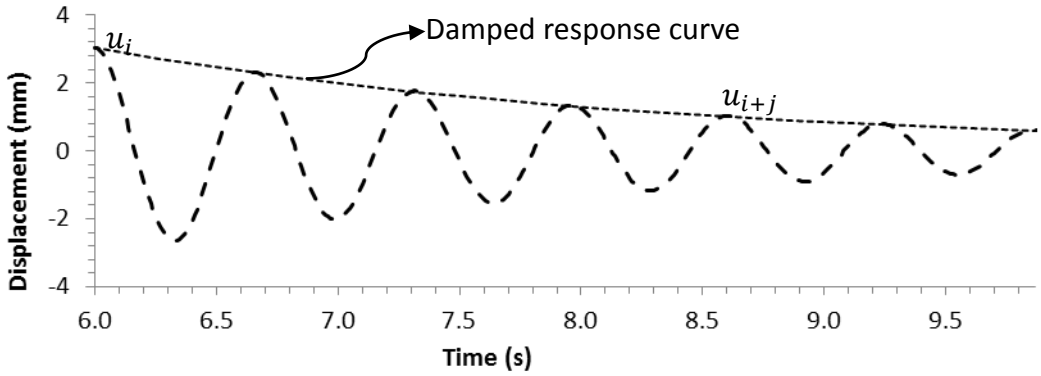


Figure 5.11: Sample damped free vibration response

For the selected peak responses, formulation of equivalent viscous damping ratio is [19];

$$\beta = \frac{1}{2\pi j} \ln \frac{u_i}{u_{i+j}} \tag{5.4}$$

where,

$u_i$ and $u_{i+j}$ : Selected peak responses

Second set consists of recorded ground motion records used in a past study including shake table tests on the same bridge setup [37]. A frequency filter between 0.1 – 8.0Hz was applied in order to exclude the frequency components exceeding the capability of the actuator. Maximum displacements of the motion set were also scaled down to approximately 150mm to stay within stroke limit of the actuator. Properties of ground motions are presented on Table 5.4 and in Figure 5.12.

Table 5.4: Properties of applied earthquake records motions [37]

| # | Earthquake Name and Date | Mw | Station | PGA (g) | PGD (cm) | Epicentral Distance (km) | Scale Factor |
|---|---|---|---|---|---|---|---|
| M1 | 17. 08. 1999 Kocaeli | 7.4 | Sakarya | 0.213 | 14.978 | 35.96 | 0.397 |
| M2 | 17. 08. 1999 Kocaeli | 7.4 | Sakarya | 0.107 | 7.546 | 35.96 | 0.200 |
| M3 | 17. 08. 1999 Kocaeli | 7.4 | Göynük | 0.135 | 4.636 | 80.68 | 1.000 |
| M4 | 12.11.1999 Düzce | 7.2 | Düzce | 0.124 | 14.548 | 8.30 | 0.370 |
| M5 | 12.11.1999 Düzce | 7.2 | Düzce | 0.067 | 7.864 | 8.30 | 0.200 |

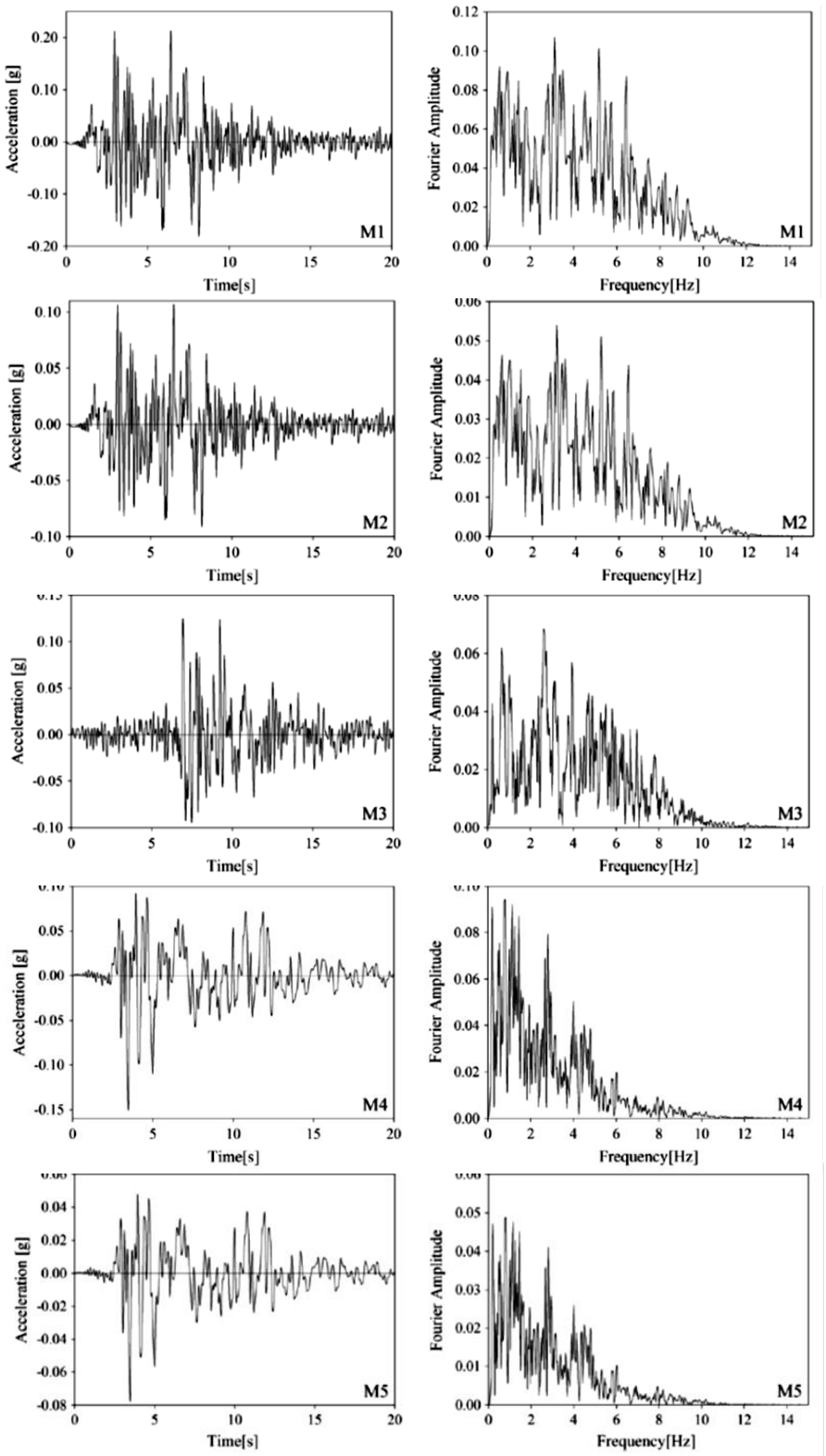


Figure 5.12: Accelerograms and Fourier amplitude graphs of applied earthquake records [37]

## 5.3 INSTRUMENTATION

Bearings located at A1, A3, C1 and C3 axes (Figure 5.2) were instrumented by LVTD's and load cells. For each exterior bearing, one LVDT was attached at the steel girder just above the bearing and another at the load cell just below to obtain shear deformations and axial forces during seismic loading.

A LVDT was attached at the middle of side of bottom slab to measure and verify input displacement history. Top slab displacement history was monitored using a LVDT attached at the middle of side of top slab. Those measurements were also used to calculate the accelerations by numerical differentiation.

Accelerometers were placed at foundation and top slab also to directly measure the acceleration values and increase redundancy of measurements. Locations of instruments are shown on (Figure 5.13).

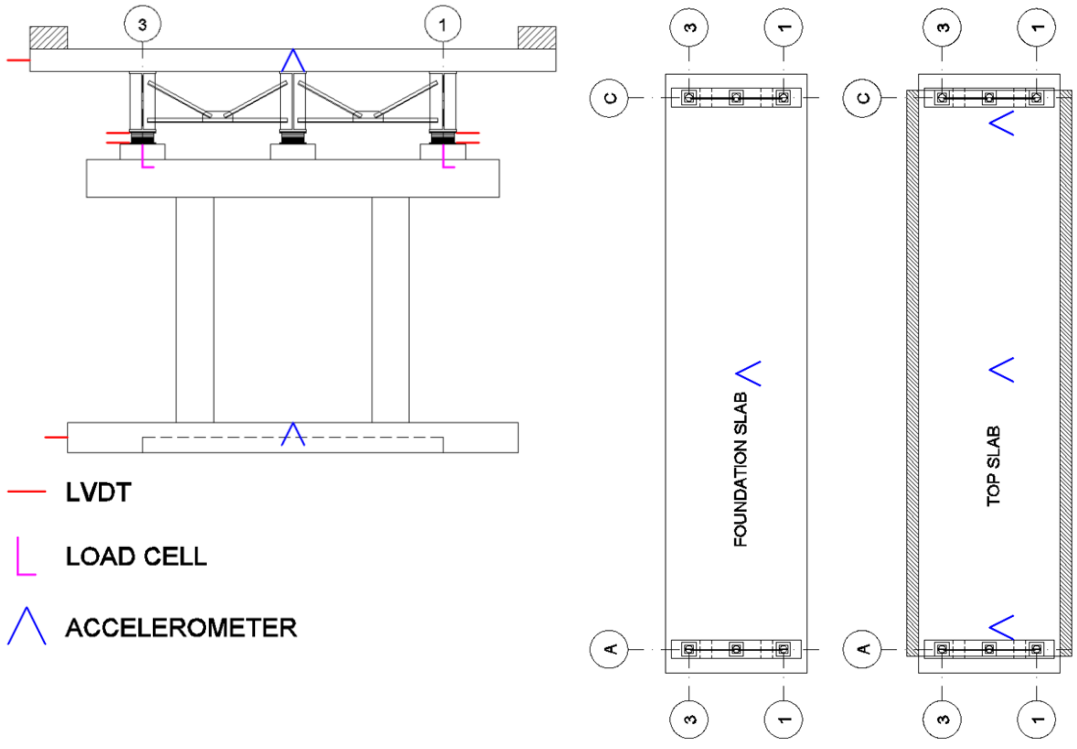


Figure 5.13: Instrumentation setup

## 5.4 BEARING TESTS

Cyclic shear tests were performed on bearings using the old and new bearing test machines in the K2 laboratory (Figure 5.14). Limits of the testing machines are as follows (old and new ones respectively):

- Maximum compressive force = 3000kN, 4000kN
- Maximum shear force = 500kN, 1000kN
- Maximum speed = N/A, 500mm

(a) Old Testing Machine


(b) New Testing Machine

Figure 5.14: Old and new bearing test machines

Using the results obtained from cyclic tests at 300mm/min loading rate, equivalent viscous damping and shear stiffness of the bearings were calculated using equations (5.5) to (5.7).

$$\beta = \frac{EDC}{2 * \pi * K_{eff} * {d_{max}}^2} \tag{5.5}$$

$$d_{max} = \frac{|d^+| + |d^-|}{2} \tag{5.6}$$

$$K_{eff} = \frac{|F^+| + |F^-|}{|d^+| + |d^-|} \tag{5.7}$$

where;

$EDC$ : Energy dissipated per cycle
$d_{max}$ : Displacement range in the cycle
$d^+$ : Maximum displacement in the cycle
$d^-$ : Minimum displacement in the cycle
$F^+$ : Maximum shear force in the cycle
$F^-$ : Minimum shear force in the cycle

Design shear stiffness of bearing can be calculated using Equations (5.8) to (5.10). Total thickness of rubber layers:

$$T_r = N * ti \tag{5.8}$$

where;

$N$ : Number of rubber layers
$t_i$ : Thickness of a rubber layer

$$A_b = \pi^2 * D_b{}^2 / 4 \quad (5.9)$$

where;

$D_b$ : Diameter of inner rubber layers (steel shim plates)

Design shear stiffness:

$$K_d = G * \mathrm{A_b}/T_r \quad (5.10)$$

where;

$G$ : Shear modulus of rubber

Using experimentally obtained shear stiffness value and solving Equation (5.6) for $G$ by substituting geometric properties of a bearing type, shear modulus of rubber can be obtained as;

$$G = K_d/(\mathrm{A_b}/T_r) \quad (5.11)$$

Properties of the tested bearings are repeated on Table 5.5 for convenience.

Table 5.5: Properties of used bearing types

| **Bearing Type** | **Shape** | **Dimensions (mm)** | **# of Rubber Layers** | **Thick. of an Int. Rubber Layer (mm)** | **Thick. of an Ext. Rubber Layer (mm)** | **Thick. of Steel Shim Plates (mm)** |
|---|---|---|---|---|---|---|
| Type-1 | Circular | $D_b = 150$ | 5 | 10 | N/A | 2 |
| Type-2 | Square | 150x150 | 4 | 8 | 4 | 2 |
| Type-3 | Square | 150x150 | 4 | 8 | 4 | (Fiber) |

### 5.4.1 TYPE-1 BEARINGS

The hysteresis loop and calculated parameters from test results are presented in Figure 5.15 and Table 5.6 respectively.

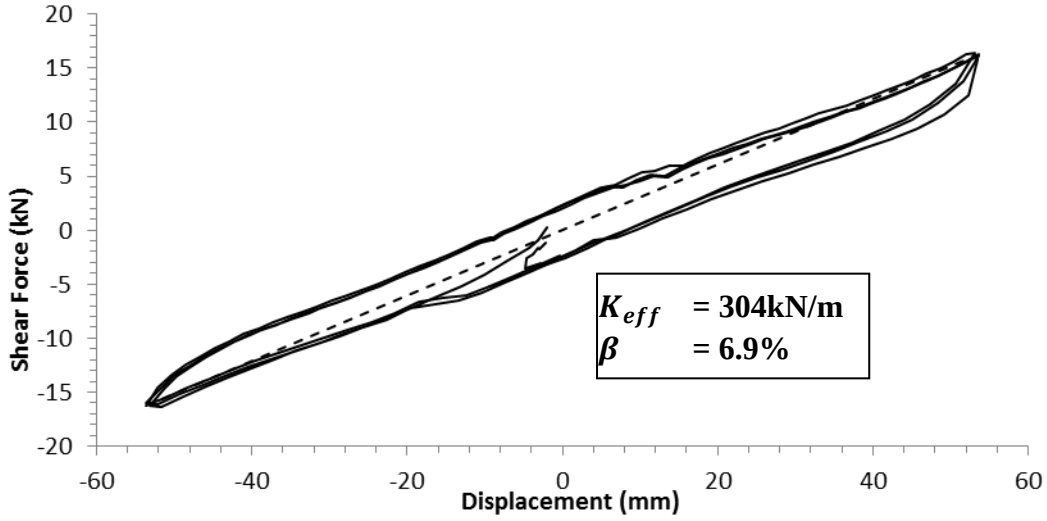


Figure 5.15: Hysteresis loop obtained from shear test under compression

Table 5.6: Calculated parameters for each test cycle

| Cycle # | $EDC$ (kN.m) | $d^+$ (m) | $d^-$ (m) | $d^{max}$ (m) | $F^+$ (kN) | $F^+$ (kN) | $K_{eff}$ (kN/m) | $\beta$ (%) |
|---|---|---|---|---|---|---|---|---|
| 1 | 0.3582 | 0.0551 | -0.0513 | 0.0532 | 16.04 | -16.74 | 308 | 6.5 |
| 2 | 0.3617 | 0.0556 | -0.0516 | 0.0536 | 15.93 | -16.41 | 302 | 6.6 |
| 3 | 0.4014 | 0.0555 | -0.0516 | 0.0535 | 15.67 | -16.66 | 302 | 7.4 |

Using average design parameters of three test cycles, G modulus is calculated as;

$K_{eff}$ = 304kN/m

$\beta$ = 6.9%

$G$ = 860KPa

### 5.4.2 TYPE-2 BEARINGS

The hysteresis loop and calculated parameters from test results are presented in Figure 5.16 and Table 5.7 respectively.

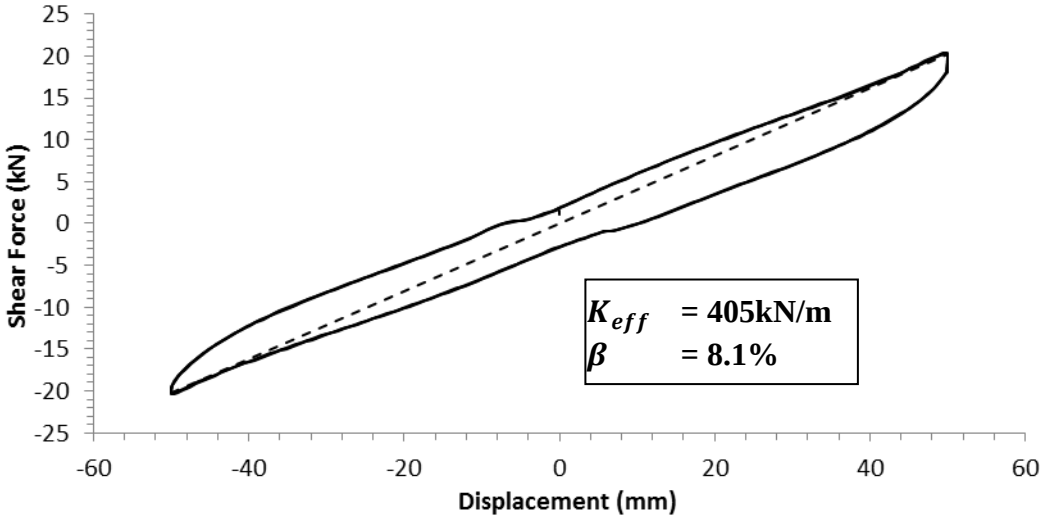


Figure 5.16: Hysteresis loop obtained from shear test under compression

Table 5.7: Calculated parameters for each test cycle

| Cycle # | $EDC$ (kN.m) | $d^+$ (m) | $d^-$ (m) | $d^{max}$ (m) | $F^+$ (kN) | $F^+$ (kN) | $K_{eff}$ (kN/m) | $\beta$ (%) |
|---|---|---|---|---|---|---|---|---|
| 1 | 0.5156 | 0.0500 | -0.0500 | 0.0500 | 20.40 | -20.34 | 407 | 8.1 |
| 2 | 0.5137 | 0.0500 | -0.0500 | 0.0500 | 20.29 | -20.24 | 405 | 8.1 |
| 3 | 0.5114 | 0.0500 | -0.0500 | 0.0500 | 20.19 | -20.16 | 404 | 8.1 |

Using average design parameters of three test cycles, G modulus is calculated as;

$K_{eff}$ = 405kN/m

$\beta$ = 8.1%

$G$ = 720KPa

### 5.4.3 TYPE-3 BEARINGS

The hysteresis loop and calculated parameters from test results are presented in Figure 5.17 and Table 5.8 respectively.

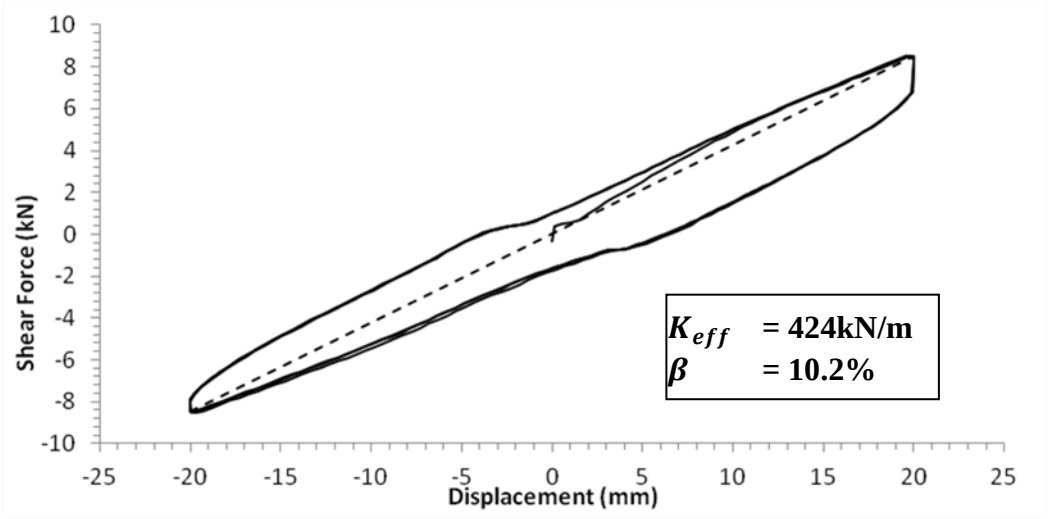


Figure 5.17: Hysteresis loop obtained from shear test under compression

Table 5.8: Calculated parameters for each test cycle

| Cycle # | $EDC$ (kN.m) | $d^+$ (m) | $d^-$ (m) | $d^{max}$ (m) | $F^+$ (kN) | $F^+$ (kN) | $K_{eff}$ (kN/m) | $\beta$ (%) |
|---|---|---|---|---|---|---|---|---|
| 1 | 0.1081 | 0.0200 | -0.0200 | 0.0200 | 8.94 | -8.13 | 427 | 10.1 |
| 2 | 0.1089 | 0.0200 | -0.0200 | 0.0200 | 8.87 | -8.07 | 424 | 10.2 |
| 3 | 0.1086 | 0.0200 | -0.0200 | 0.0200 | 8.86 | -8.05 | 423 | 10.2 |

Using average design parameters of three test cycles, G modulus is calculated as:

$K_{eff}$ = 424kN/m

$\beta$ = 10.2%

$G$ = 754KPa

### 5.4.4 UNIDIRECTIONAL FRICTION TESTS

Static shear tests were conducted on Type-2 bearings to estimate the coefficient of friction between steel and rubber. Tests were repeated under various compression stress levels and loading rates. Test setup is shown in Figure 5.18.

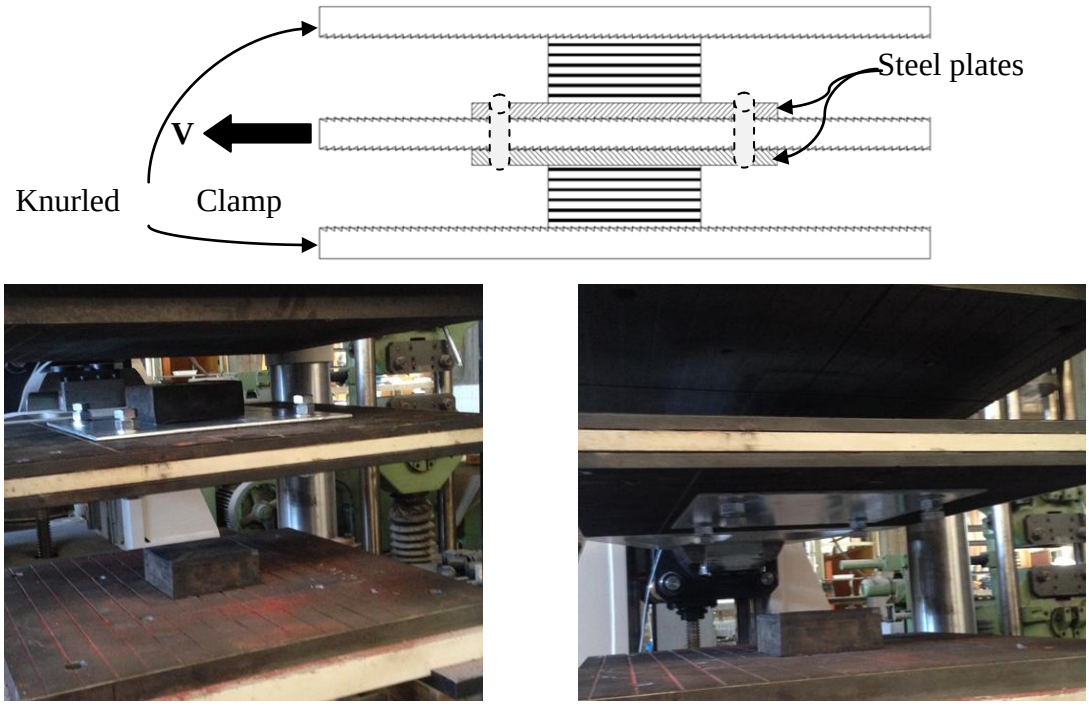


Figure 5.18: Test setup to obtain coefficient of friction between rubber and steel

Two identical steel plates were mounted to the middle board of the testing machine. During shear tests, one surface of a bearing contacted with those steel plates, and the other surface was in contact with the knurled clamp board of the machine. By doing so, it is aimed that the slip would occur between bearings and the mounted steel surfaces before the knurled clamp boards.

First, coefficient of friction between bearings and galvanized steel plates shown in Figure 5.18 were tested. Static shear loadings up to 100mm displacements were performed at varying loading rates and compression values.

Figure 5.19: Galvanized steel plates used in unidirectional friction tests

Shear force (total force of two bearings) vs lateral bearing displacement graphs at different loading rates under compressive forces of 20, 33, 50 and 75kN (compressive stresses of respectively 0.89, 1.47, 2.22 and 3.33MPa) are presented in Figures 5.20 and 5.21.

Results clearly indicated that loading rate, *s*, has a significant effect on the friction force (i.e. coefficient of friction) between bearings and steel plates. Under 33kN compressive force, frictional resistance was reached and kinetic coefficient of friction could be estimated for loading rates of 10 and 25 mm/min as 0.35 and 0.40 respectively. Static coefficients of friction were estimated as 0.37 and 0.40 respectively.

At higher loading rates of 50, 100, 300 and 500mm/min, ratios of shear to compressive force were 0.54, 0.59, 0.81 and 0.73 respectively at 100mm displacement. At the slowest loading rate of 5mm/min, the same ratio was 0.32 at 100mm displacement. Static coefficient of friction values related those loading rates would likely be higher than the ratio of shear to compressive forces as frictional resistance was not reached yet.

For 20kN compressive force, static coefficient of friction could only be estimated at the loading rate of 5mm/s, yielding value of 0.51.

At loading rates of 10, 25 and 50 mm/min, ratios of shear to compressive force were measured to be 0.60, 0.77 and 0.77 in the order given. At the highest loading rates of 100, 300 and 500mm/min, bearing seemed to slip from knurled clamp boards after 90mm displacement. Measured peak ratios of shear to compressive force were 0.91, 1.13 and 1.09 respectively.

At 50 and 75kN compressive force levels, static coefficient of friction could not be reached, as shear force vs displacement graphs did not exhibit a peak followed by a decrease in force up to 100mm displacements. For tests under 50kN compressive forces, measured ratios of shear force to compressive force were 0.28, 0.35, 0.38, 0.39, 0.42, 0.57 and 0.60 for loading rates of 5, 10, 25, 50, 100, 300 and 500mm/min respectively. At 75kN compressive forces, same ratios are obtained as 0.18, 0.21, 0.22, 0.22, 0.30, 0.37 and 0.38 in the same order given.

Results indicated that coefficient of friction is highly dependent to loading rate. To summarize, static coefficient of friction for long term service loads were measured to be greater than 0.35. Moreover, for seismic loading (speeds higher than 3000mm/min) bearings were unlikely to slip before rolling occurs under any compressive force level tested.

Results presented on Figure 5.21 indicated that as loading rate increases, shear force vs displacement behavior became nearly identical due to reducing slip. For example at loading rates of 500mm/min, measured shear forces are nearly the same at 40mm displacement (%100 shear strain), indicating zero to negligible slipping values.

To induce slipping at the loading rate of 500mm/min, surface of the bearings contacting galvanized steel plates were lubricated with hydraulic oil. Tests were repeated under 25, 33, 50 and 75kN compressive forces and results are presented on Figure 5.22. Results indicated peak shear to compressive load ratios of 0.11, 0.16, 0.14 and 0.10 under compressive forces of 20, 33, 50 and 75kN.

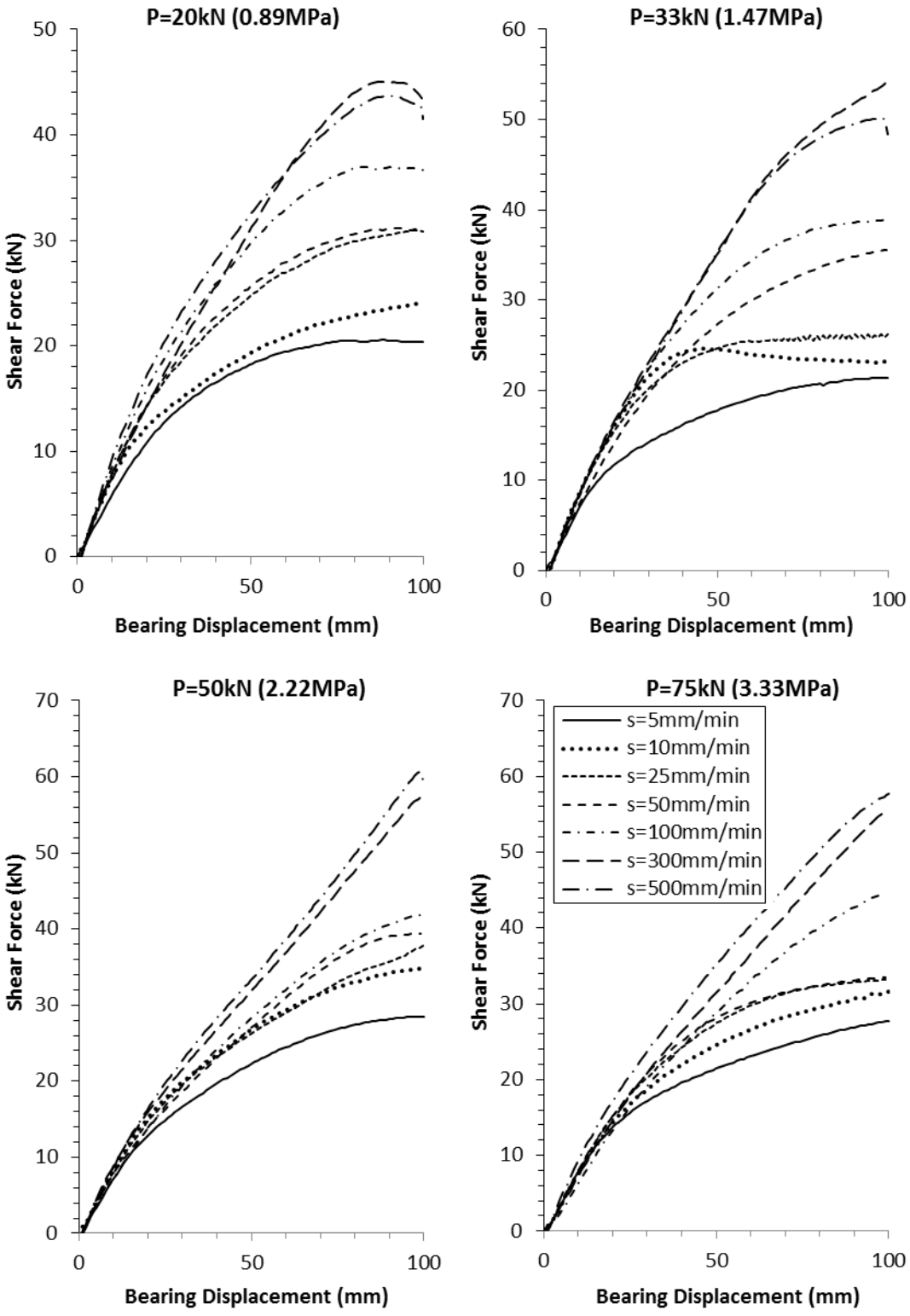


Figure 5.20: Shear force (sum of two bearings) vs lateral bearing displacement (shear deformation) under varying compressive forces

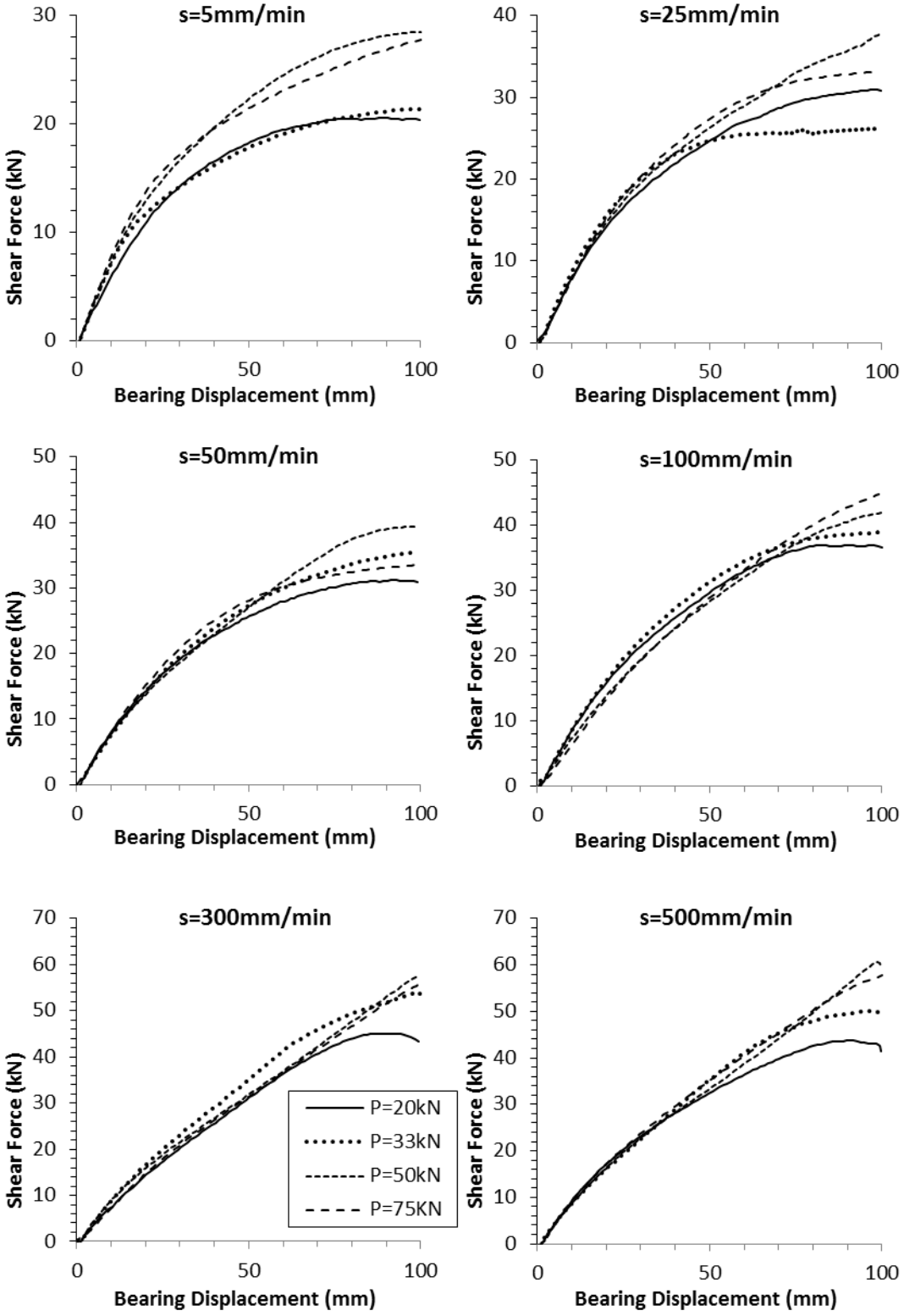


Figure 5.21: Shear force (sum of two bearings) vs lateral bearing displacement under varying loading rates

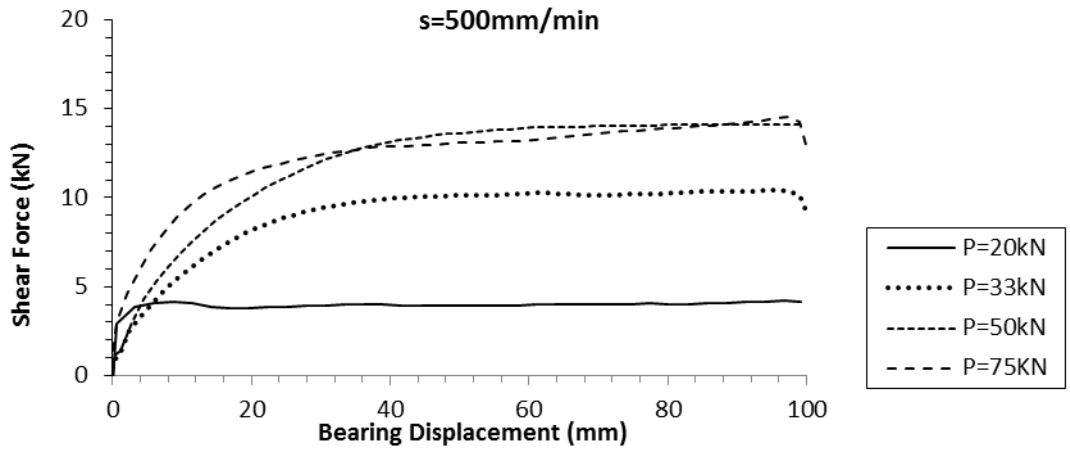


Figure 5.22: Shear force (sum of two bearings) vs lateral bearing displacement under varying compressive forces, using lubricated galvanized steel plates

### 5.4.5 CYCLIC FRICTION TESTS

Cyclic shear tests were carried out on Type-2 bearings to explore the shear behavior and slipping under highest loading rate that could be applied by the test machine (500mm/min) using steel plates having different finishes. Tests were repeated under various levels of compression stress and results were compared with the hysteresis loops obtained from cyclic shear tests.

Four different steel plates are used to observe the effect of finish on the friction response under highest loading rate (500mm/min) Figure 5.23. A test setup similar to the one explained in Section 5.4.4 was used for raw steel (c) and galvanized steel (d) plates.

For slightly rusted steel (a) and moderately sanded galvanized steel (b) plates, a test setup containing only one friction plate at top of the knurled clamp board was used as only one plate for each finish could be obtained (Figure 5.24).

Four full cycles up to 50mm (125% shear starin) lateral displacements were applied to the bearings. Results are presented in Figure 5.25. It can be seen that, value of compressive force had negligible effect on the bearing shear behavior on any of the surfaces, meaning zero to negligible slipping occurred during cyclic loadings.

Test results are organized by compressive force values on Figure 5.26, such that results obtained on different steel surfaces for an axial load level are plotted together including results of tests under clamped conditions.

Results again indicated that, surface type did not have a significant effect on shape and magnitude of hysteresis loops and obtained response is nearly identical with the clamped test results; i.e. zero to negligible slipping occurred during loadings.

(a) Slightly rusted stainless steel

(b) Moderately sanded and galvanized steel

(c) Raw steel

(d) Galvanized Steel

Figure 5.23: Steel plates with different surface finishes used in cyclic friction tests

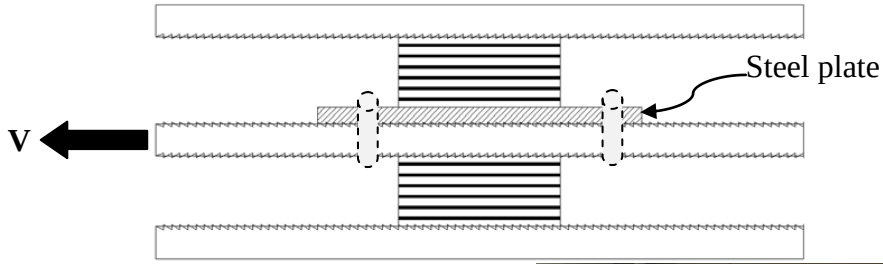


(a) Slightly rusted stainless steel

(b) Moderately sanded and galvanized steel

Figure 5.24: Test setup with one plate on top of the knurled clamp board

.

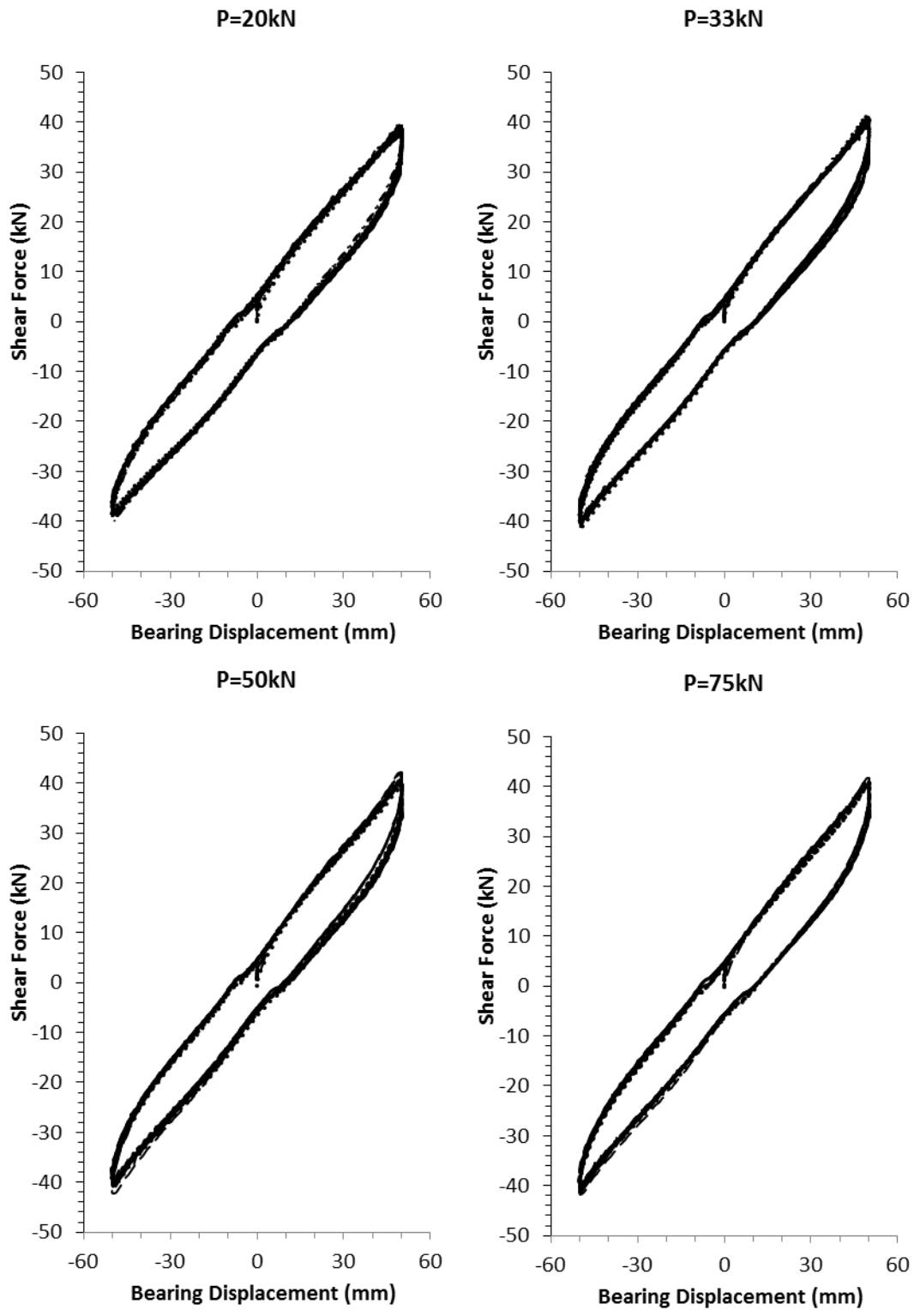


Figure 5.25: Results of cyclic friction tests organized by compressive forces

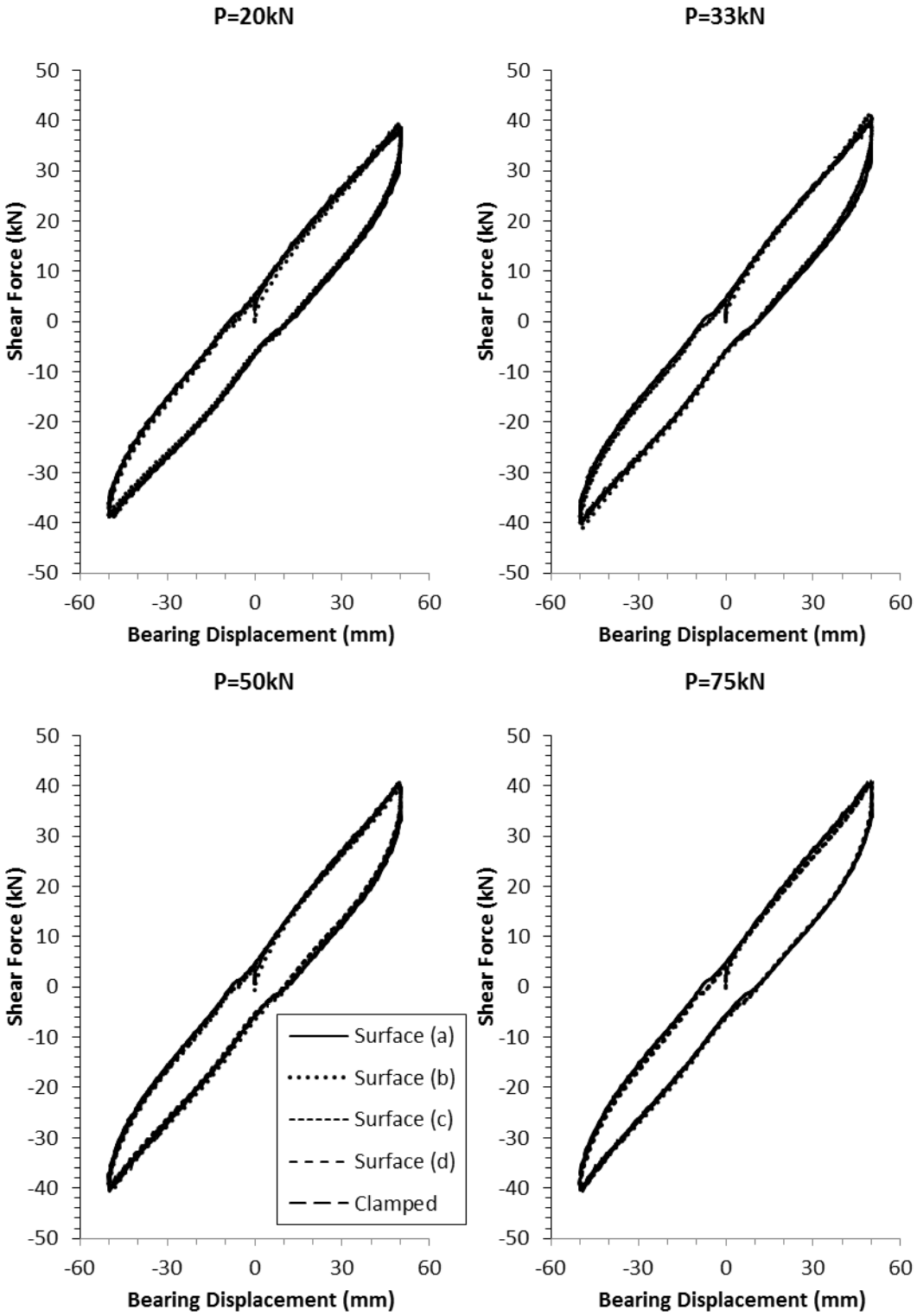


Figure 5.26: Results of cyclic friction tests organized by steel surfaces

## 5.5 HARMONIC LOADING TESTS

Theoretical and measured input acceleration and displacement histories were compared and presented for loading frequencies of 0.6Hz and 1.0Hz in Figure 5.36. Results indicate no major discrepancies existed.

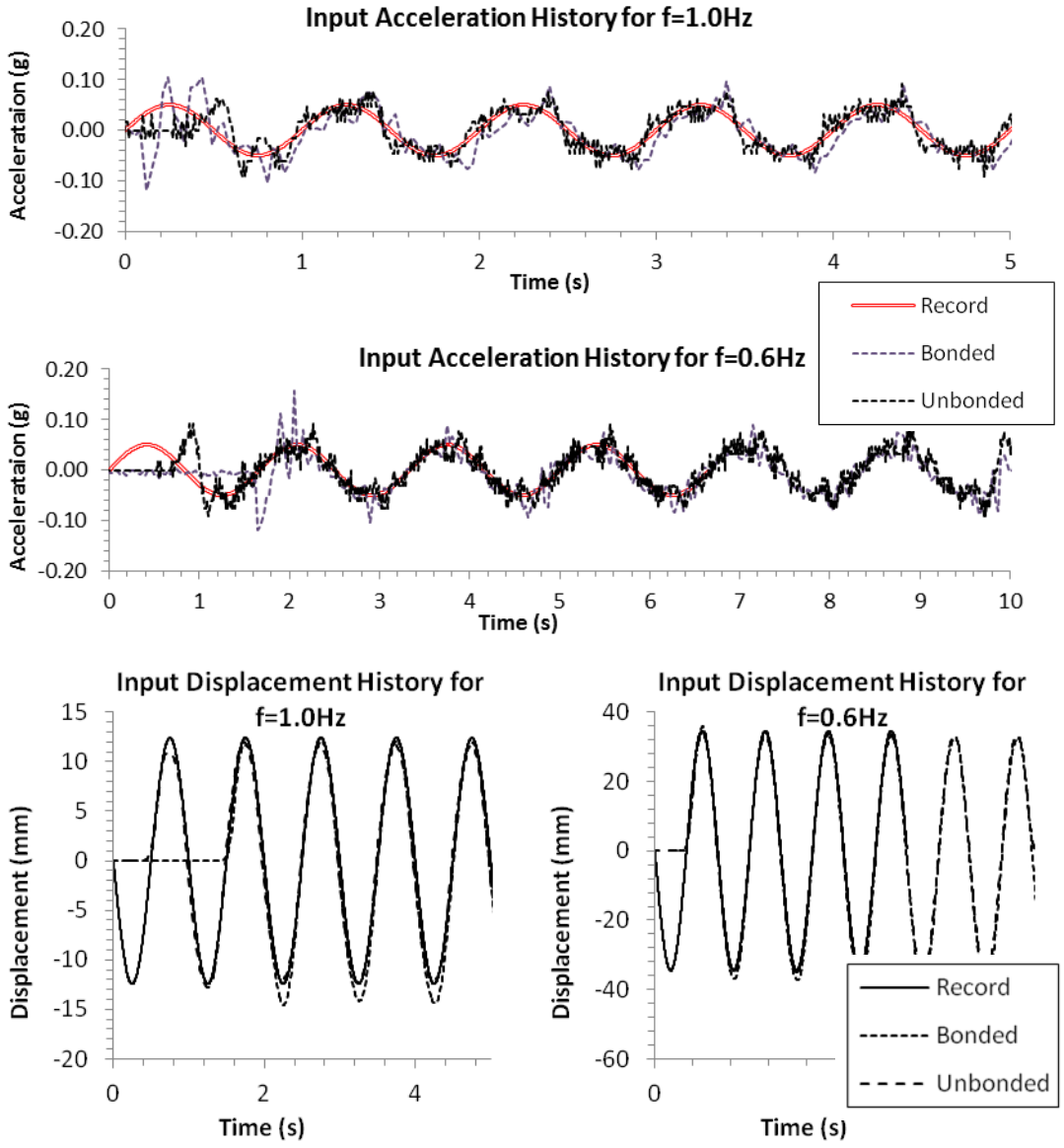


Figure 5.27: Comparison of theoretical and measured acceleration and displacement histories of applied harmonic loads

### 5.5.1 BONDED SETUP

Frequency response curve and damped free vibration response considering deck displacements are presented in Figure 5.28.

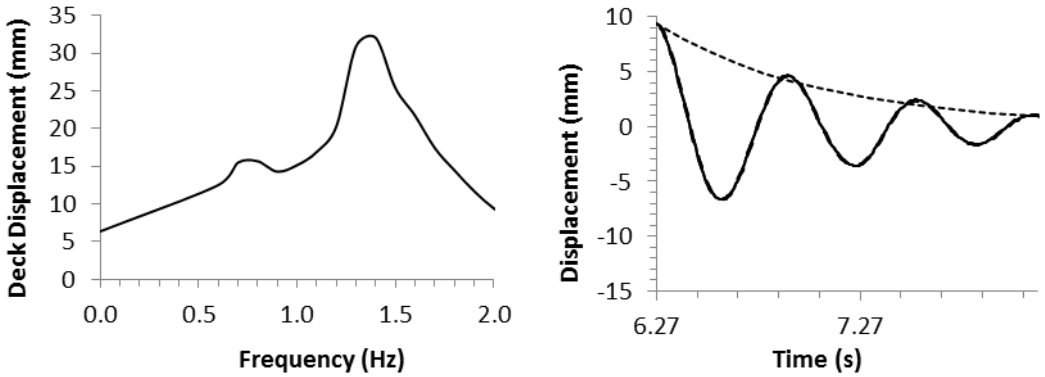


Figure 5.28: Frequency response curve of deck displacements and damped free vibration response of bearing displacements for bonded setup

Damped fundamental frequency of the system is in the vicinity of $f_1 = 1.40Hz$. Equivalent damping ratio of the structure is calculated using the formulation given in Section 5.2 as;

$p_0 = 6.34mm$

$p_{max} = 32.05mm$

$$\Rightarrow \beta_1 = \frac{p_0}{2p_{max}} = \frac{6.34}{2 * 32.05} = 9.9\%$$

Using the damped free vibration response history and substituting in Equation (5.4), same structural properties were calculated as follows;

$u_1 = 6.78mm, t_1 = 6.27s$

$u_2 = 3.13mm, t_2 = 6.93s \rightarrow \beta_{2-1} = 12.3\% \rightarrow f_{D,2-1} = 1.52Hz$

$u_3 = 1.54mm, t_3 = 7.57s \rightarrow \beta_{3-2} = 11.3\% \rightarrow f_{D,3-2} = 1.56Hz$

$u_4 = 0.66mm, t_4 = 8.14s \rightarrow \beta_{4-3} = 13.4\% \rightarrow f_{D,4-3} = 1.75Hz$

$$\Rightarrow \beta_{4-1} = \frac{1}{2\pi * 3} \ln \frac{6.78}{0.66} = 12.3\% \quad , f_{D,4-1} = 1.60Hz$$

$$\Rightarrow f_{n,4-1} = 1.62Hz$$

Based on the results, equivalent damping ratio of the system was considered to be equal to approximately 10% for FEA.

### 5.5.2 UNBONDED SETUP

Frequency response curve and damped free vibration response considering deck displacements are presented in Figure 5.29.

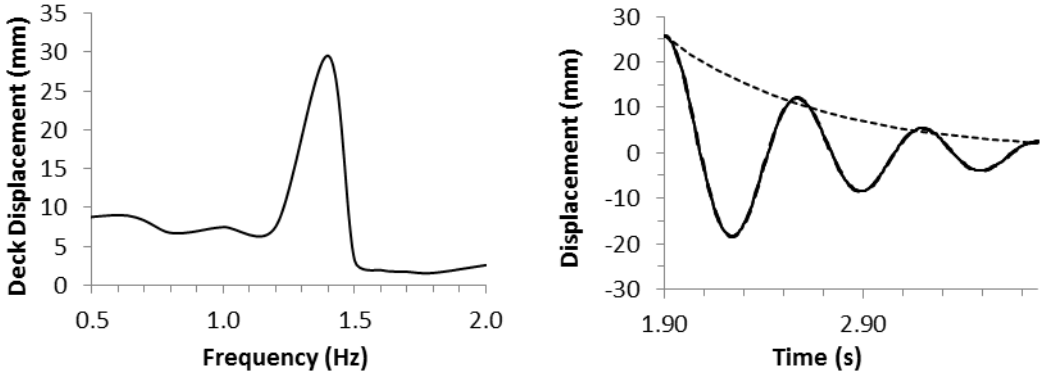


Figure 5.29: Frequency response curve of deck displacements and damped free vibration response of bearing displacements for unbonded setup

Results indicated that damped fundamental frequency of the system is in the vicinity of $f_1 = 1.40Hz$.

Equivalent damping ratio of the structure is calculated using the formulation given in Section 5.2 as;

$p_0 = 6.34mm$

$p_{max} = 29.54mm$

$$\Rightarrow \beta_1 = \frac{p_0}{2p_{max}} = \frac{6.34}{2 * 29.54} = 10.7\%$$

Using the damped free vibration response history and substituting in Equation (5.4), same structural properties were calculated as follows;

$u_1 = 15.30mm, t_1 = 1.90s$

$u_2 = 6.61mm, t_2 = 2.57s \rightarrow \beta_{2-1} = 13.4\% \rightarrow f_{D,2-1} = 1.49Hz$

$u_3 = 2.87mm, t_3 = 3.20s \rightarrow \beta_{3-2} = 13.3\% \rightarrow f_{D,3-2} = 1.59Hz$

$u_4 = 1.30mm, t_4 = 3.78s \rightarrow \beta_{4-3} = 12.7\% \rightarrow f_{D,4-3} = 1.72Hz$

$$\Rightarrow \beta_{4-1} = \frac{1}{2\pi * 3} \ln \frac{15.30}{1.30} = 12.3\% \quad , f_{D,4-1} = 1.60Hz$$

$$\Rightarrow f_{n,4-1} = 1.61Hz$$

Based on the results, equivalent damping ratio of the system was considered be equal to approximately 10.0% for FEA.

## 5.6 STATIC LOADING TESTS

To estimate the coefficient of friction and to investigate the static response of the bridge at low loading rates, a setup was prepared to push the bridge in longitudinal direction.

Longitudinal and lateral movements of the deck were measured by LVDT's, and axial forces in bearings were obtained using load cells. Total static force acting on deck was measured by a load cell mounted to top of concrete slab (Figure 5.30).

Load was applied at an average speed of 0.34mm/s (20mm/min). Displacement vs time and load vs time graphs is presented in Figures 5.31 and 5.32 respectively.

Results did not indicate any lateral deck movement as expected. Load vs displacement graph is presented in Figure 5.33. Force and displacement values measured at labeled points are presented on Table 5.9.

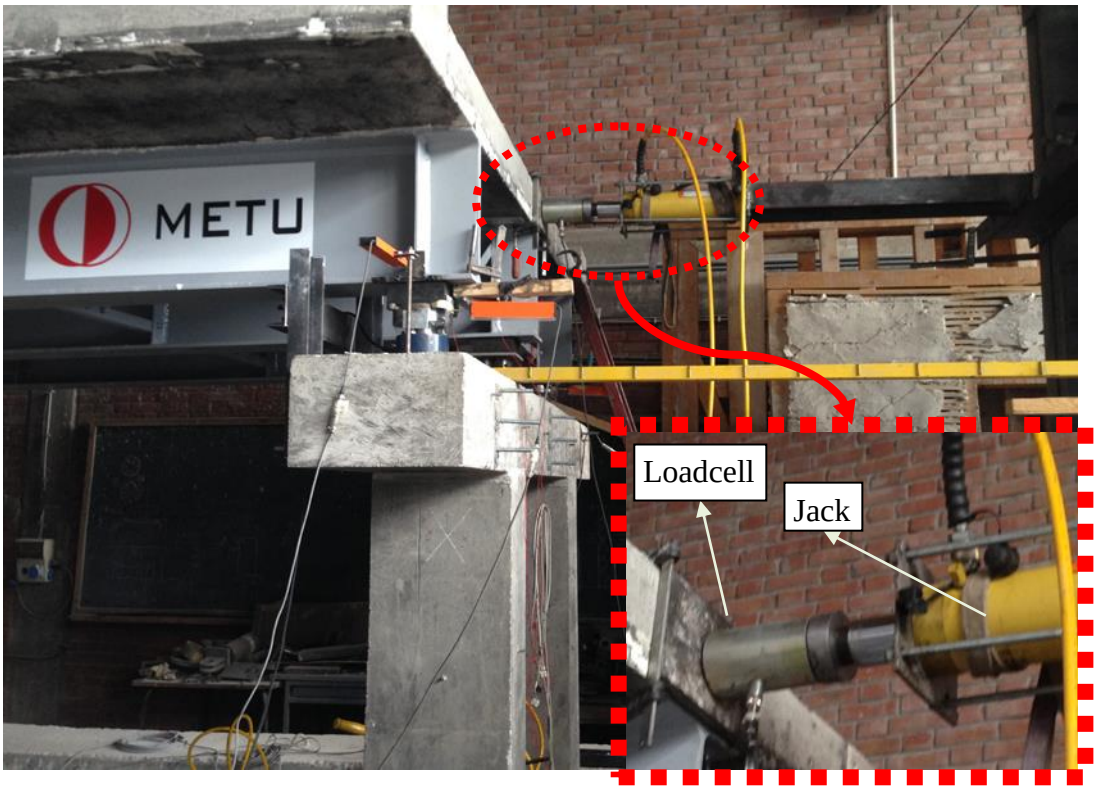


Figure 5.30: Test setup for static loading

Theoretical no-slip behavior of the bridge is plotted on the same graph, using the hysteretic loading results of the bearings.

It is seen that two load vs displacement graphs parted ways at loading force value of 41.9kN (point 1), indicating which slipping initiated.

Recalling that weight of the superstructure is 200kN, the coefficient of friction value where slipping starts is 0.20. When longitudinal force reached up to 57.6kN (point 2), full slipping observed yielding a static friction coefficient of 0.29.

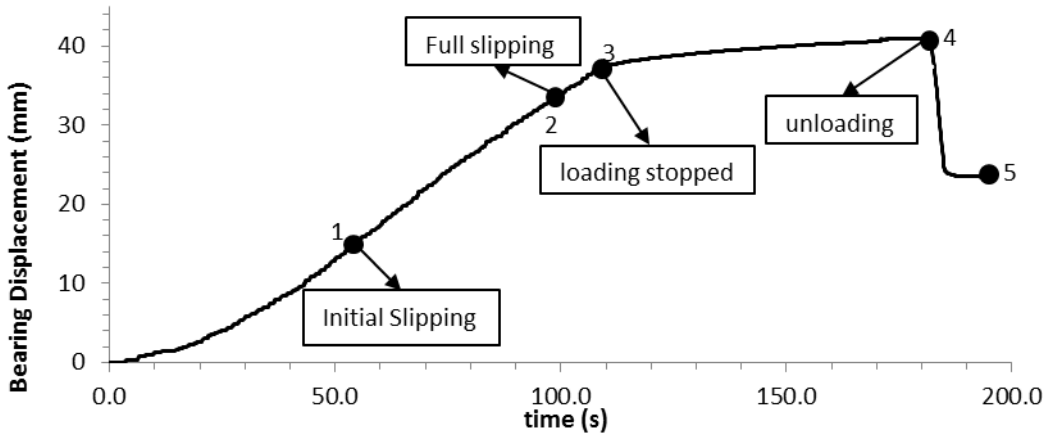


Figure 5.31: Bearing Displacement vs time graph obtained of static loading test

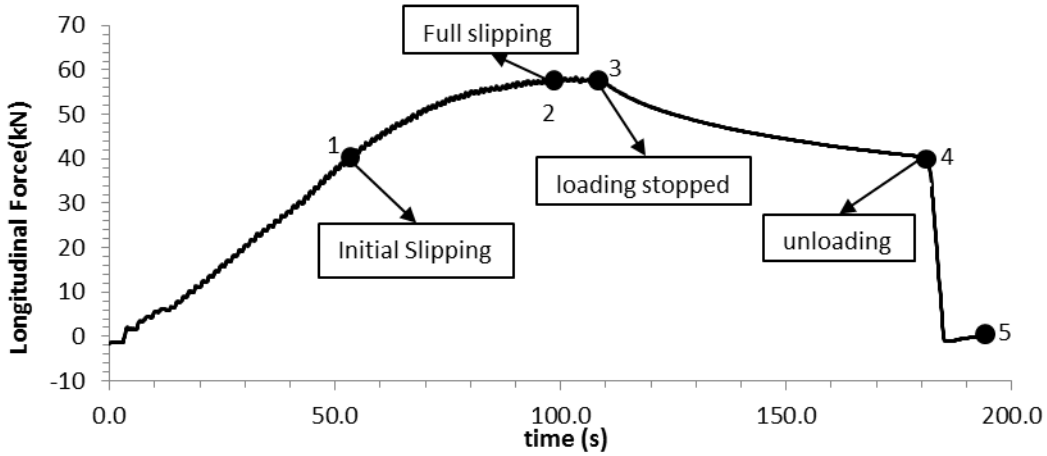


Figure 5.32: Load vs time graph obtained of static loading test

After loading of hydraulic jack is stopped (point 3), slip continued until load reduced to 40.3kN (point 4), suggesting dynamic coefficient of friction may be equal or lower than 0.20.

Permanent displacement, i.e. magnitude of the slip, was measured as 23.4mm from LVDT readings, and also verified by measurements from the setup as shown in Figure 5.34.

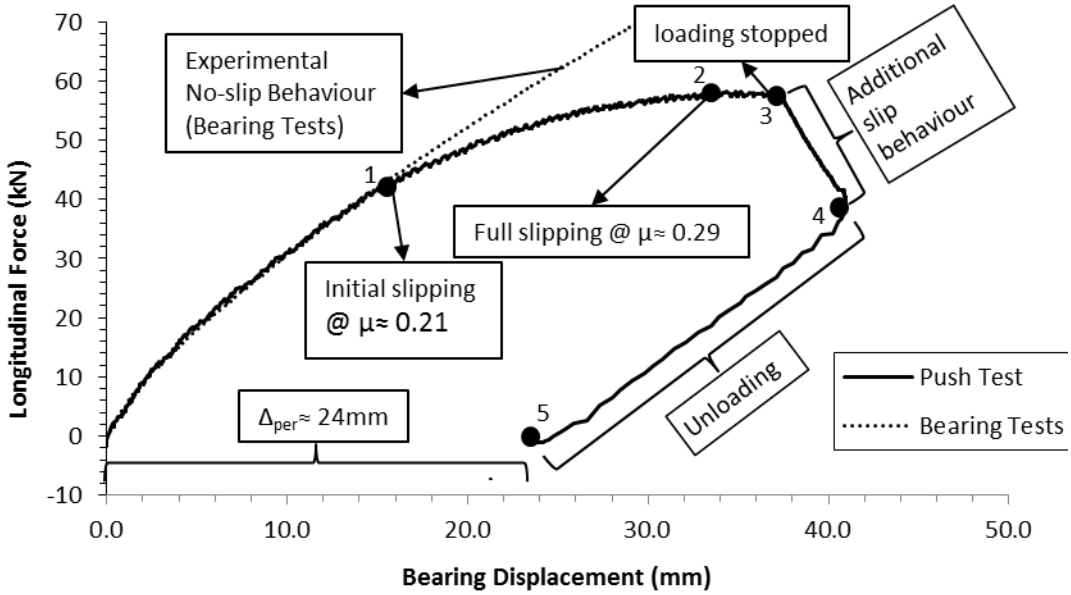


Figure 5.33: Load vs displacement graph of static loading test

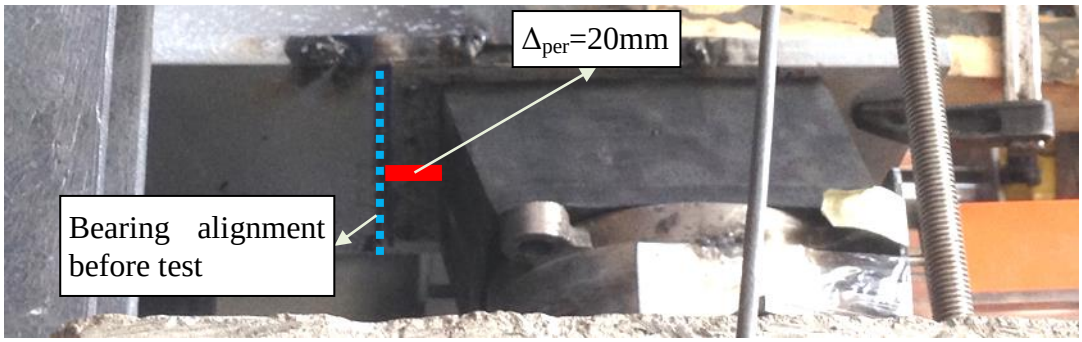


Figure 5.34: Measured slip value

Table 5.9: Measured force and displacement during static loading test

| Point | $F$ (kN) | Δ (mm) |
|---|---|---|
| 1 (Initial slip) | 41.9 | 15.4 |
| 2 (Full slipping) | 57.6 | 33.3 |
| 3 (Loading stopped) | 57.9 | 37.1 |
| 4 (Unloading) | 40.3 | 40.9 |
| 5 (End) | 0.0 | 23.4 |

Measured permanent displacement (i.e. slip) of 24.4mm can also be verified as follows; at point 4, where unloading took place, elastic displacement can be estimated from the first portion of the loading curve as 13.5mm. This yields a theoretical slip value of 40.9-13.5=27.4mm, which is quite close to the measured value of 23.4mm. The difference between is likely due to viscoelastic bearing displacement occurred during test, which should be added to the calculated elastic displacement.

## 5.7 SEISMIC LOADING TESTS

Theoretical and measured input displacement histories were compared and presented in Figure 5.35. Results indicate no major discrepancies existed, but comparison of M1 and M4 records showed that actuator had possibly reached its displacement limits at some point. Although careful consideration was given to center the actuator after each test, the issue could not be prevented and exact cause is yet to be understood.

However, by comparing Figures 5.12 and 5.35, it can be seen that the time intervals where disparities were observed do not include peak acceleration points of the motion record. Thus this relatively small incompatibility is unlikely to affect the result of the seismic loading tests. Comparison of input acceleration histories are also provided in Figures 5.36 and 5.37. Measured and theoretical values showed reasonable agreement.

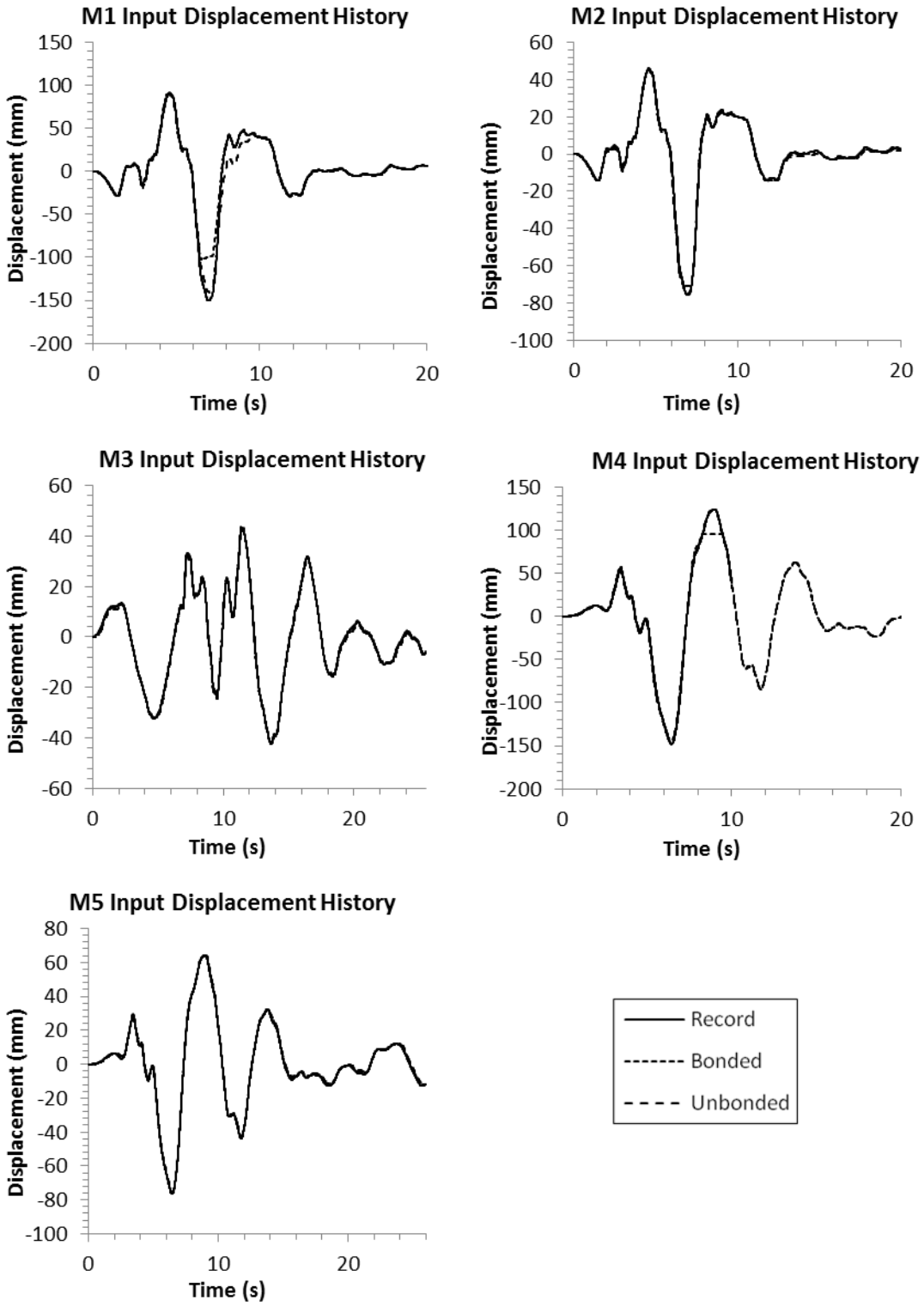


Figure 5.35: Comparison of input displacements of applied ground motion records

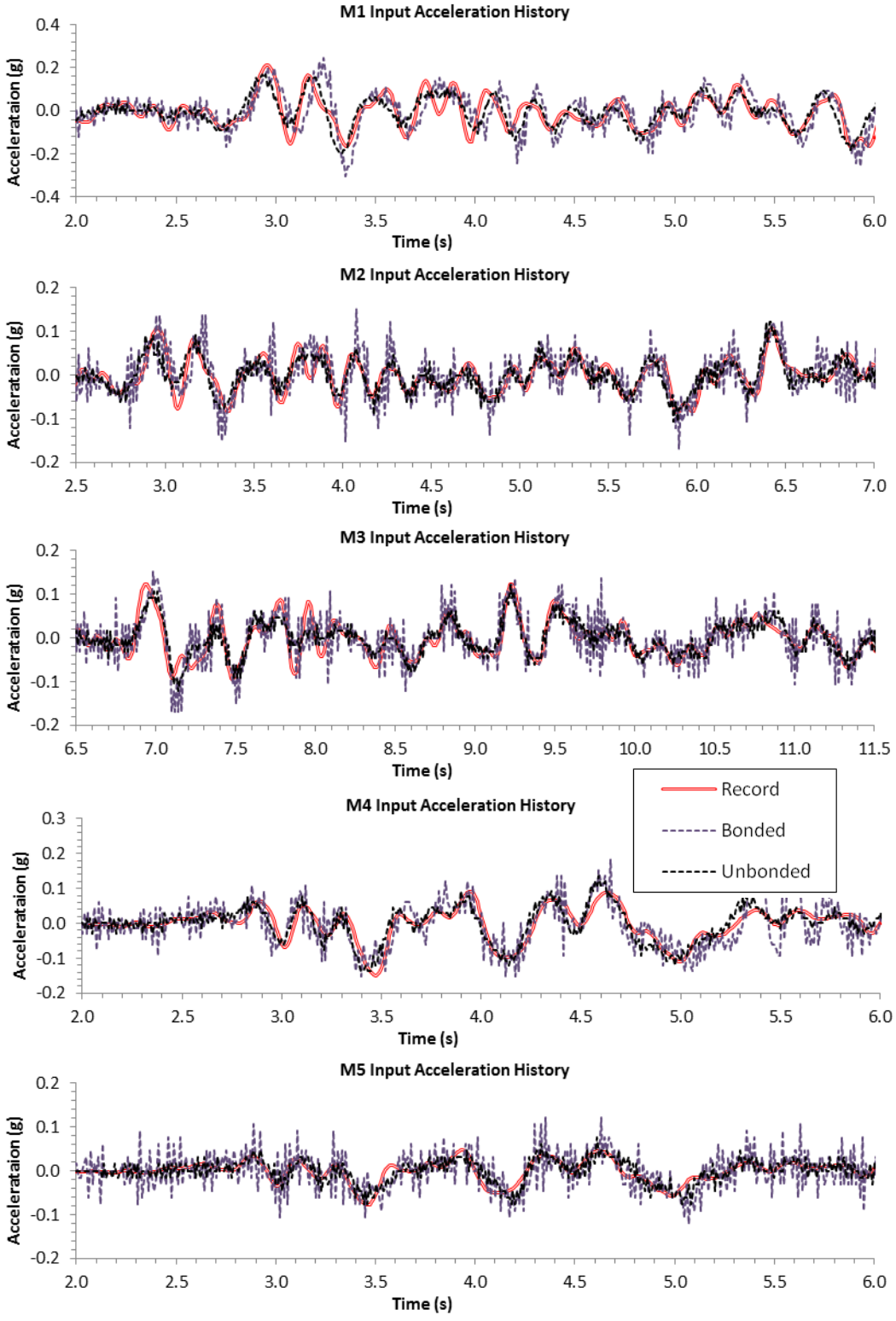


Figure 5.36: Comparison of theoretical and measured input accelerations of applied ground motion records

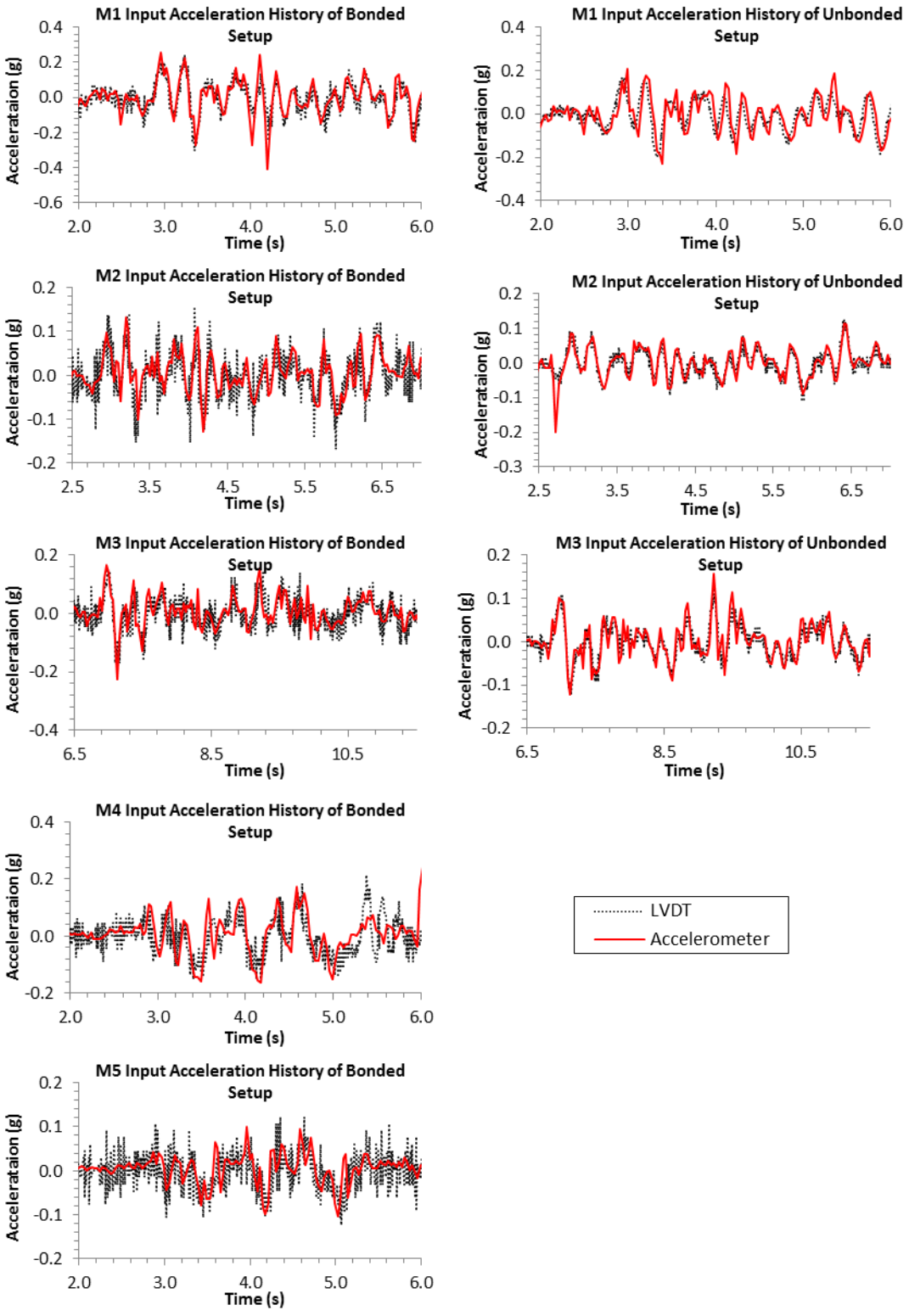


Figure 5.37: Comparison of input accelerations obtained from LVDT readings and accelerometers

### 5.7.1 BONDED SETUP

Seismic component of bearing axial forces and lateral displacement histories are presented in Figure 5.39 to Figure 5.41. Maximum and minimum values of seismic bearing axial forces and lateral displacement are presented on Table 5.10.

Table 5.10: Maximum and minimum values of seismic component of bearing axial forces and bearing shear deformations for bonded setup

| EQ | Axial Bearing Forces (kN) | | Lateral Bearing Displacements (mm) | |
|---|---|---|---|---|
| | Max | Min | | Max |
| M1 | 7.9 | -10.8 | 21.6 | -24.6 |
| M2 | 5.1 | -5.2 | 8.2 | -12.5 |
| M3 | 5.8 | -6.2 | 9.1 | -12.5 |
| M4 | 7.7 | -22.8 | 31.8 | -30.7 |
| M5 | 4.3 | -4.3 | 8.6 | -9.5 |

Maximum responses were obtained from M4 ground motion record. Bearings did not exhibit absolute uplift. Peak decrease and increase in bearing axial forces were 24% and 69% respectively. Maximum shear deformations were measured as 64%. No permanent lateral displacements of bearings or deck were observed, meaning restoring forces were able to recenter the deck after seismic loading. Maximum relative velocity of top of bearings with respect to bottom was 236 mm/s (≈14m/s).

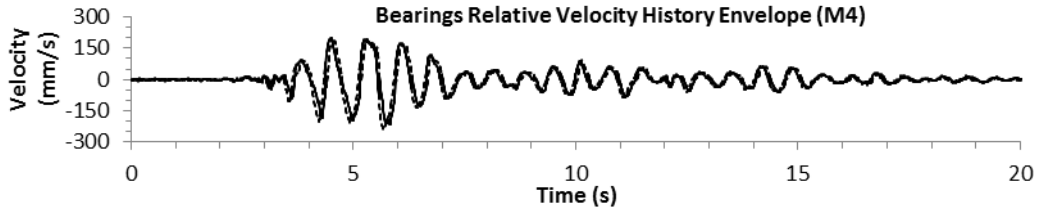


Figure 5.38: Measured bearing shear velocity history

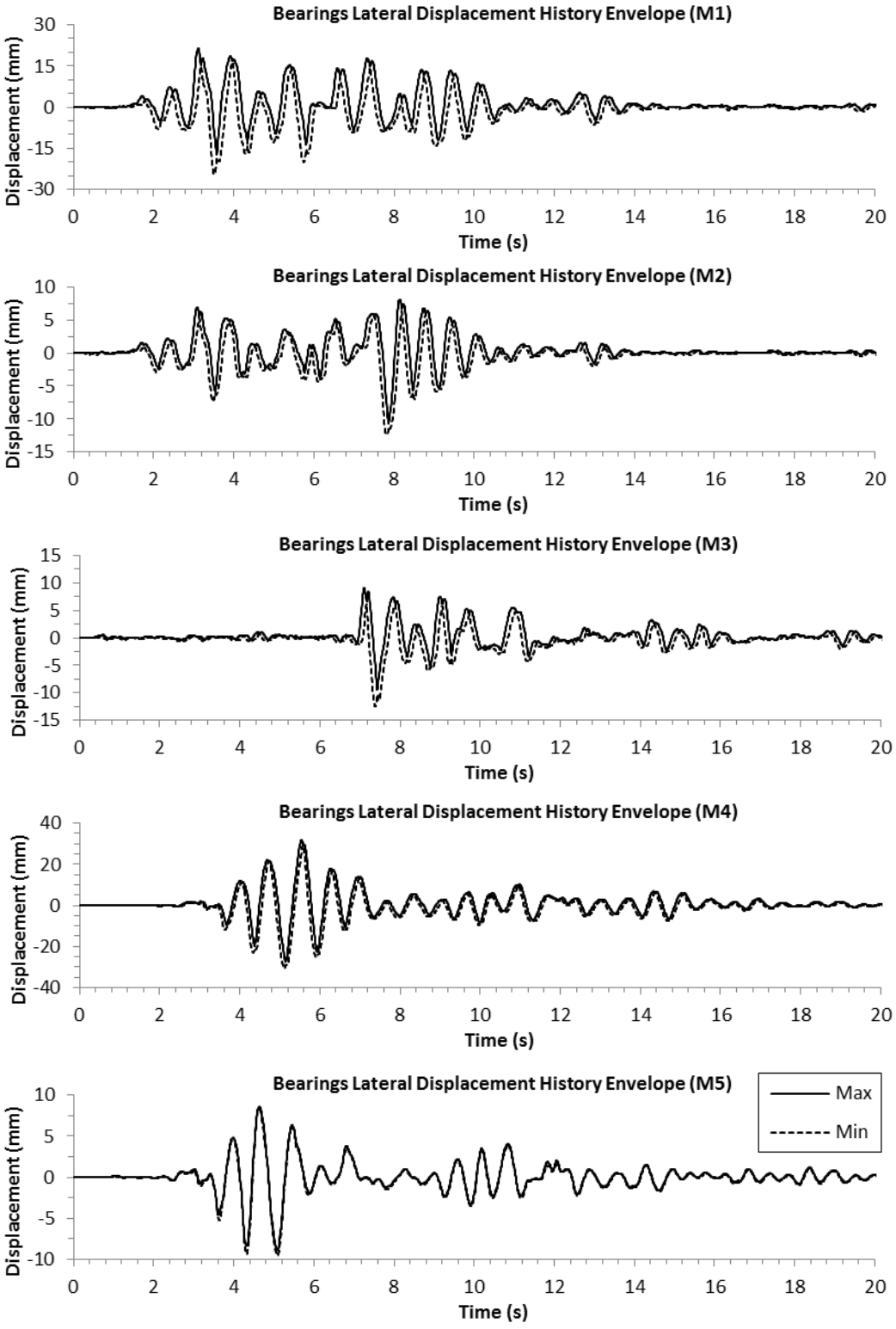


Figure 5.39: Envelopes of bearing shear deformations for bonded setup

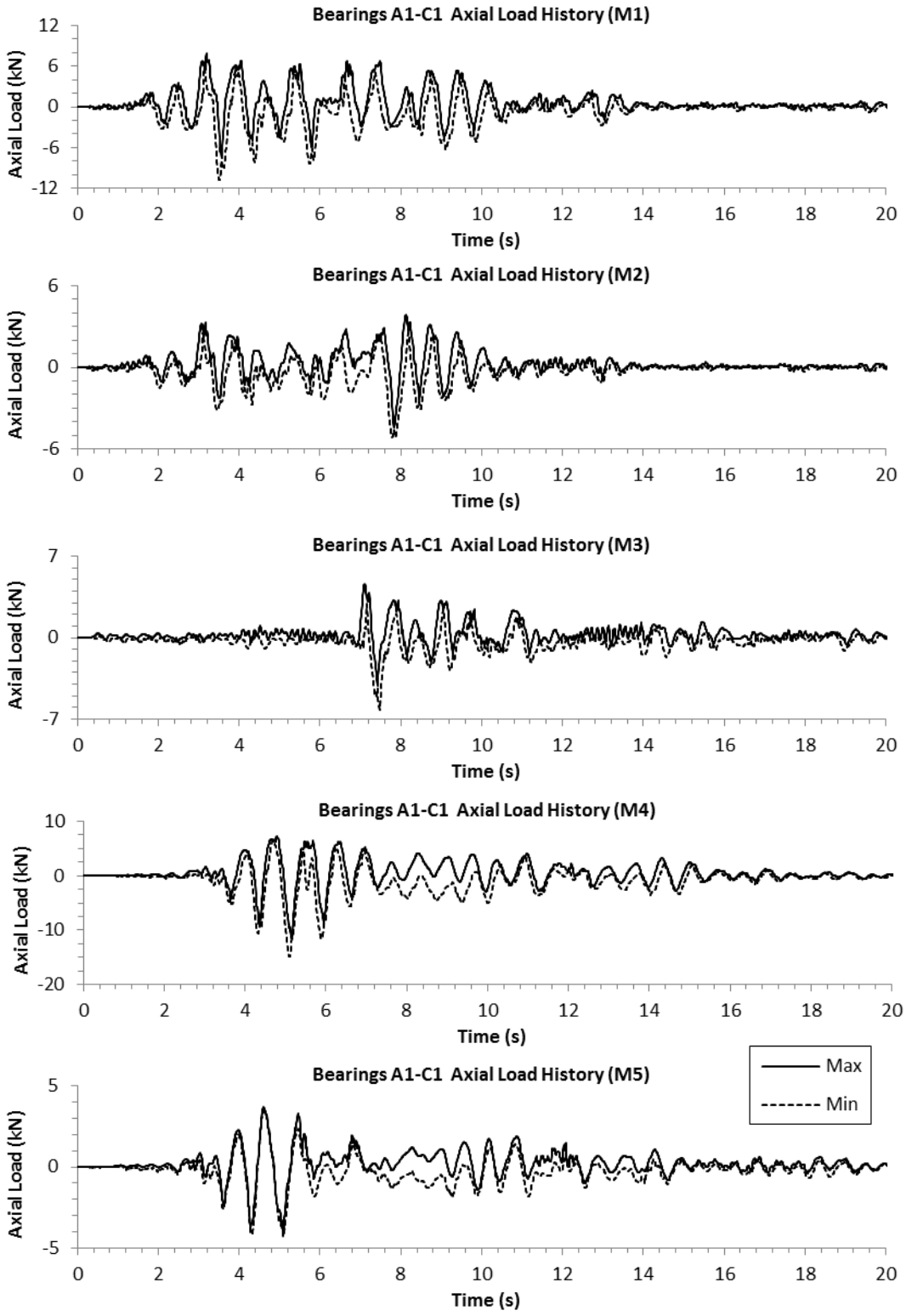


Figure 5.40: Envelopes of seismic axial loads for bearings A1-C1 for bonded setup

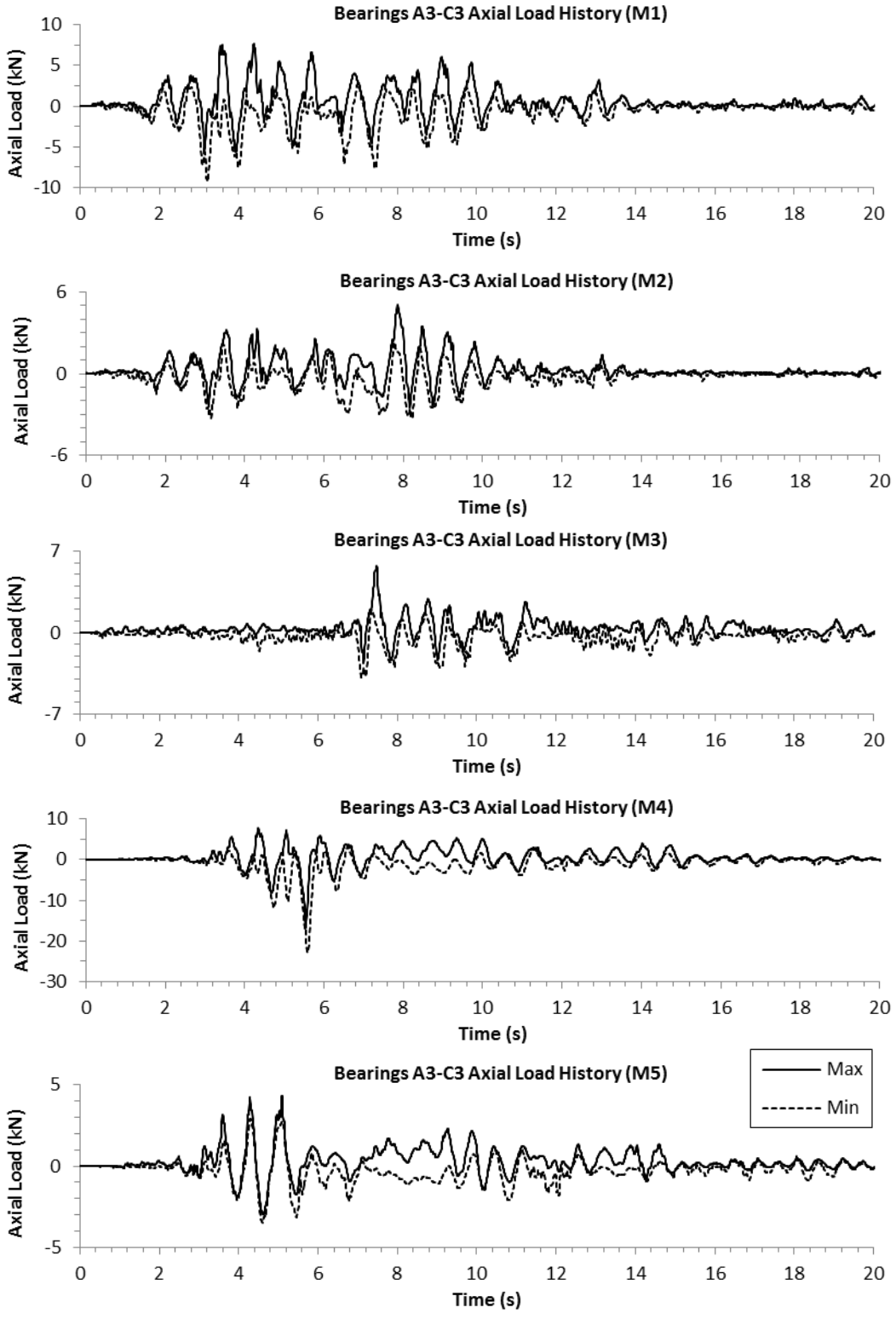


Figure 5.41: Envelopes of seismic axial loads for bearings A3-C3 for bonded setup

### 5.7.2 UNBONDED SETUP

Seismic component of bearing axial forces and lateral displacement histories are presented in Figure 5.43 to Figure 5.45. Maximum and minimum values of seismic bearing axial forces and lateral displacement are presented on Table 5.11.

Table 5.11: Maximum and minimum values of seismic component of bearing axial forces and bearing shear deformations for unbonded setup

| EQ | Axial Bearing Forces (kN) | | Lateral Bearing Displacements (mm) | |
|---|---|---|---|---|
| | Max | Min | Max | Min |
| M1 | 3.4 | -25.7 | 14.2 | -16.1 |
| M2 | 2.8 | -9.2 | 4.4 | -7.4 |
| M3 | 3.9 | -10.5 | 5.8 | -7.8 |
| M4 | 3.8 | -26.8 | 15.1 | -17.1 |
| M5 | 2.5 | -6.2 | 5.5 | -5.6 |

Maximum responses were obtained from M4 ground motion record. Bearings did not exhibit absolute uplift. Peak decrease and increase in bearing axial forces were 12% and 81% respectively. Maximum shear deformations were measured as 43%. No permanent lateral displacements of bearings or deck were observed, meaning zero to negligible slip occurred. Maximum relative velocity of top surface of bearings with respect to bottom was 172 mm/s (≈ 10m/s).

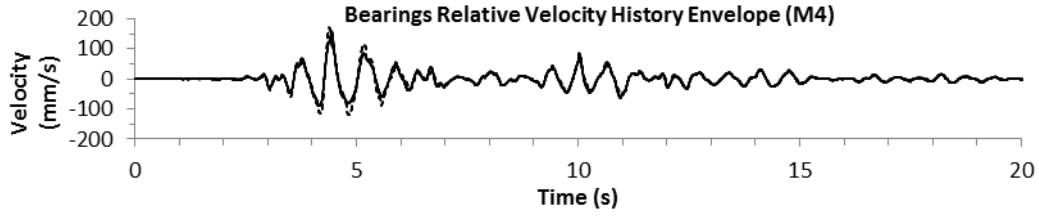


Figure 5.42: Measured bearing shear velocity history

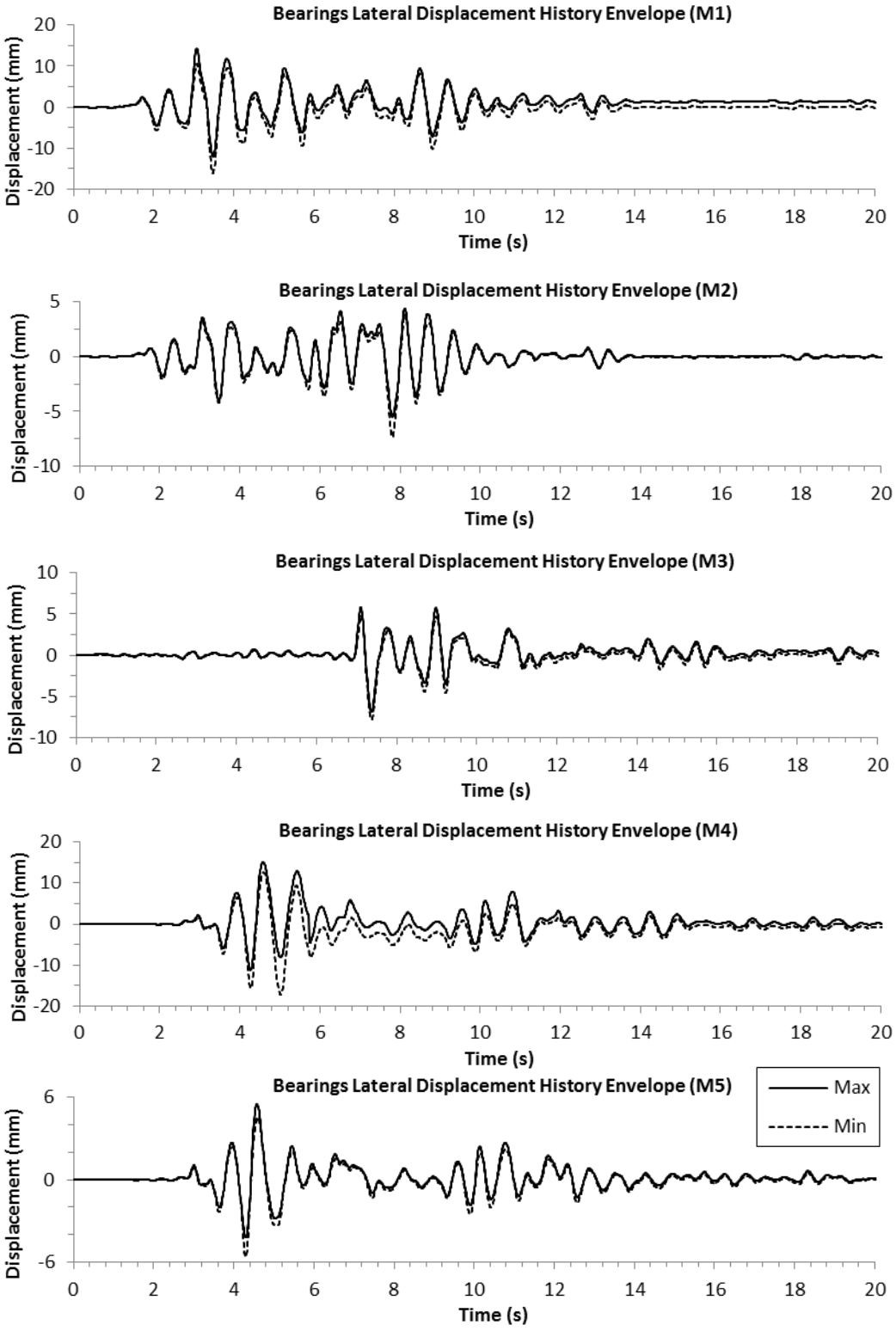


Figure 5.43: Envelopes of bearing shear deformations for unbonded setup

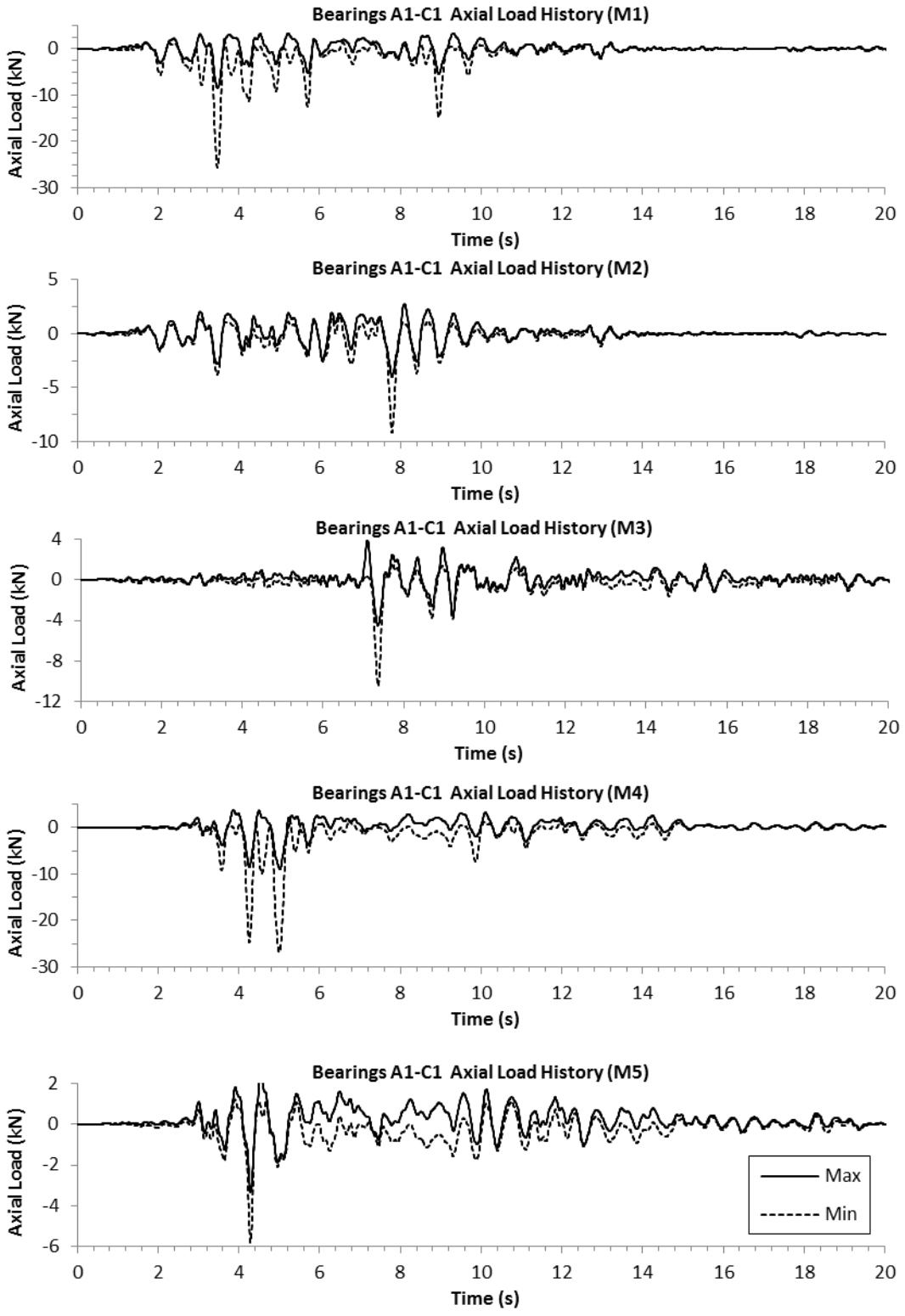


Figure 5.44: Envelopes of seismic axial loads for bearings A1-C1 for unbonded setup

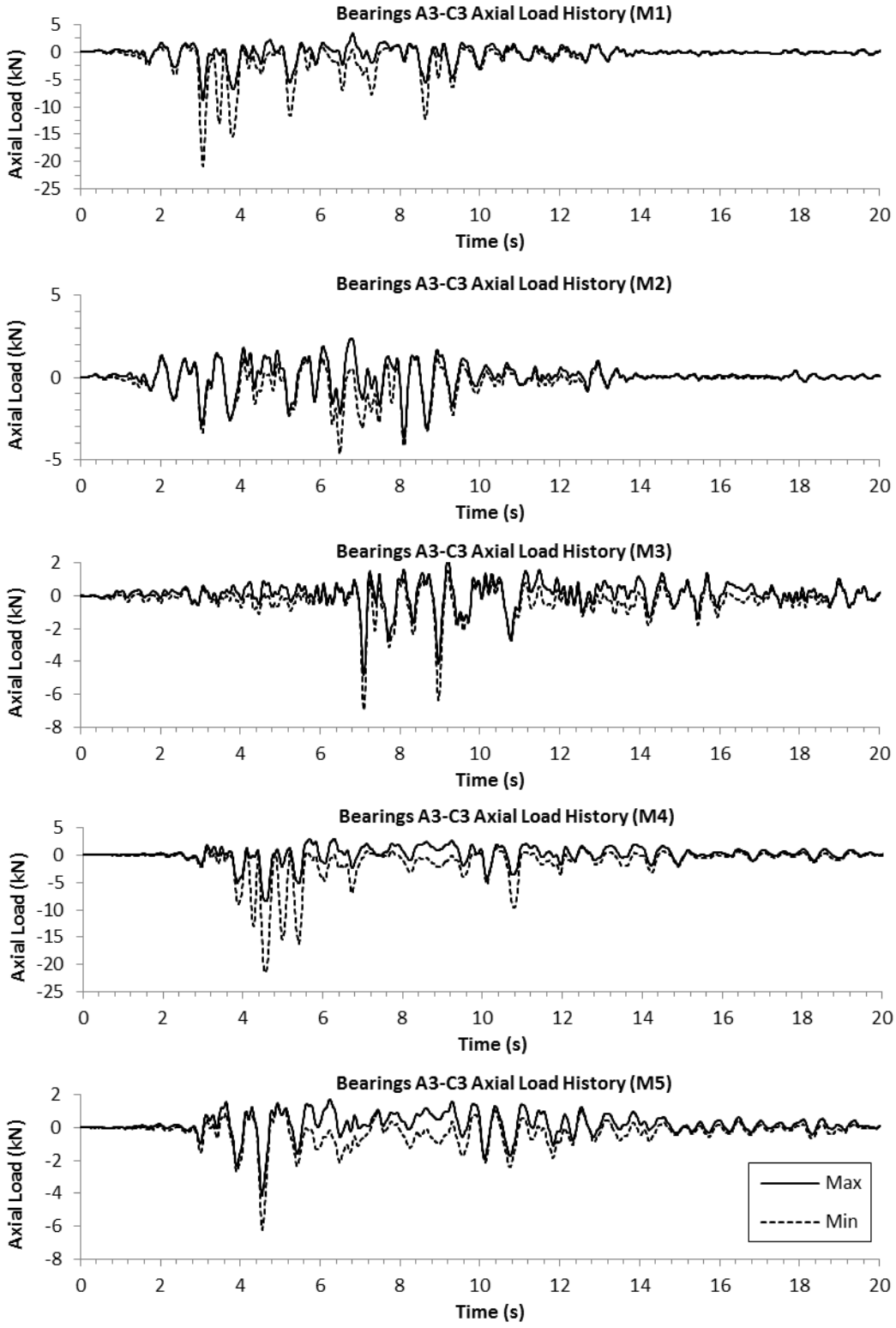


Figure 5.45: Envelopes of seismic axial loads for bearings A3-C3 for unbonded setup

### 5.7.3 COMPARISON WITH FEA RESULTS

CSI Bridge software is used for finite element analysis. Overview of the detailed 3-D finite element model (FEM) is shown in Figure 5.46.

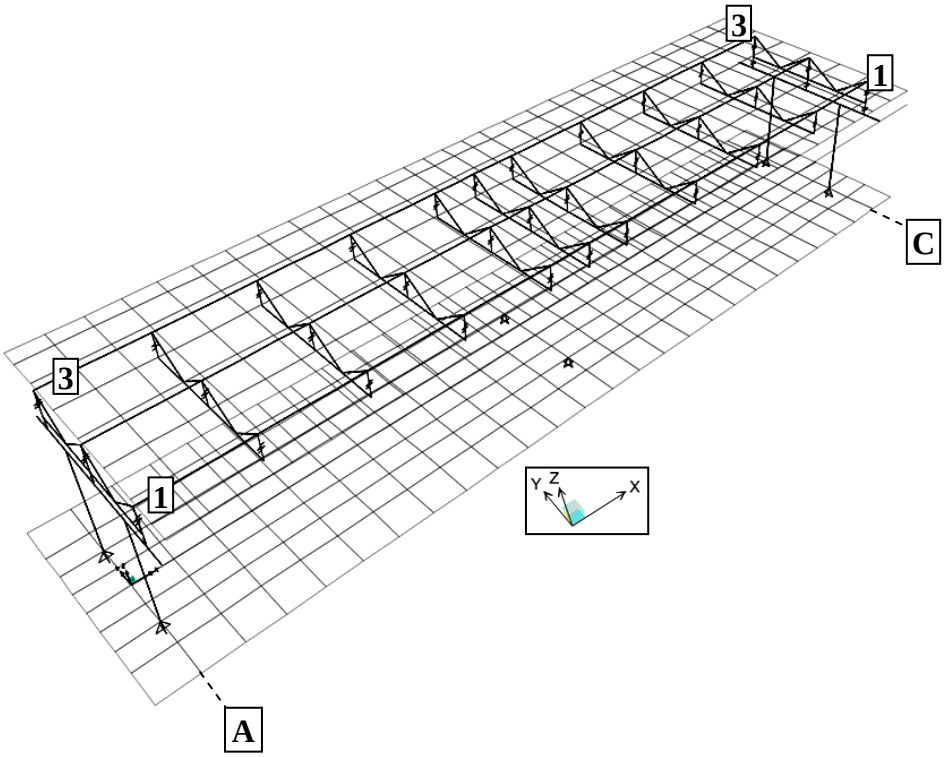


Figure 5.46: Overview of finite element model

To calibrate the model, vibrational characteristics of the bridge and actual bearing shear stiffness calculated in Sections 5.5.1 and 5.4.1 were used initially. Fundamental frequency of the bridge in lateral axis (Y) was calculated as 1.41Hz.

As explained in Section 5.1, test setup was able to exert excitation only in the lateral axis (Y) of the bridge. Considering the symmetry of the model around the same axis, a simplified FEA (finite element analysis) model in YZ plane was constructed (Figure 5.47).

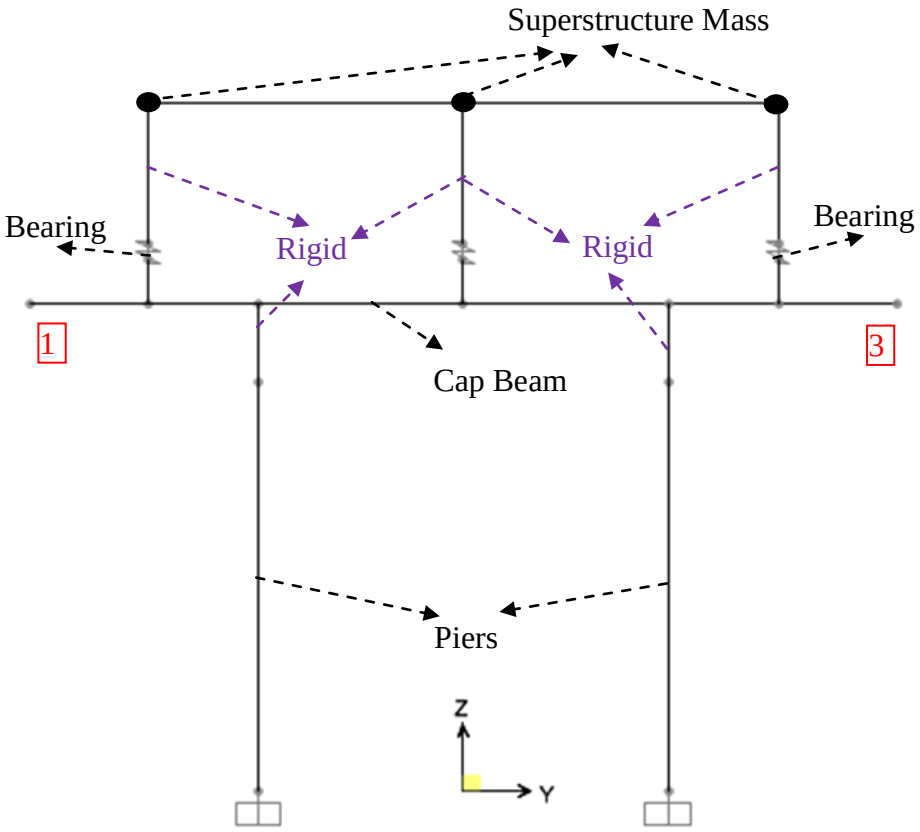


Figure 5.47: Representation of simplified FEA model

Fundamental frequency of the simplified model was calculated as 1.48Hz being in conformity with the detailed FEA model.

Experimentally determined bearing properties (Sections 5.4.1 to 5.4.3) are summarized on Table 5.12.

Table 5.12: Results of bearing tests

| **Bearing Type** | $K_{eff}$ **(kN/m)** | $\beta$ **(%)** |
|---|---|---|
| Type-1 | 304 | 6.9 |
| Type-2 | 405 | 8.1 |
| Type-3 | 424 | 10.2 |

Experimentally calculated fundamental frequency ranges and equivalent viscous damping ratios of the bridge with bonded and unbonded bearings (Sections 5.5.1 and 5.5.2) are presented on Table 5.13.

Table 5.13: Results of harmonic load tests

| **Bridge Setup** | **Fundamental Frequency (Hz)** | $\boldsymbol{\beta_{system}}$ **(%)** |
|---|---|---|
| Bonded | 1.40-1.60 | 10.0 |
| Unbonded | 1.40-1.72 | 10.0 |

As nonlinear time-history analyses were to be performed using varying coefficient of friction between bearings and structure, Rayleigh Damping coefficients had to be used. Values were selected to make the average damping ratio equal to 10% between frequency values of 0.50 – 2.00Hz (Figure 5.48).

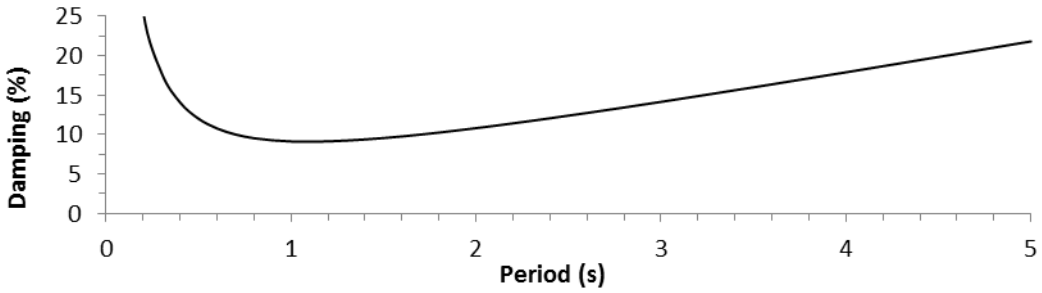


Figure 5.48: Selected Rayleigh damping coefficients

Experimental bearing stiffness values were used without any modification to adjust fundamental frequency of the FEA models, since they are the most directly measured parameters to describe stiffness of the structure.

Fundamental frequencies of prepared FEA models are presented on Table 5.14. Results were in conformity with those obtained from experimental studies.

Table 5.14: Fundamental frequencies of FEA models

| FEA Model | Fundamental Frequency (Hz) |
|---|---|
| Bonded | 1.48 |
| Unbonded | 1.61 |

Comparison of experimental data and FEA results of the bonded setup for M1 and M4 loading are presented in Figures 5.52 and 5.53. Although bearing displacement histories were in good agreement, greater compressive bearing forces had been observed in shake table tests.

Comparison of experimental data and FEA results for the unbonded setup also indicated similar results (Figures 5.54 and 5.55). Compressive bearing forces measured during shake table tests were greater than the results of FEA. Bearing shear deformations showed reasonable agreement.

FEA also showed that absolute uplift of bearings did not occurred, i.e. seismic tensile loads on bearings did not exceed dead loads acting on bearings (≈ 33kN).

FEA of unbonded setup using various friction coefficients (frictional bearing element is explained in Section 6.4) indicated that, significant slip began to occur when a friction coefficient of 0.2 was used (Figure 5.51). A simplified formulation can be derived to calculate necessary lateral pseudo acceleration that must act on the deck to initiate bearing slip as follows:

$$F_L/6 > \mu.(F_D - F_1) \tag{5.12}$$

where;

$F_L$ : Lateral inertial force acting on superstructure (Figure 5.49)

$F_D$ : Dead load on bearings = 33kN

$F_1$ : Seismic uplift force on bearings (Figure 5.49)

$\mu$ : Friction coefficient between bearings and girders

Recalling Equation (2.6) and arranging for two piers;

$$F_1 = F_L.H/(4.d) \quad (5.13)$$

where;

H : Center of mass of deck measured from bottom (Figure 5.49) = 0.45

d : Transverse spacing of bearings (Figure 5.52) = 1.00

Substituting Equation (5.13) into (5.12) gives;

$$F_L > 6.\mu.[F_D - F_L.H/(4.d)] \quad (5.14)$$

⇨ $F_L > 200.\mu.(1 + 0.675.\mu)$

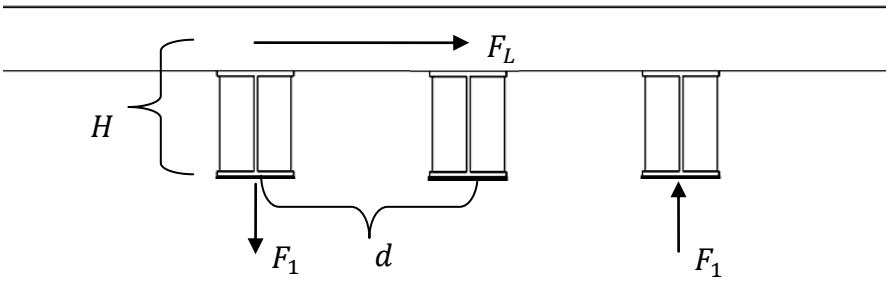


Figure 5.49: Bearing uplift forces in test bridge setup due to transverse excitations

Recalling total weight of the deck is 200kN, required deck pseudo acceleration will be $A_d = F_L/200$. Solution of Equation (5.14) for different values of friction coefficient is presented on Table 5.15. M1 and M4 records were severe enough to initiate slipping when friction coefficient is equal to 0.30 or lower (Figure 5.50).

Table 5.15: Required deck pseudo accelerations to initiate bearing slipping

| $\mu$ | $F_L$ (kN) | $A_d\ (g)$ |
|---|---|---|
| 0.20 | 35.2 | 0.176 |
| 0.30 | 49.9 | 0.249 |
| 0.50 | 74.8 | 0.374 |
| 0.75 | 99.6 | 0.498 |
| 1.00 | 119.4 | 0.597 |

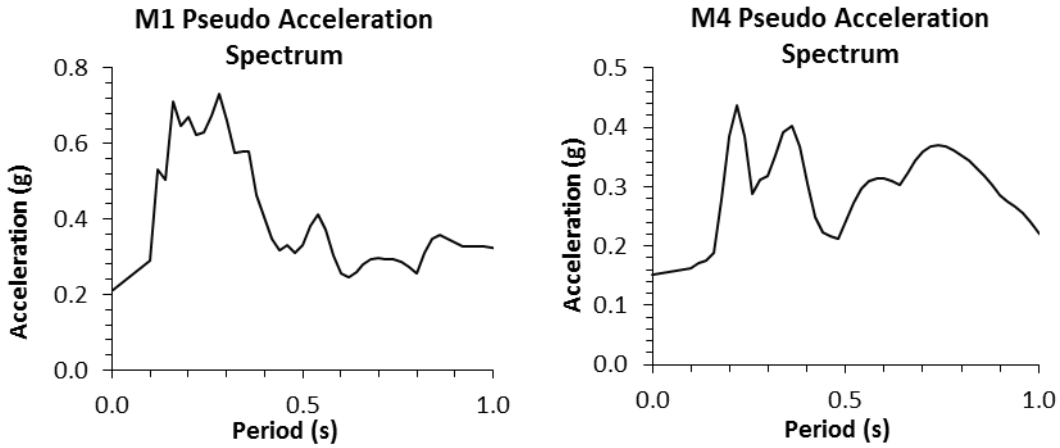


Figure 5.50: Response spectrum of M1 and M4 records

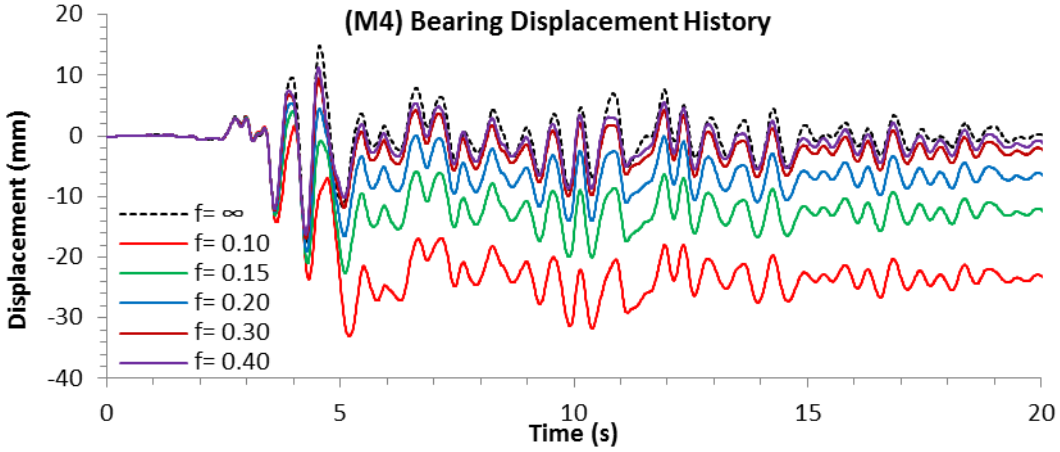


Figure 5.51: Bearing displacements for various friction coefficients under M4 ground motion record

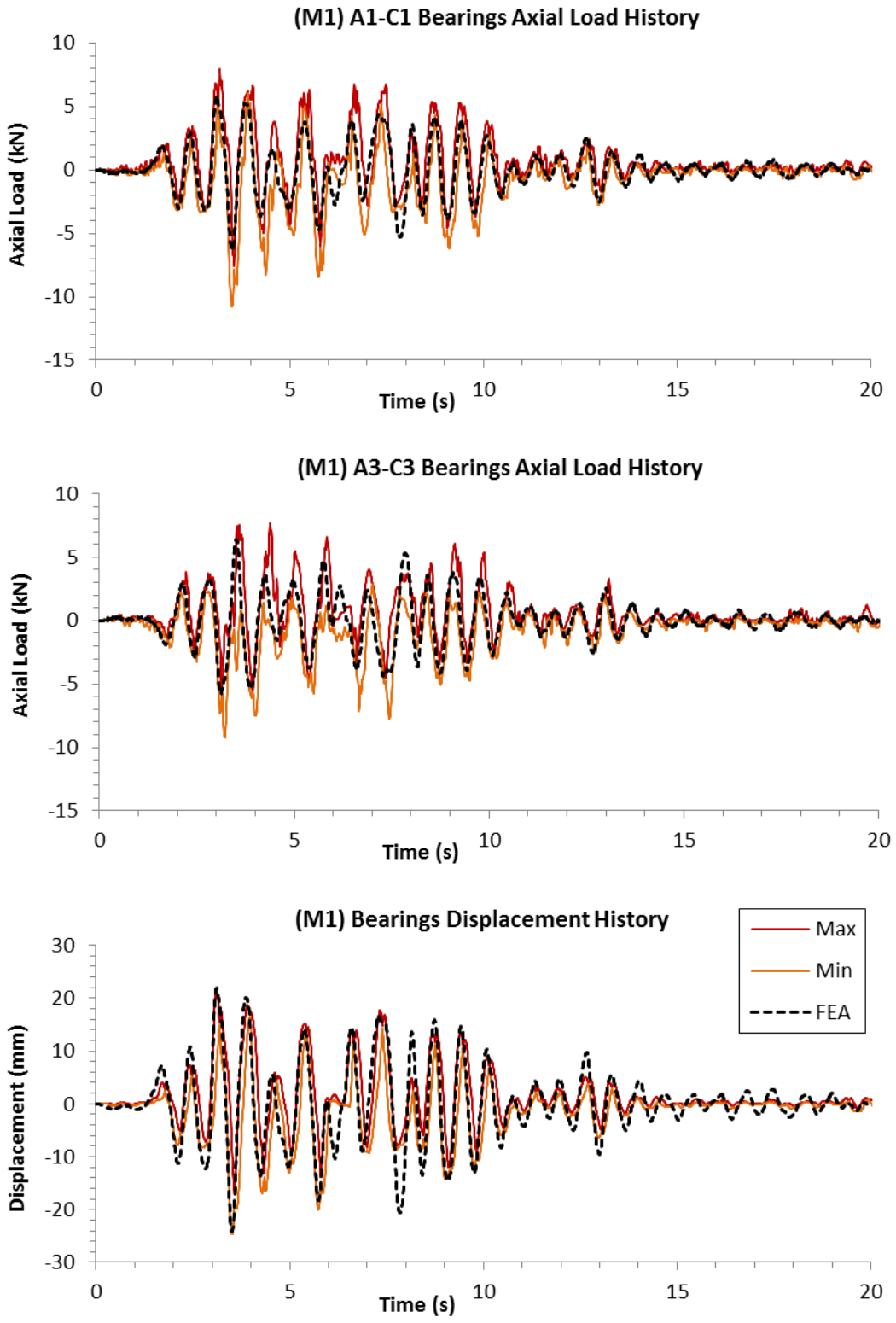


Figure 5.52: Comparison of experimental data and FEA results for bonded setup under M1 loading

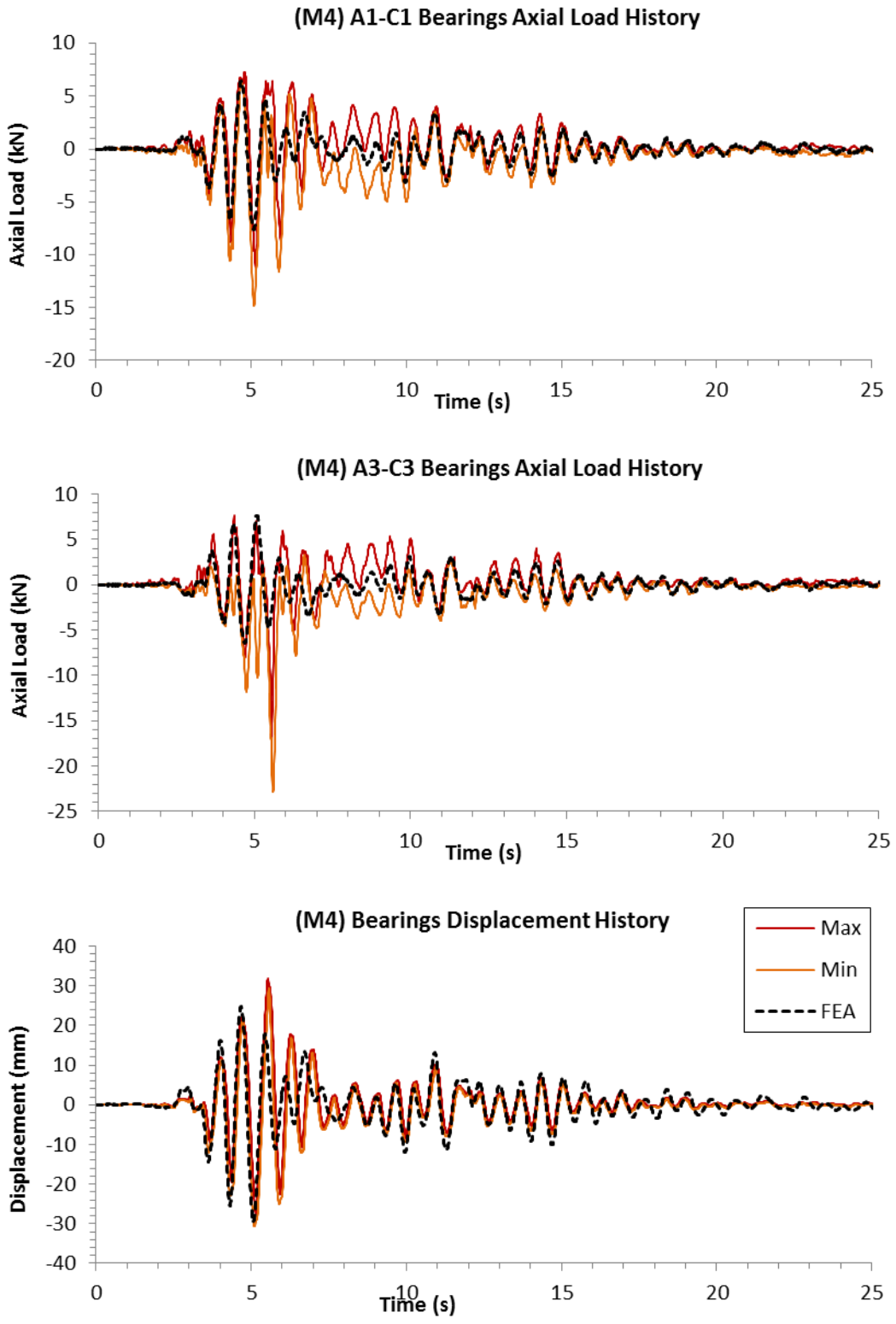


Figure 5.53: Comparison of experimental data and FEA results for bonded setup under M4 loading

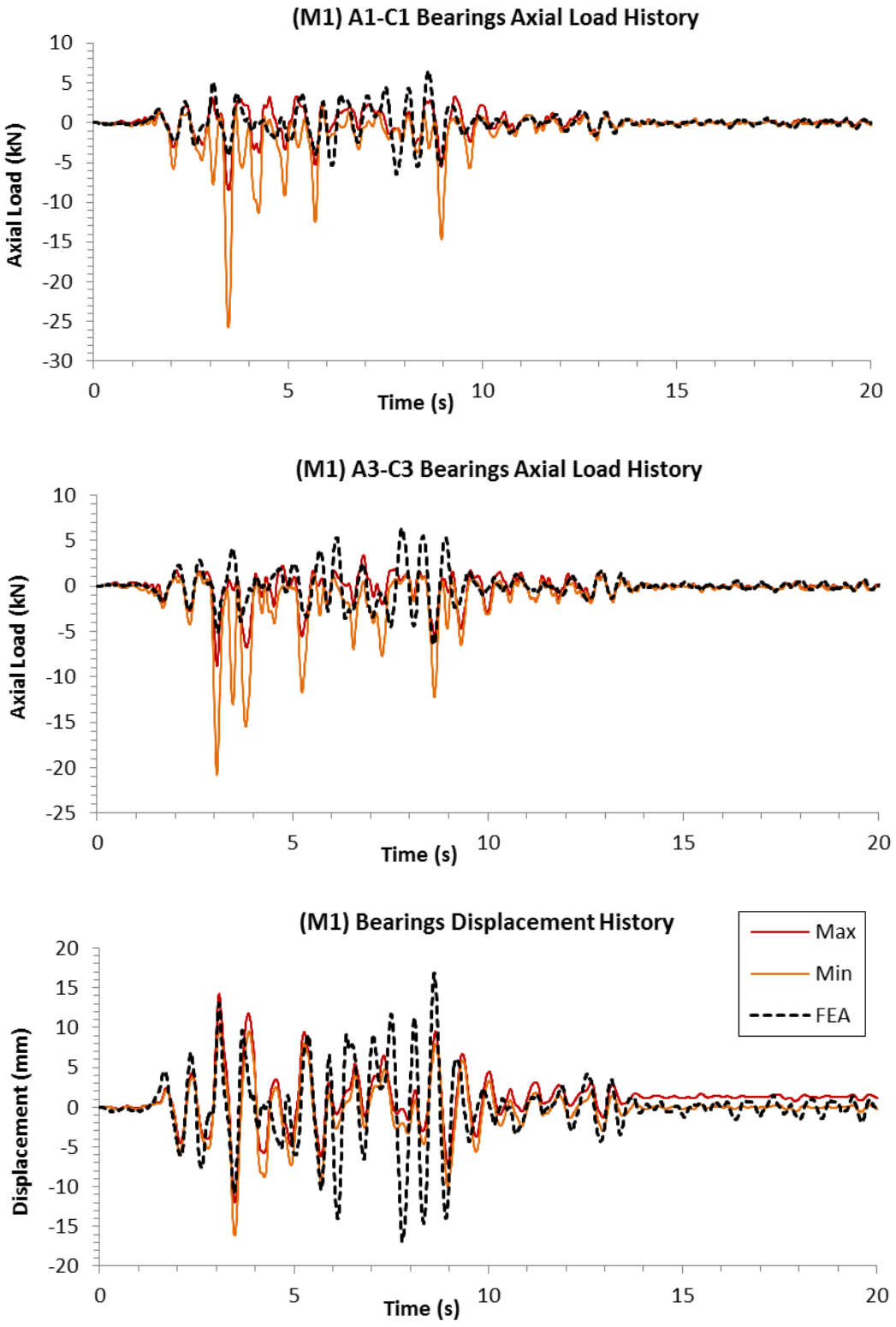


Figure 5.54: Comparison of experimental data and FEA results for unbonded setup under M1 loading

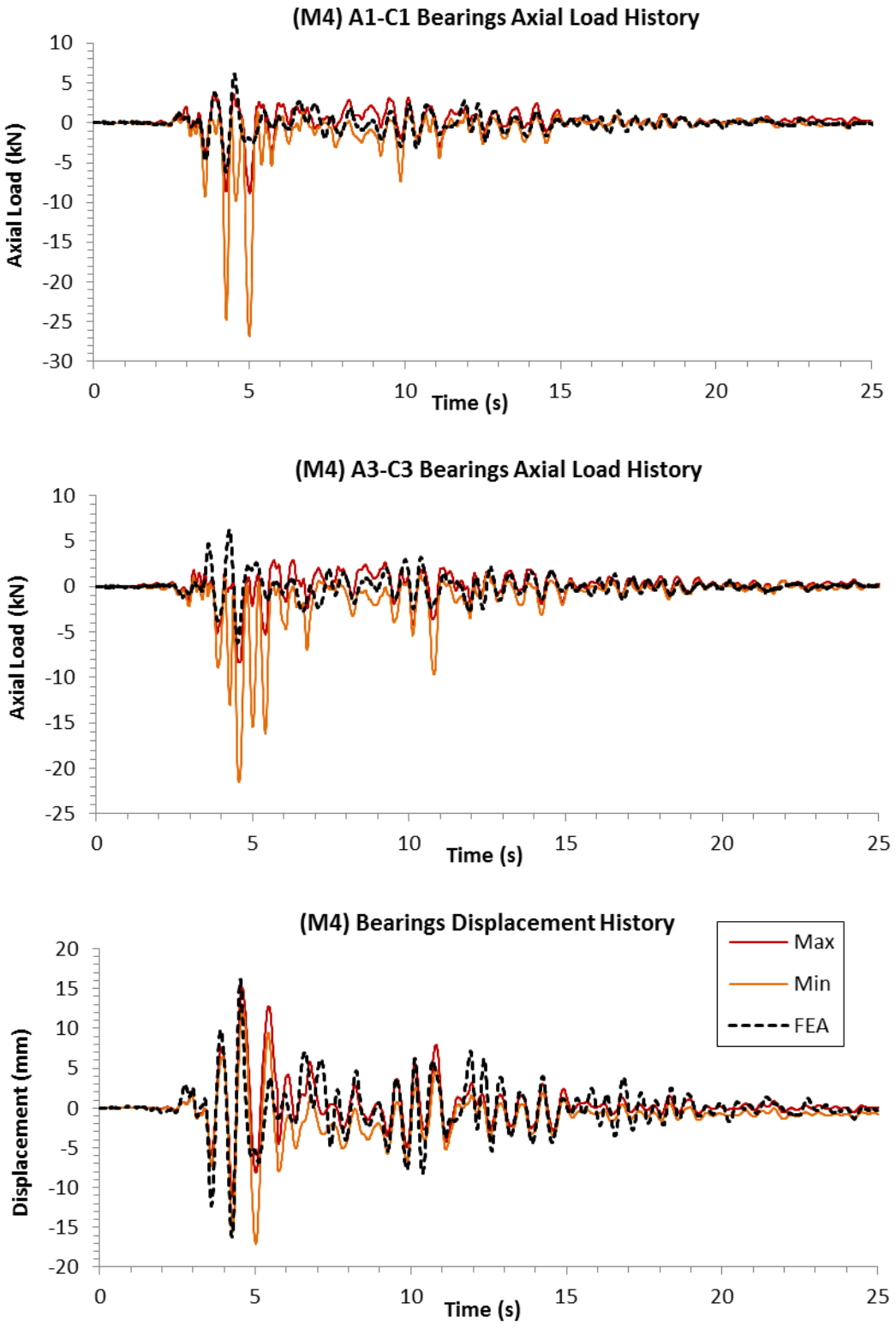


Figure 5.55: Comparison of experimental data and FEA results for unbonded setup under M4 loading

# CHAPTER 6

# PARAMETRIC STUDIES

## 6.1 EXPLANATION

Results of experimental studies and FEA performed through this thesis indicated that friction coefficient between bearings and steel girders increased significantly in proportion with the loading rate (Section 5.4.4) and bearings did not slip during seismic loading (Section 5.7.2). However, if coefficient of friction was assumed to be 0.20, significant slipping began to initiate according to FEA (Section 5.7.3).

In this parametric study, seismic behavior of a one span bridge utilizing unbonded elastomeric bearings was examined by carrying out approximately 800 nonlinear time history analyses and the dependence of seismic displacement demands and uplift forces on bearings to the following parameters was investigated:

- Friction coefficient between bearings and substructure/superstructure: It defines the resistance of an unbonded bearing to slip during seismic loading. Investigated values are $\mu$=0.05, 0.10, 0.15, 0.20, 0.25, 0.30, 0.40, 0.50, 0.75 and 1.00.
- Coefficient of acceleration, Cs, per AASHTO: Seismic loads acting on the deck are directly proportional to acceleration coefficient. Investigated values are A=0.10, 0.20, 0.30 and 0.40.
- Skew angle of the bridge: Investigated values are S=0°, 10°, 20°, 30°, 40°, 50° and 60°.

- Height-to-width ratio of the deck: Recalling explanations presented in Section 2.2 and derivation of Equation (2.5) regarding uplift forces, it is concluded to include this parameter in this parametric study. Investigated values are h/w=0.125, 0.25, 0.50, 0.75 and 1.00.
- Fundamental frequency of the bridge: Fundamental frequency of the bridge was adjusted by changing shear stiffness of bearings accordingly. Investigated values are f=0.607, 0.854, 1.196, 1.658 and 2.262.

## 6.2 CONSTRUCTION AND APPLICATION OF SPECTRUM COMPATIBLE RECORDS

9 set of spectrum compatible earthquake records were prepared to be able to include the coefficient of acceleration per AASHTO as a parameter in the study, as majority of the bridges are designed using response spectrum provided by the same specification without carrying out any local site specific study.

Records S1 to S6 were constructed by modifying the frequency content of actual ground motion records and each have three separate orthogonal components. Records S7, S8 and S9 were generated artificially and have one component.

Four design response spectra were constructed for coefficient of acceleration ($A$) values of 0.1, 0.2, 0.3 and 0.4 (Figure 6.1) using Equations (4.1) and (4.2), which is repeated here for convenience;

$$C_s = \frac{1.2 * A * S}{T^{2/3}} \tag{4.1}$$

where;

$A$ = Acceleration coefficient
$S$ = Soil site coefficient
$T$ = Period

and $C_s$ need not exceed $2.5A$. For soil profiles III or IV where $A \geq 0.30$, $C_s \leq 2.0A$. Where $T$ exceeds 4.0s;

$$C_s = \frac{3*A*S}{T^{4/3}} \tag{4.2}$$

Table 6.1: Summary of spectrum compatible ground motion records

| # | Earthquake Name and Date | Mw | Station | Epicentral Distance (km) | Scale Factor |
|---|---|---|---|---|---|
| S1 | 17. 08. 1999 Kocaeli | 7.4 | Gebze | 7.74 | Spectrum Compatible |
| S2 | 12.11.1999 Düzce | 7.2 | Düzce | 8.30 | Spectrum Compatible |
| S3 | 17. 08. 1999 Kocaeli | 7.4 | Düzce | 17.06 | Spectrum Compatible |
| S4 | 17. 08. 1999 Kocaeli | 7.4 | Yarımca | 4.80 | Spectrum Compatible |
| S5 | 01.15.1995 Kobe | 7.3 | Nishi-Akashi | 8.00 | Spectrum Compatible |
| S6 | 06.28.1966 Parkfield | 6.2 | Cholame #5 | 12.60 | Spectrum Compatible |
| S7 | Synthetic | N/A | N/A | N/A | Spectrum Compatible |
| S8 | Synthetic | N/A | N/A | N/A | Spectrum Compatible |
| S9 | Synthetic | N/A | N/A | N/A | Spectrum Compatible |

For all case studies, soil profile was assumed to be of type I (rock site) to eliminate the complexity of soil-structure interaction.

Vertical excitation was applied simultaneously with the horizontal components. Vertical response spectrum was assumed to be 2/3 of the horizontal one.

A freeware program named “RSCA”, released under GNU public license by Thiele M. [39] and modified by the author, was used to modify and generate acceleration records. Algorithms implemented in the software and modifications done were explained in the author’s M.Sc. thesis [21].

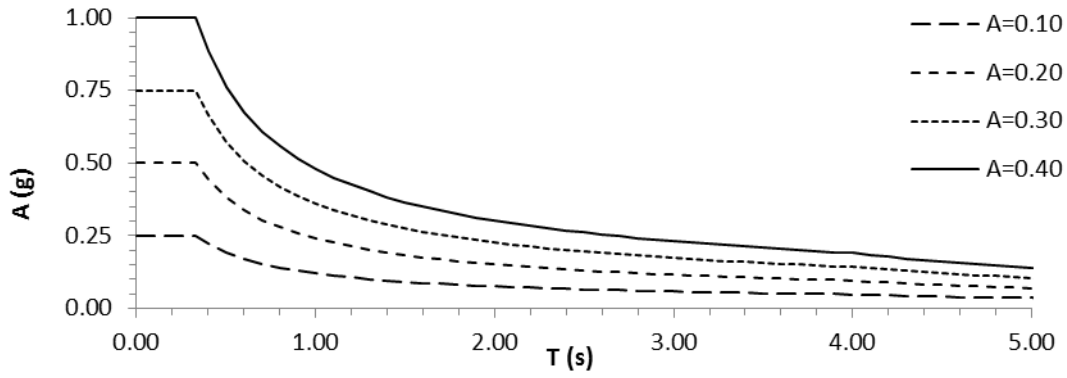


Figure 6.1: Design Response Spectra per AASHTO [2 and 3]

## 6.3 FEA MODELING

CSI Bridge software was used for finite element analysis. Simplified model explained in Section 5.7.3 was extended to 3D in order to represent the investigated skew angles (Figure 6.2). Structural properties of the bridge test setup were used.

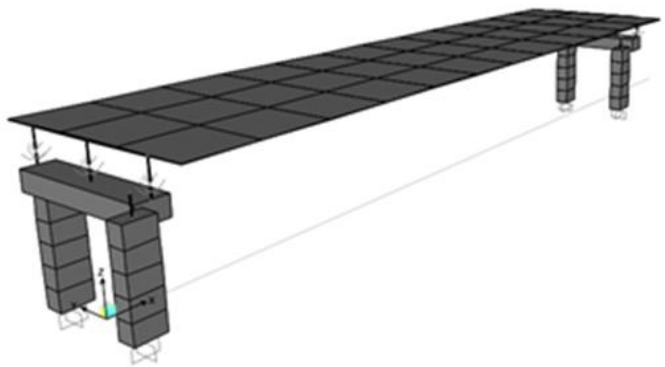

Figure 6.2: FEA model used in the parametric study

## 6.4 BEARING ELEMENT FORMULATION FOR FRICTION MODELING

CSI Bridge software includes a friction pendulum element, of which parameter ranges are flexible enough to model friction on flat surfaces. Simplifying the formulation by assuming unidirectional shear behavior, shear force in the element becomes [20];

$$f_u = f_{uf} + f_{up} \tag{6.1}$$

where friction component is;

$$f_{uf} = -P\mu z \tag{6.2}$$

where $\mu$ is the coefficient of friction and $z$ is called internal hysteretic variable. Friction coefficient is calculated as;

$$\mu = fast - (fast - slow)e^{-rv} \tag{6.3}$$

where $slow$ is the static friction coefficient at zero velocity, $fast$ is the dynamic friction coefficient at fast velocities and v is the velocity of sliding. Formulation of the effective inverse velocity parameter, $r$, is given by;

$$r = rate \tag{6.4}$$

which is inverse of characteristic sliding velocity. The pendulum contribution to the shear force is;

$$f_{up} = -P\frac{d_u}{radius} \tag{6.5}$$

where $P$ is the compressive force on the bearing.

By equating $rate$ to zero, $radius$ to infinity, $slow$ to the desired friction coefficient value and solving related equations, equation (6.1) simply becomes;

$$f_u = P.slow.\text{z} \tag{6.6}$$

making pendulum part equal to zero.

Detailed explanation of hysteretic variable z and solution for two shear degree of freedoms can be found in the analysis manual [20] of the software.

A verification of the bearing element was conducted by comparing the results of the two different hysteretic loading applied to ADINA frictional contact model (explained in Section 3.3) and CSI Bridge model.

In the first set of verification analyses, a lateral displacement was applied using the loading vs time function presented on Figure 6.3. Friction coefficient is set to 0.3 and a constant compressive load of 33kN was applied to bearing.

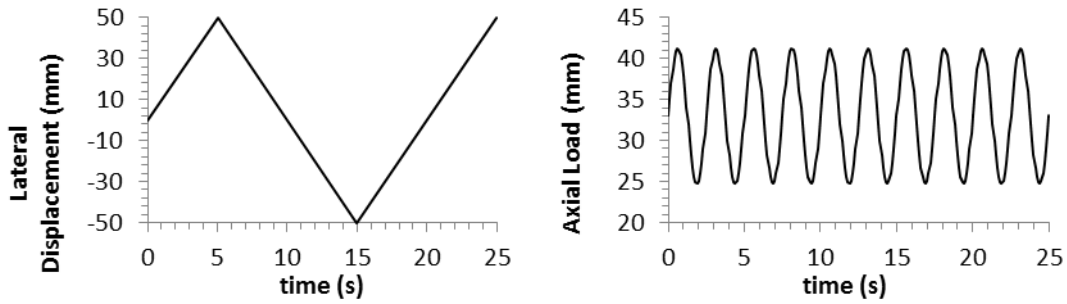


Figure 6.3: Load vs time function for the applied lateral displacement and axial forces to bearings

Results indicated hysteresis loops and frictional damping values obtained from ADINA and CSI BRIDGE analyses were in reasonable agreement (Figure 6.4).

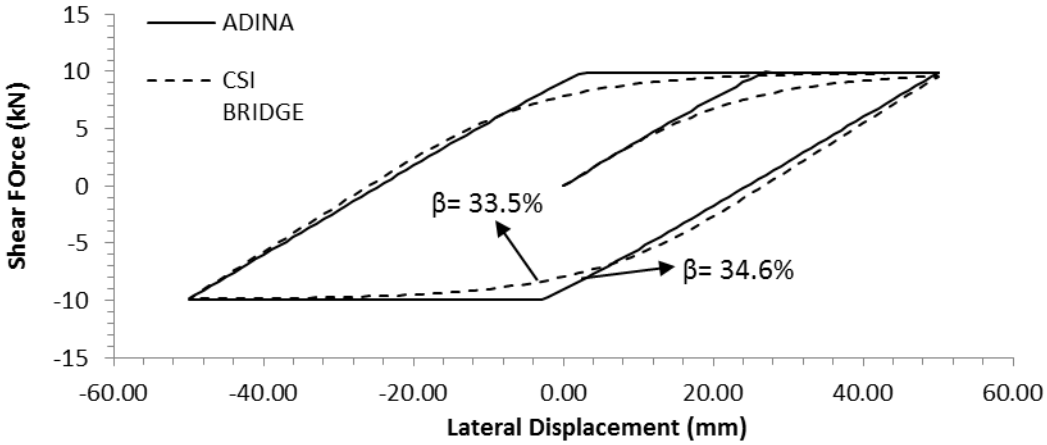


Figure 6.4: Comparison of results of ADINA and CSI Bridge analyses

In the second set of verification analyses, a variation to axial bearing forces was introduced by applying a sin function. Compressive force vs time graph is presented on Figure 6.3. Same lateral displacement function from the first loading was used and results are shown on Figure 6.5.

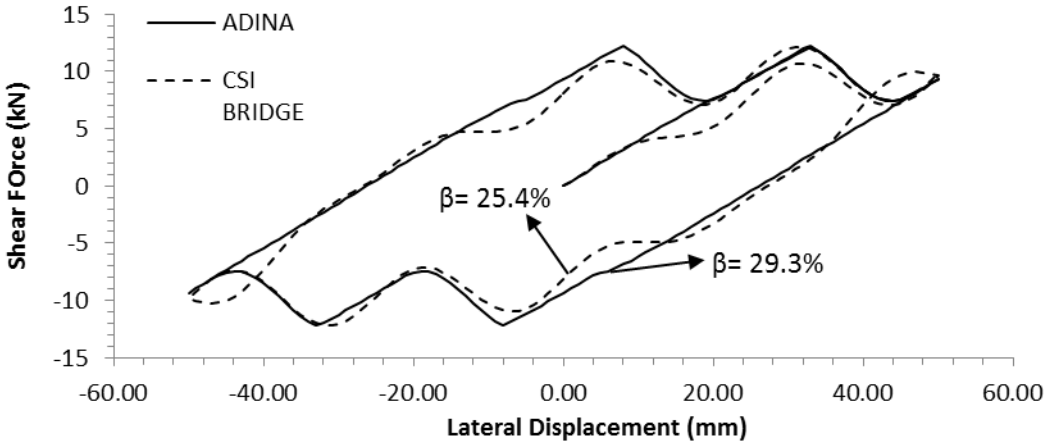


Figure 6.5: Comparison of results of ADINA and CSI Bridge analyses

Results again indicated hysteresis loops obtained from ADINA and CSI BRIDGE have a reasonable match. The deviation at the corners occurred due to the hysteretic variable (z) present in the element model of CSI Bridge.

This refined model provided a smoother behavior than Coulomb friction model used in ADINA. Calculated damping values were within ±15% of each other (Figure 6.5).

## 6.5 RESULTS OF FEA

Results of the parametric study are explained in this section for each parameter investiaged.

### 6.5.1 EFFECT OF FRICTION COEFFICIENT

Longitudinal, lateral and resultant deck displacement histories over bearing A1 (relative to top of piers) for various friction coefficient values and seismic acceleration coefficients are given on Figure 6.10 to Figure 6.21.

Results indicated that deck displacements increased rapidly when coefficient of friction is smaller than a particular value. For all seismic coefficient magnitudes, this critical value was observed to be between 0.15-0.30 (Figure 6.6).

Normalized resultant deck displacements with respect to the response obtained using linear bearing elements for the same system without any friction interface are plotted on Figure 6.8. For low seismic hazard ($A = 0.10$), no significant amplification of deck displacements was observed provided that friction coefficient is greater than 0.20. For higher seismic loadings, deck displacements were stable in the friction coefficient range of 0.30-0.60, increasing outside the range.

Maximum amount of slipping in bearings and maximum seismic uplift forces are presented in Figures 6.7 and 6.8 respectively. Although a decrease in seismic uplift force occurred where friction coefficient is approximately 0.10, magnitude of uplift was not observed to be highly dependent to friction coefficient values greater than 0.30.

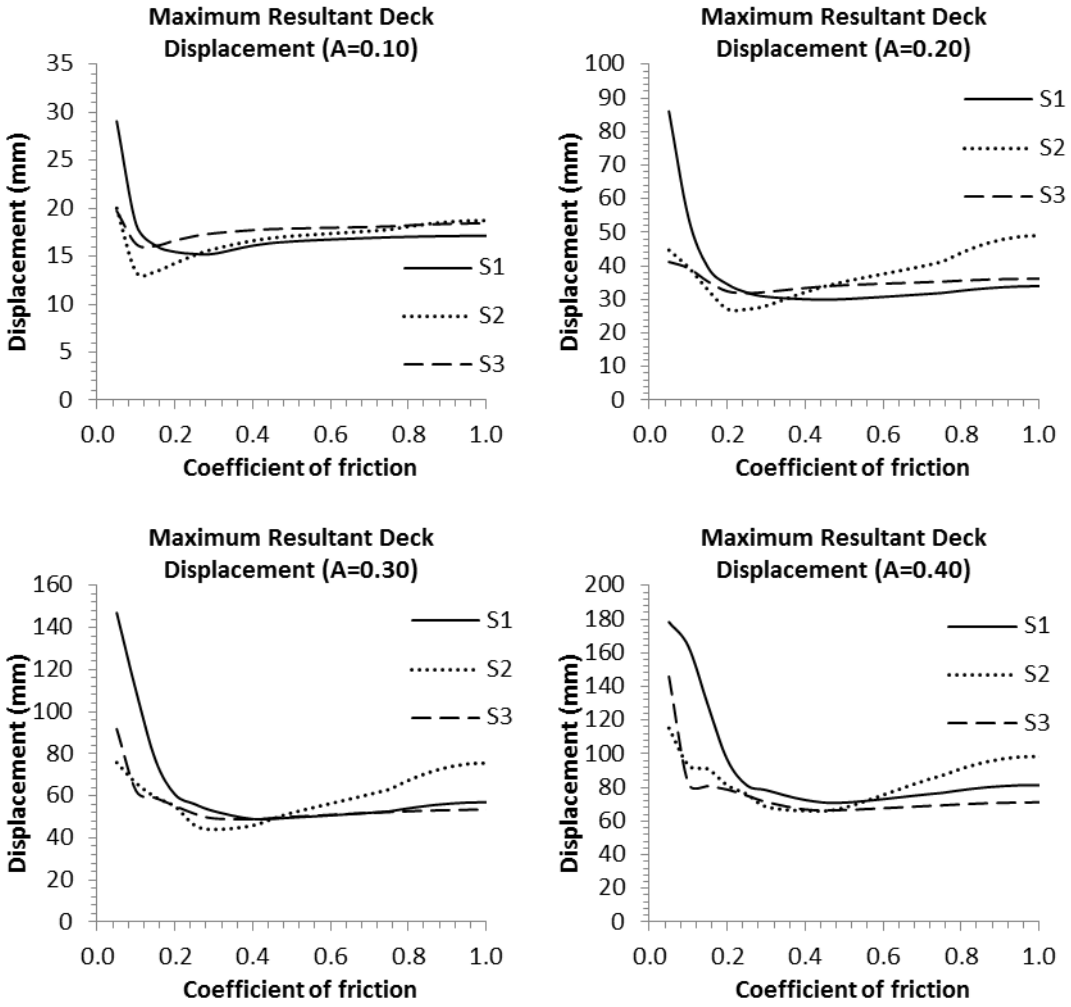


Figure 6.6: Maximum resultant deck displacements as a function of friction coefficient

Maximum slip did not seem to have a systematic behavior as a function of friction coefficient. In some cases, amount of slip even increased with coefficient of friction. Recalling that shear resistance of an unbonded bearing is a function of axial force acting on the bearings, this highly nonlinear behavior is difficult to be expressed by simple formulations. Such an irregular shear behavior can be observed from hysteresis loop of a bearing calculated from seismic analysis with a friction coefficient of 0.75 and $A = 0.40$ (Figure 6.9).

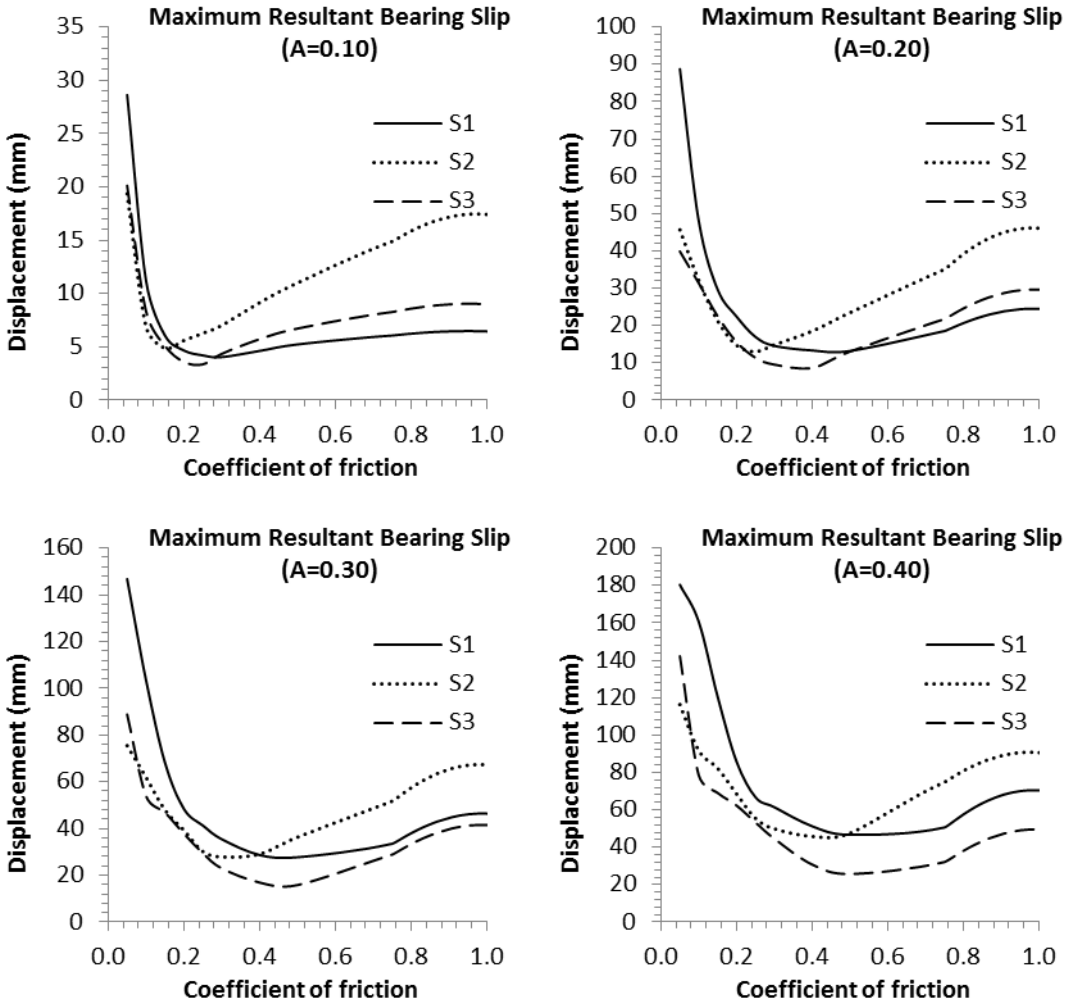


Figure 6.7: Maximum bearing slip as a function of friction coefficient

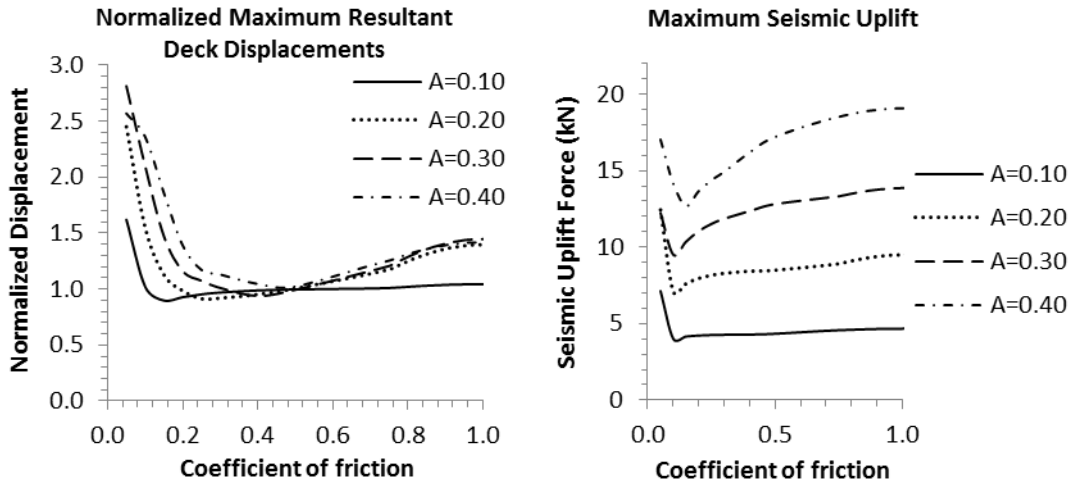


Figure 6.8: Normalized maximum relative deck displacements as a function of friction coefficient

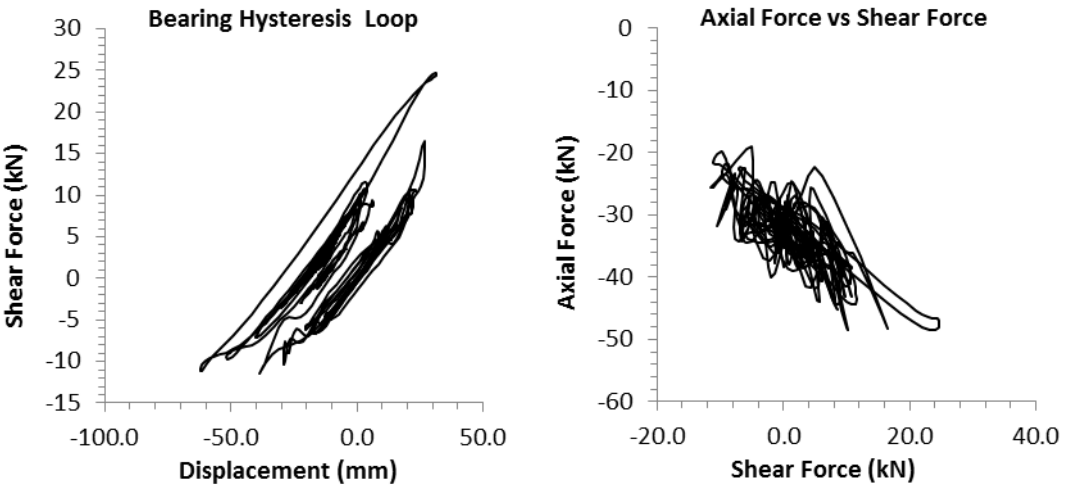


Figure 6.9: Hysteresis loops and axial force vs shear force plot of a bearing under S1 loading with friction coefficient of 0.75 and $A = 0.40$

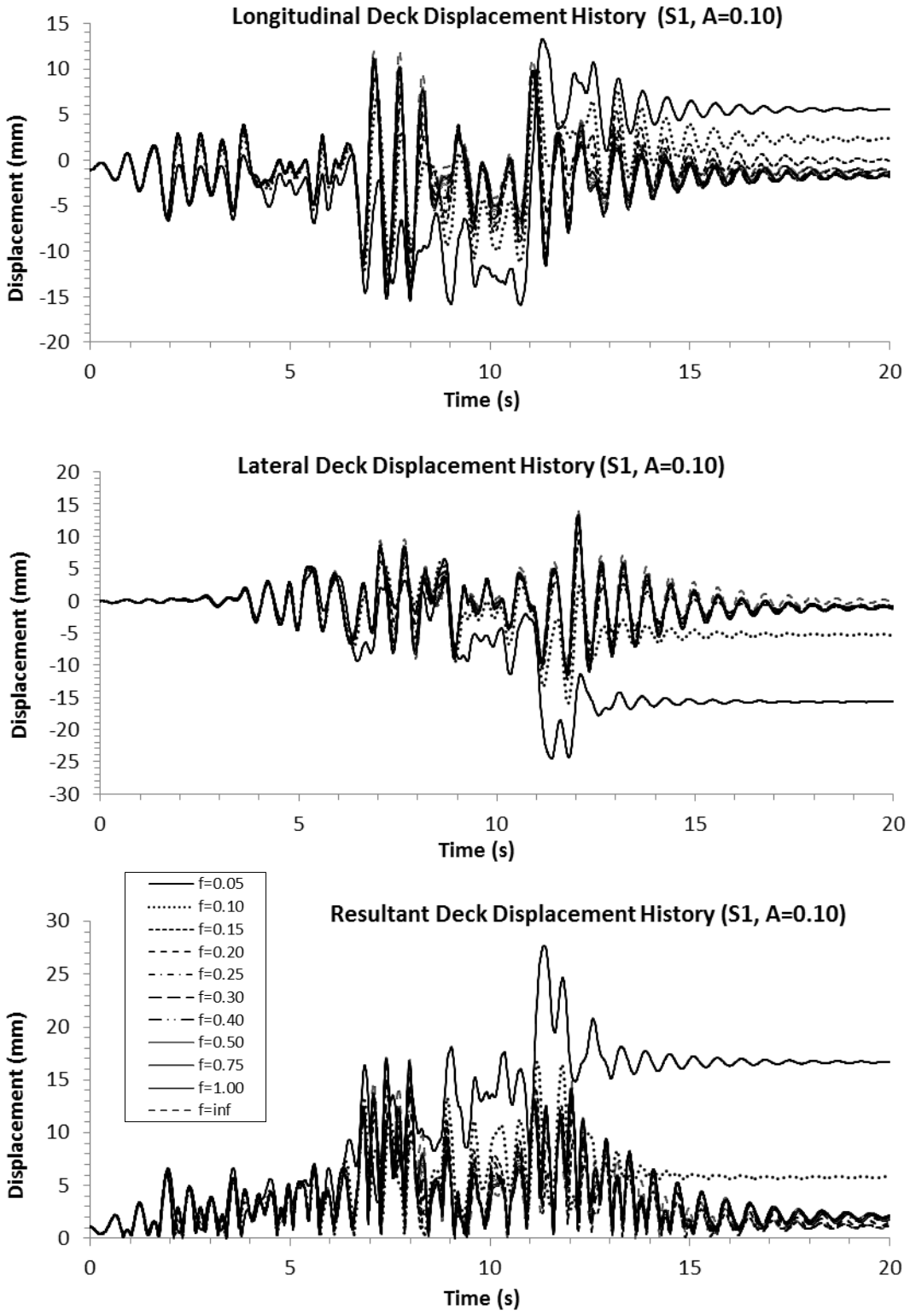


Figure 6.10: Longitudinal, lateral and resultant relative deck displacement histories for varying friction coefficients under S1 ground motion loading with $A = 0.10$

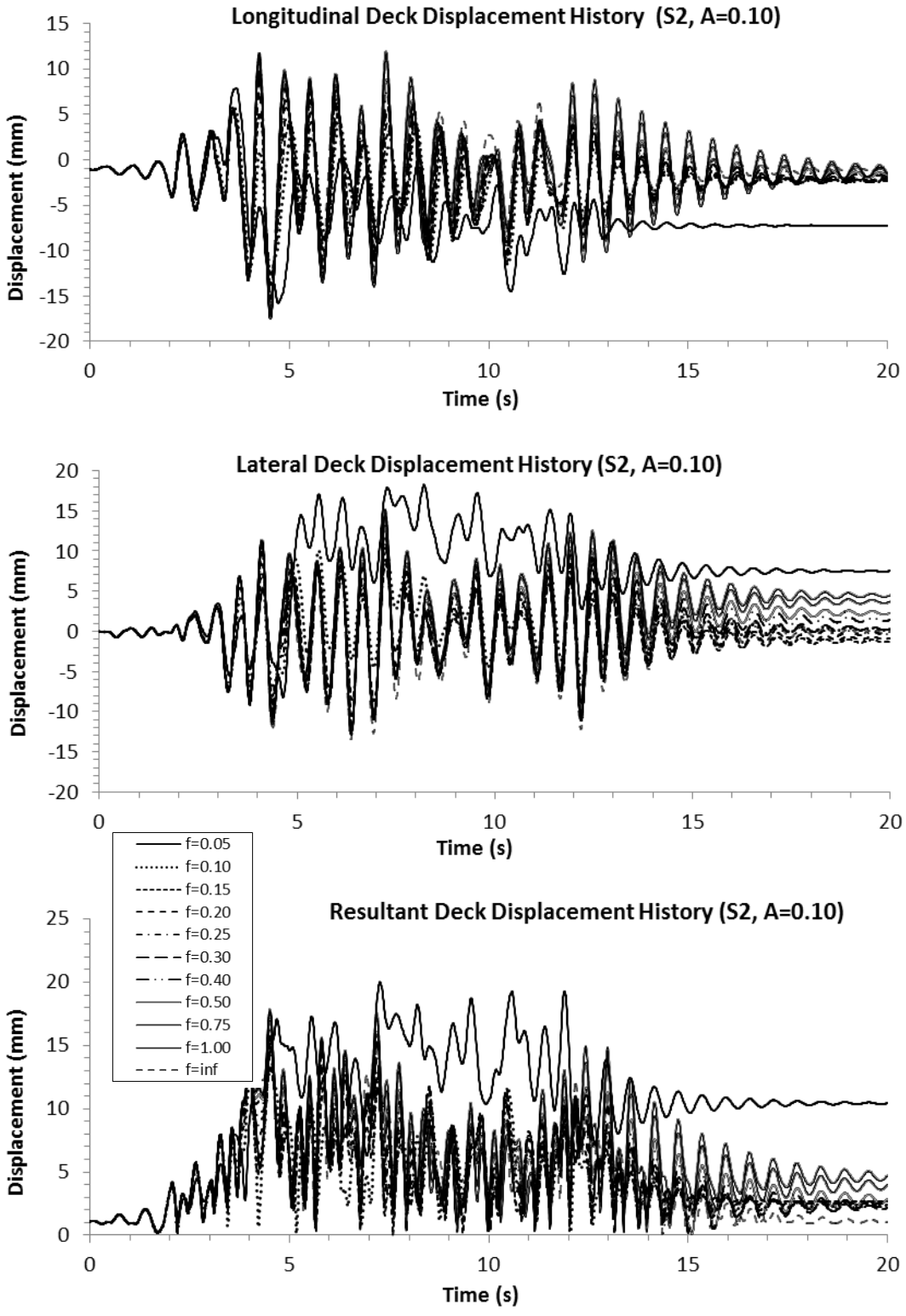


Figure 6.11: Longitudinal, lateral and resultant relative deck displacement histories for varying friction coefficients under S2 ground motion loading with $A = 0.10$

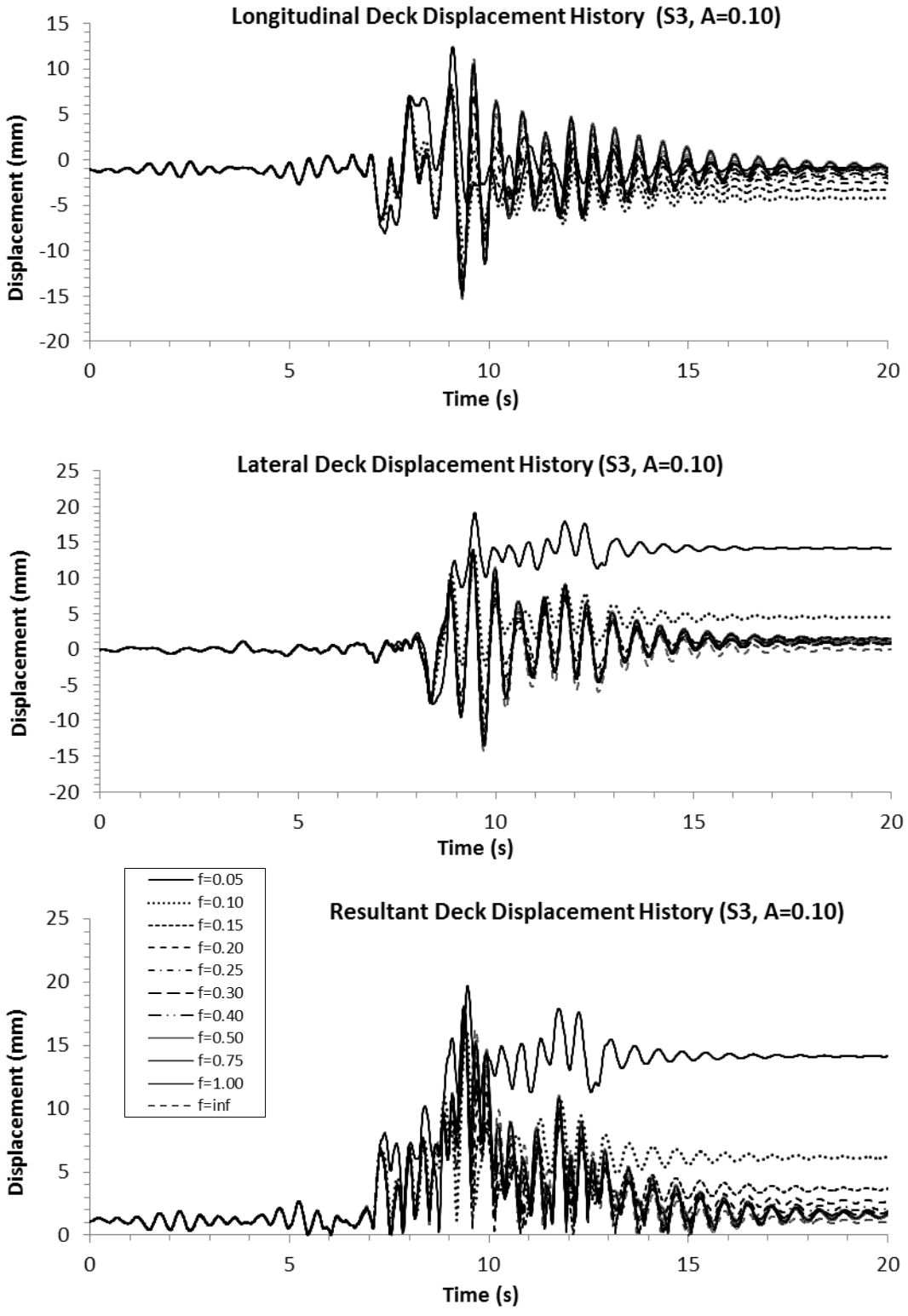


Figure 6.12: Longitudinal, lateral and resultant relative deck displacement histories for varying friction coefficients under S3 ground motion loading with $A = 0.10$

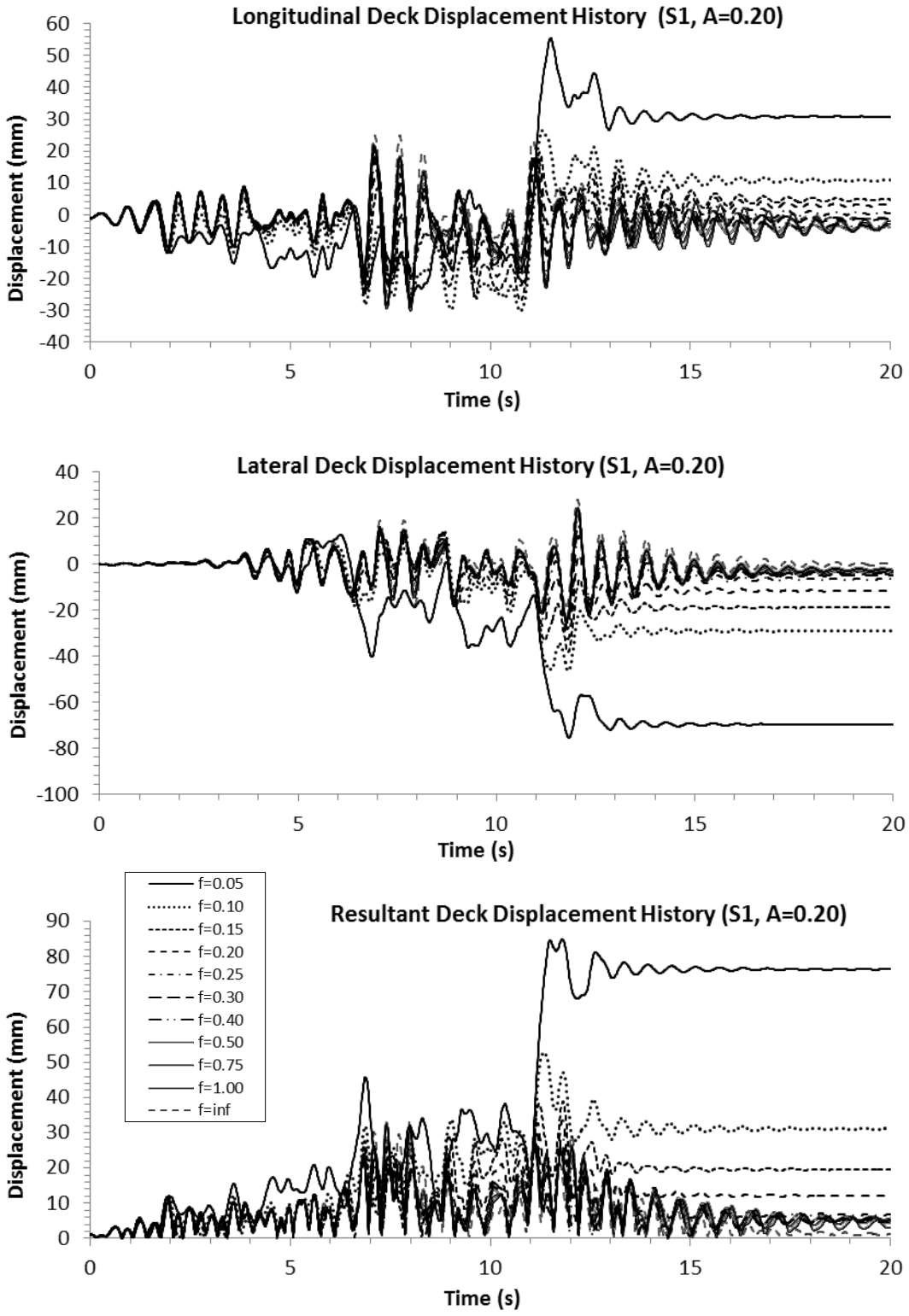


Figure 6.13: Longitudinal, lateral and resultant relative deck displacement histories for varying friction coefficients under S1 ground motion loading with $A = 0.20$

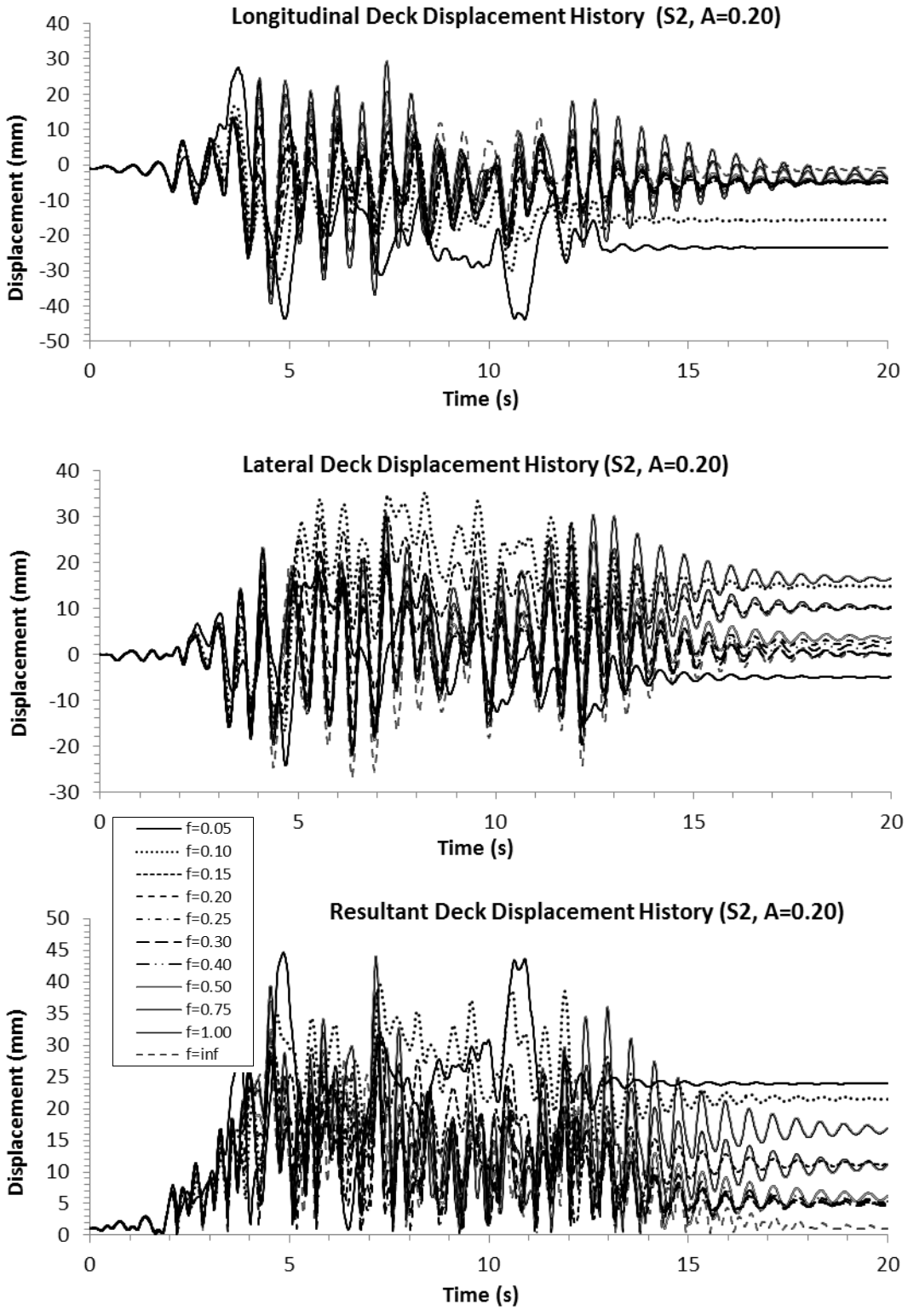


Figure 6.14: Longitudinal, lateral and resultant relative deck displacement histories for varying friction coefficients under S2 ground motion loading with $A = 0.20$

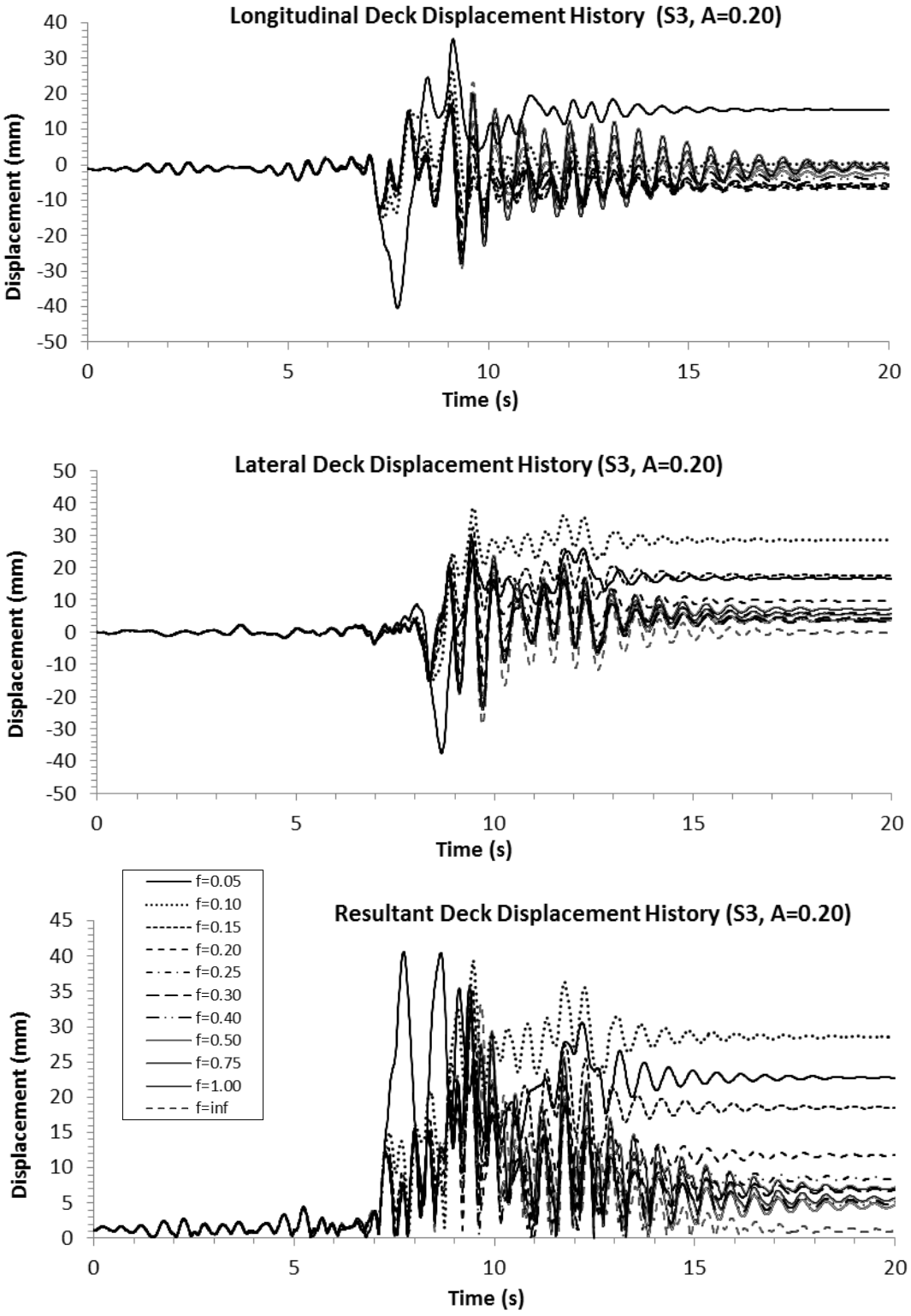


Figure 6.15: Longitudinal, lateral and resultant relative deck displacement histories for varying friction coefficients under S3 ground motion loading with $A = 0.20$

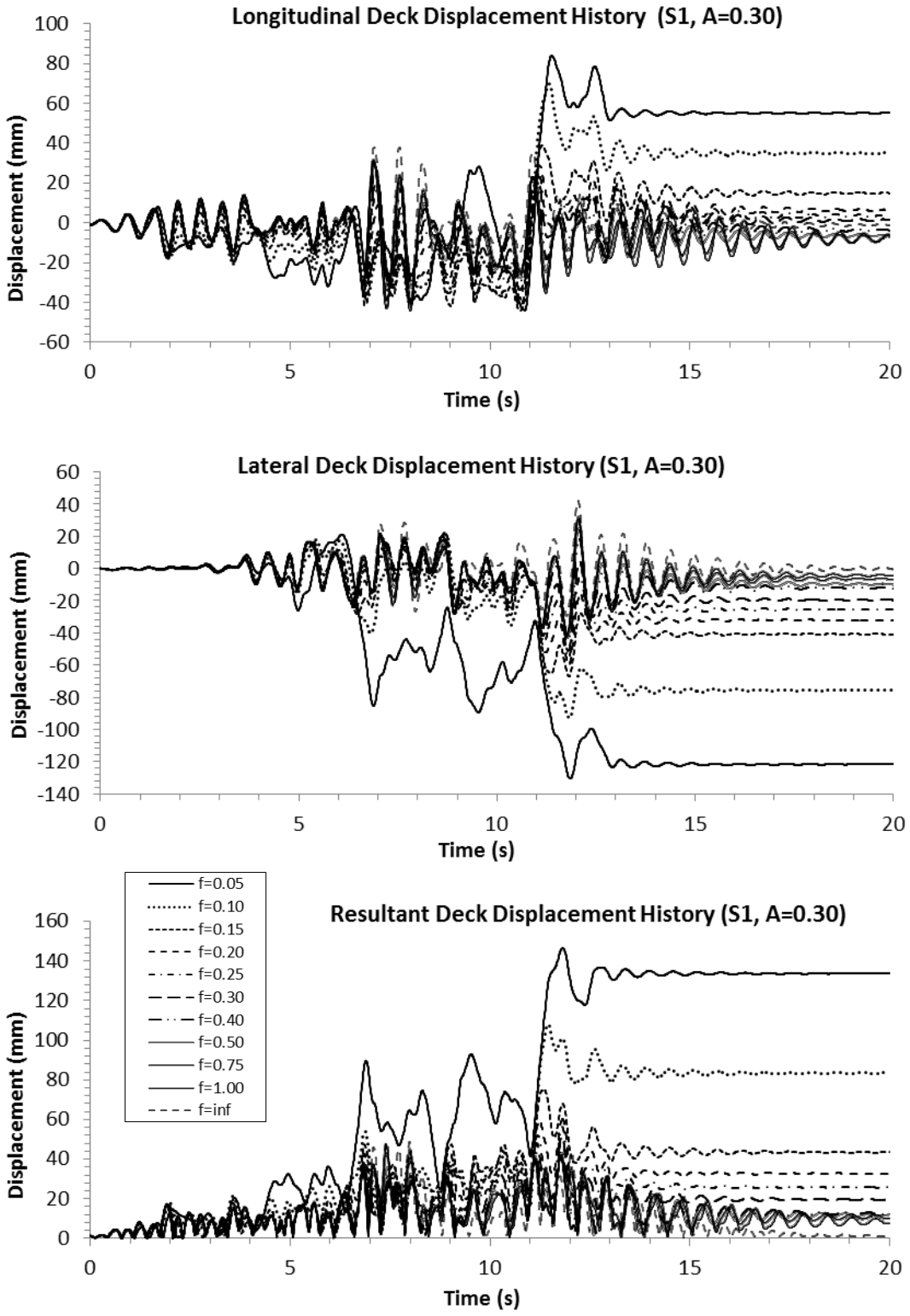


Figure 6.16: Longitudinal, lateral and resultant relative deck displacement histories for varying friction coefficients under S1 ground motion loading with $A = 0.30$

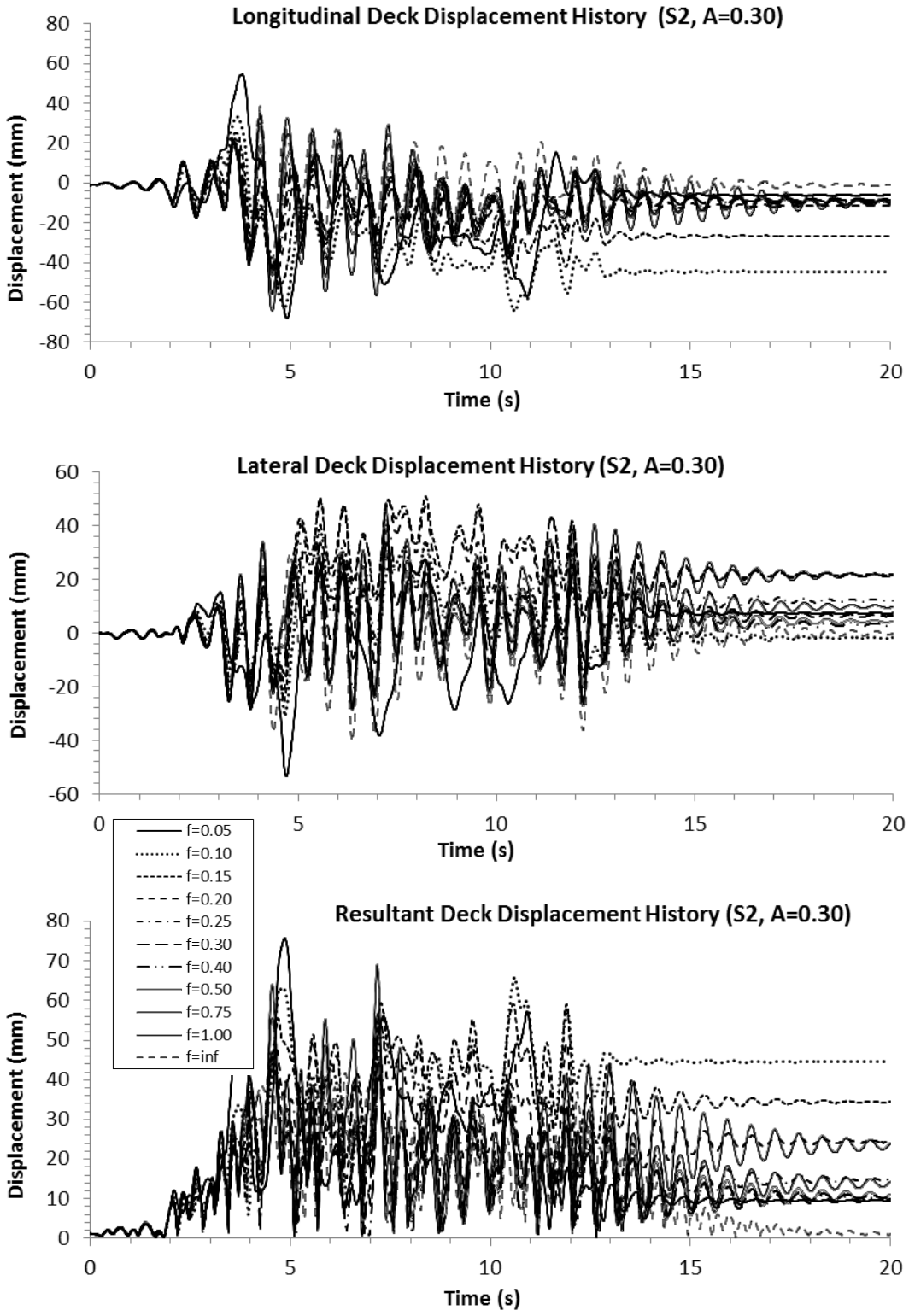


Figure 6.17: Longitudinal, lateral and resultant relative deck displacement histories for varying friction coefficients under S2 ground motion loading with $A = 0.30$

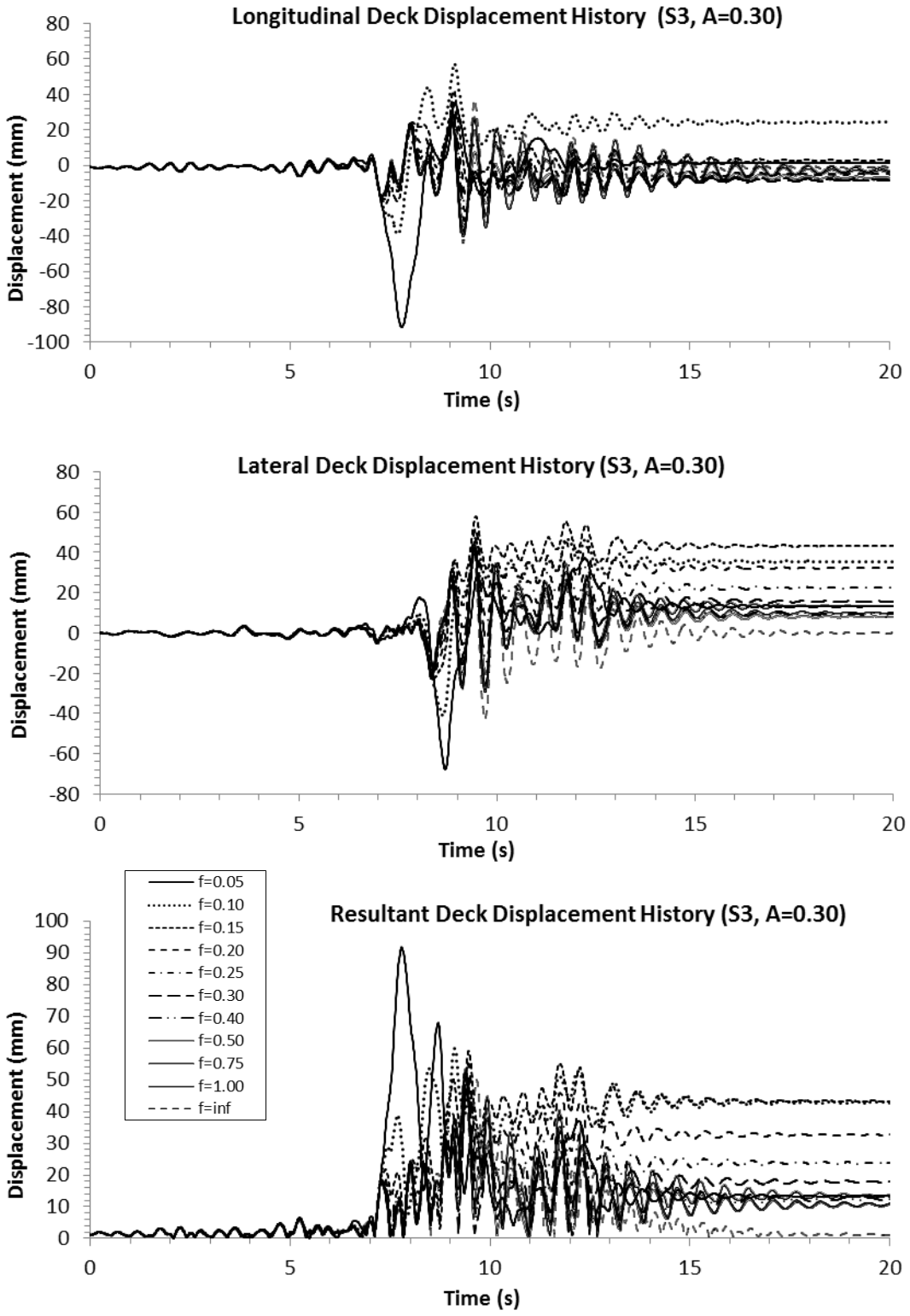


Figure 6.18: Longitudinal, lateral and resultant relative deck displacement histories for varying friction coefficients under S3 ground motion loading with $A = 0.30$

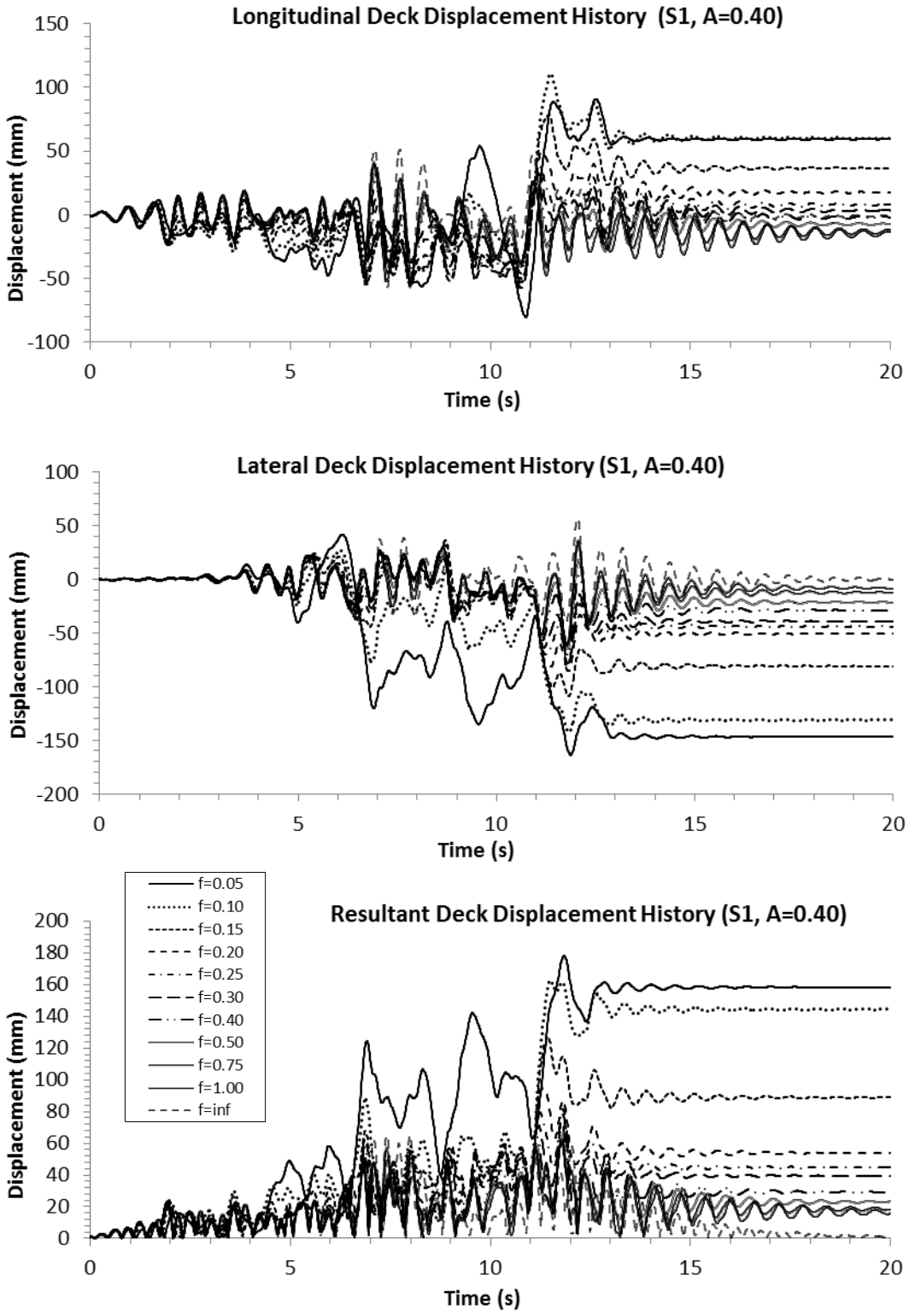


Figure 6.19: Longitudinal, lateral and resultant relative deck displacement histories for varying friction coefficients under S1 ground motion loading with $A = 0.40$

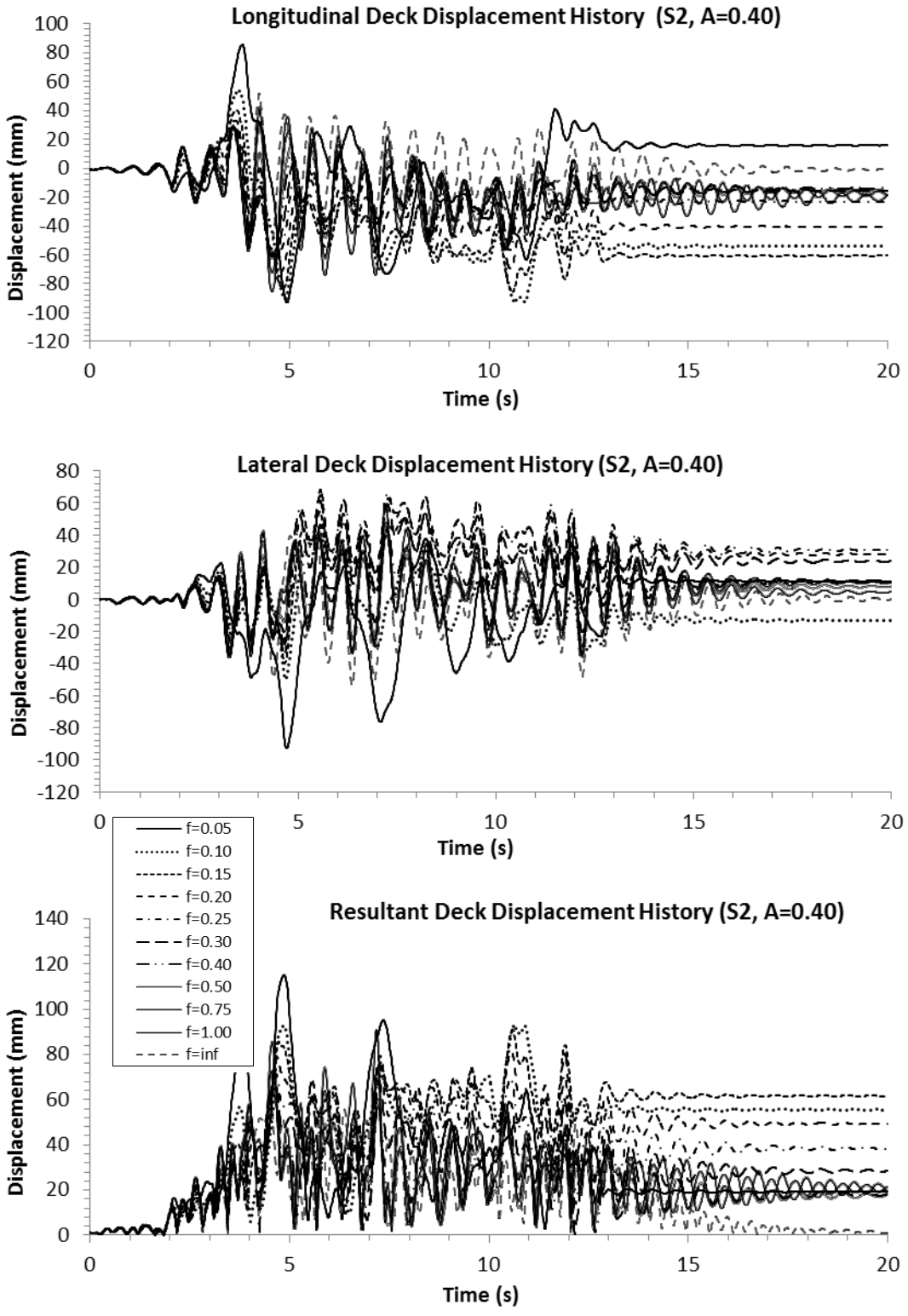


Figure 6.20: Longitudinal, lateral and resultant relative deck displacement histories for varying friction coefficients under S2 ground motion loading with $A = 0.40$

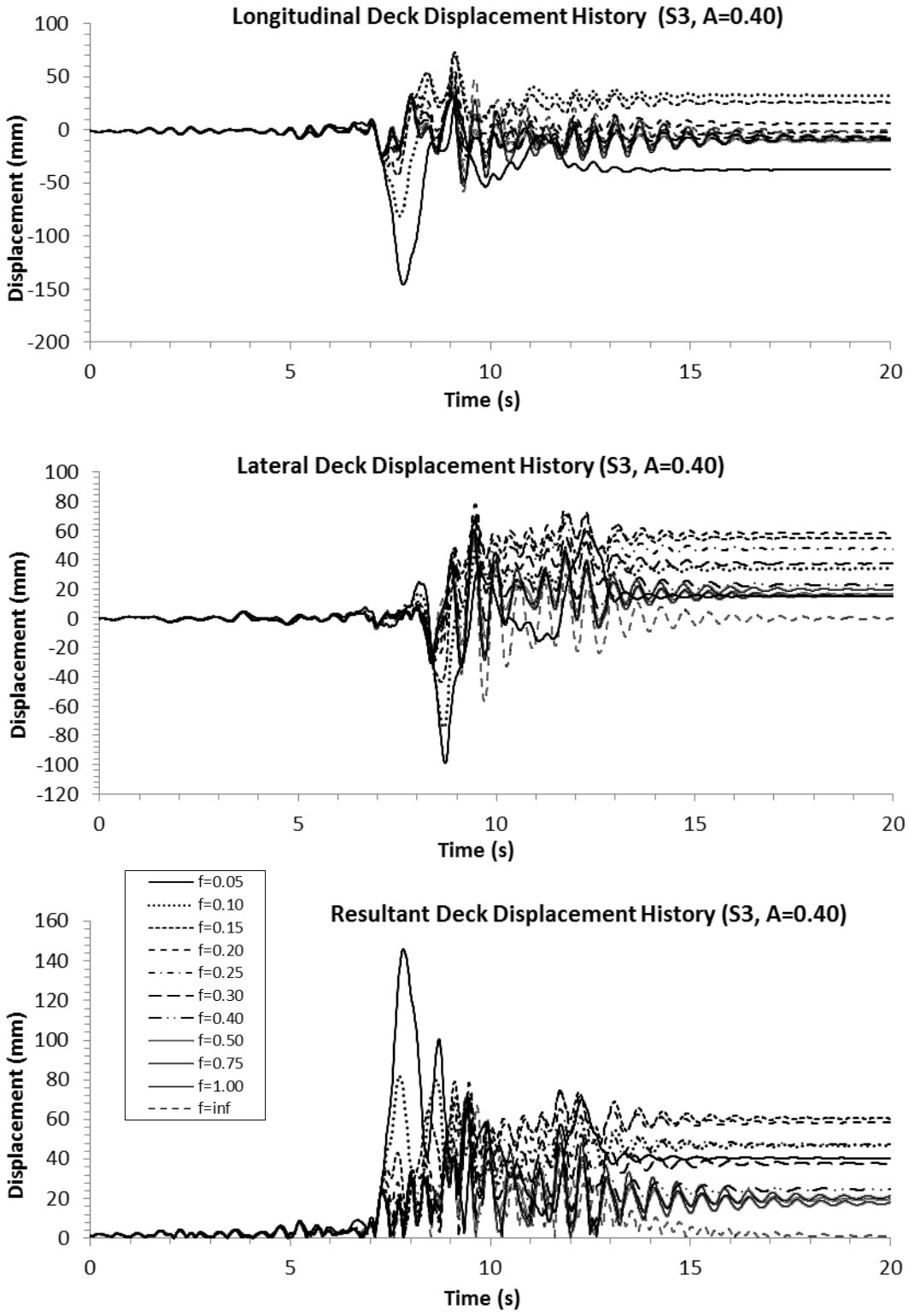


Figure 6.21: Longitudinal, lateral and resultant relative deck displacement histories for varying friction coefficients under S3 ground motion loading with $A = 0.40$

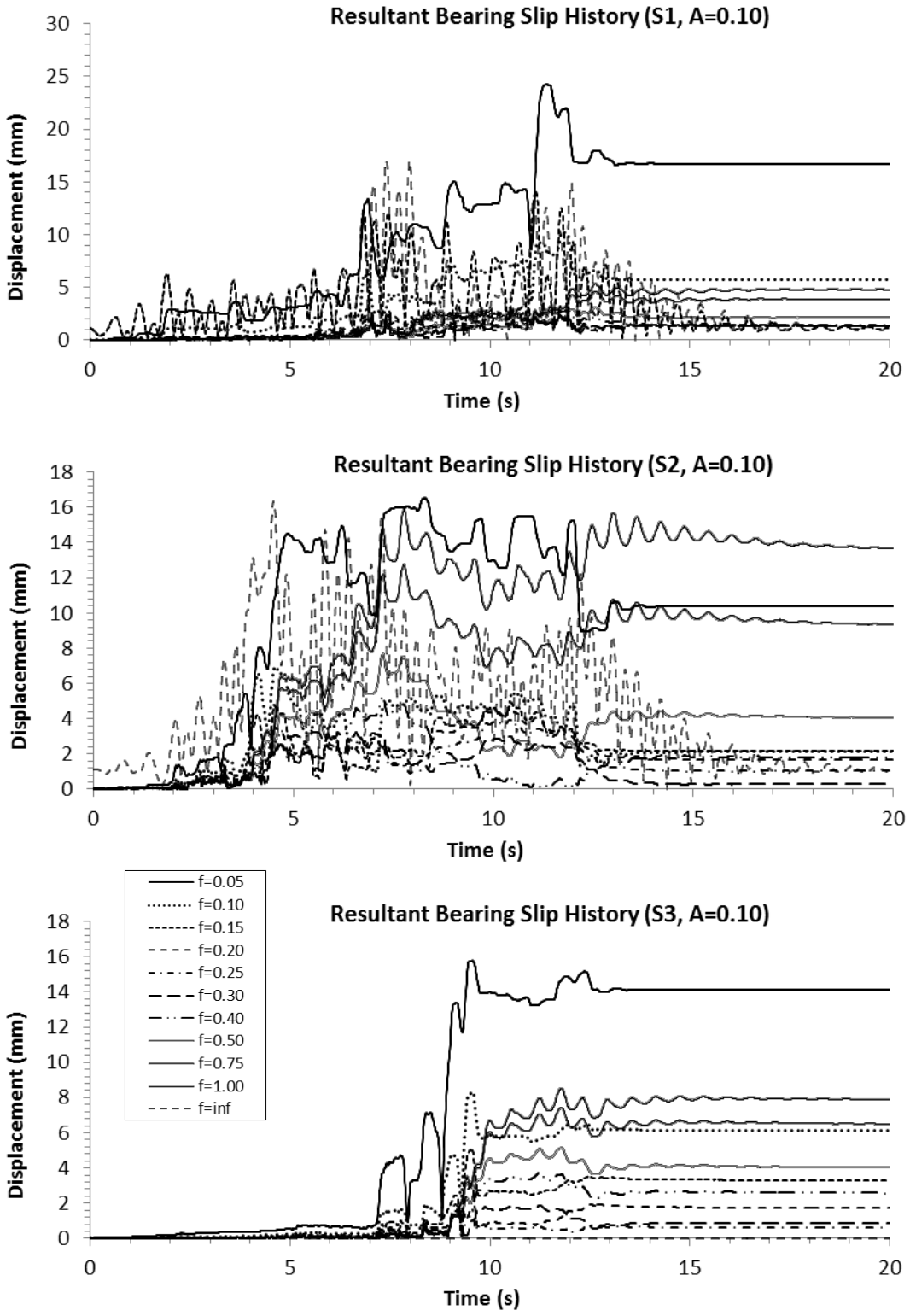


Figure 6.22: Resultant bearing slip histories for varying friction coefficients under for $A = 0.10$

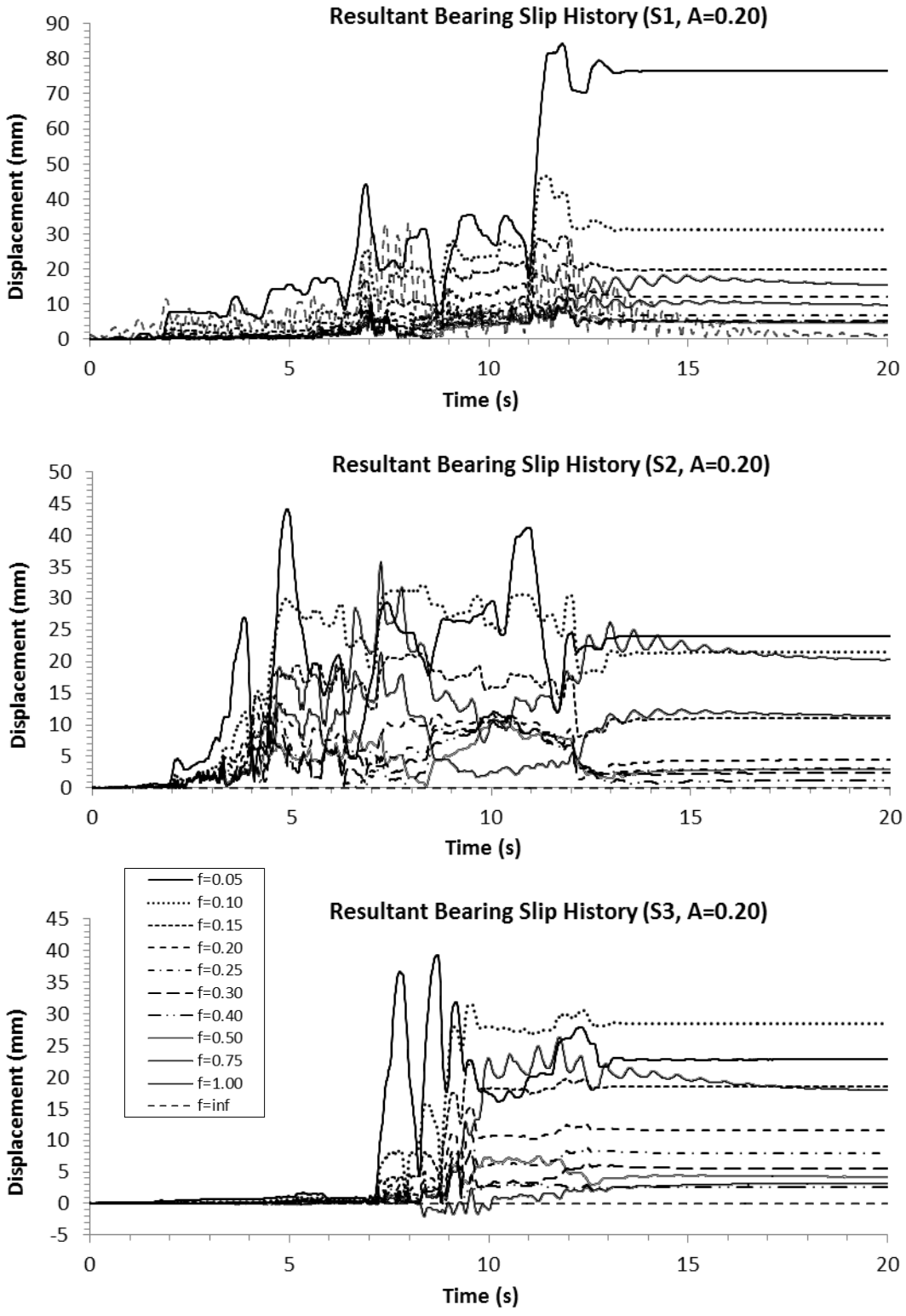


Figure 6.23: Resultant bearing slip histories for varying friction coefficients under for $A = 0.20$

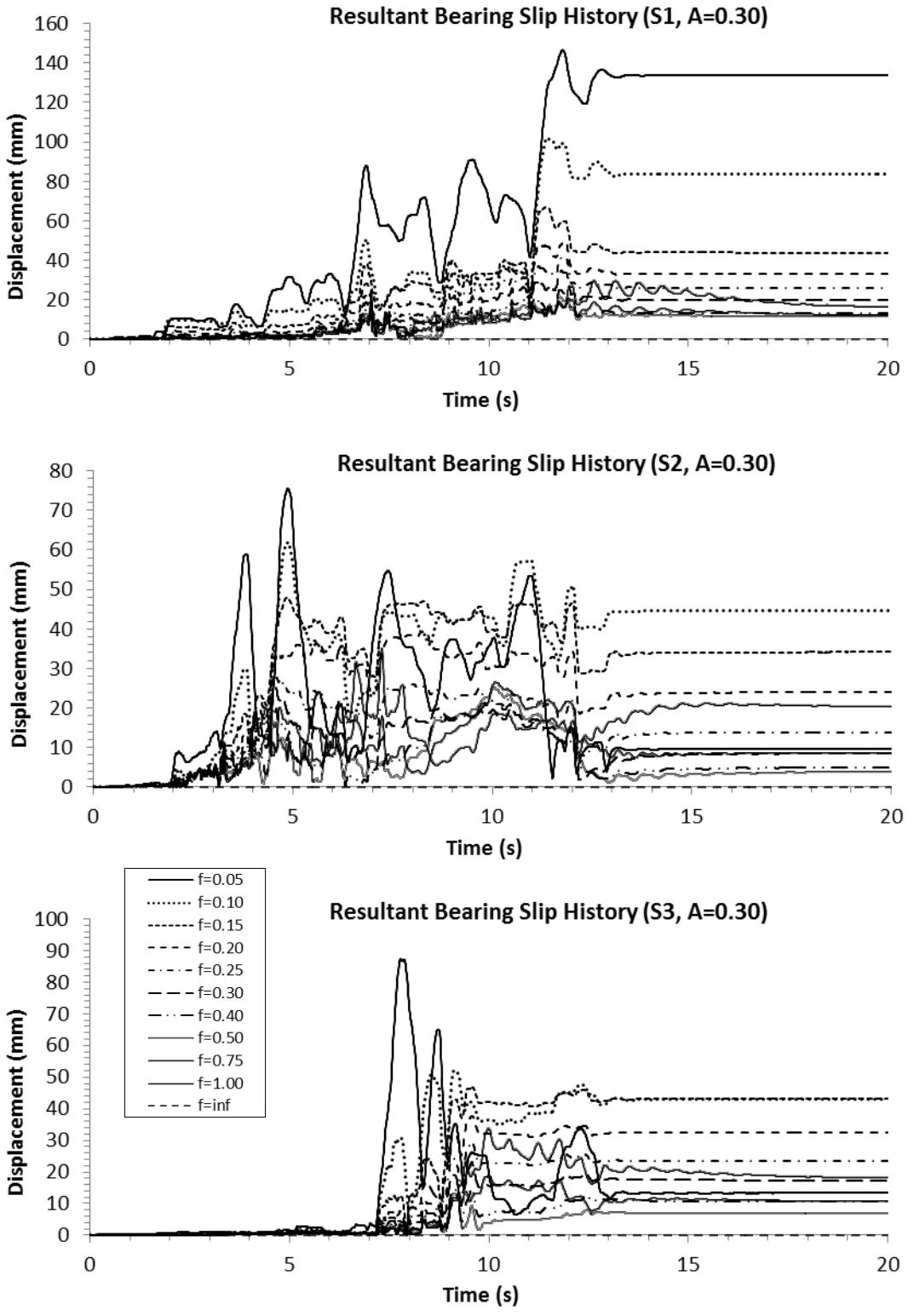


Figure 6.24: Resultant bearing slip histories for varying friction coefficients under for $A = 0.30$

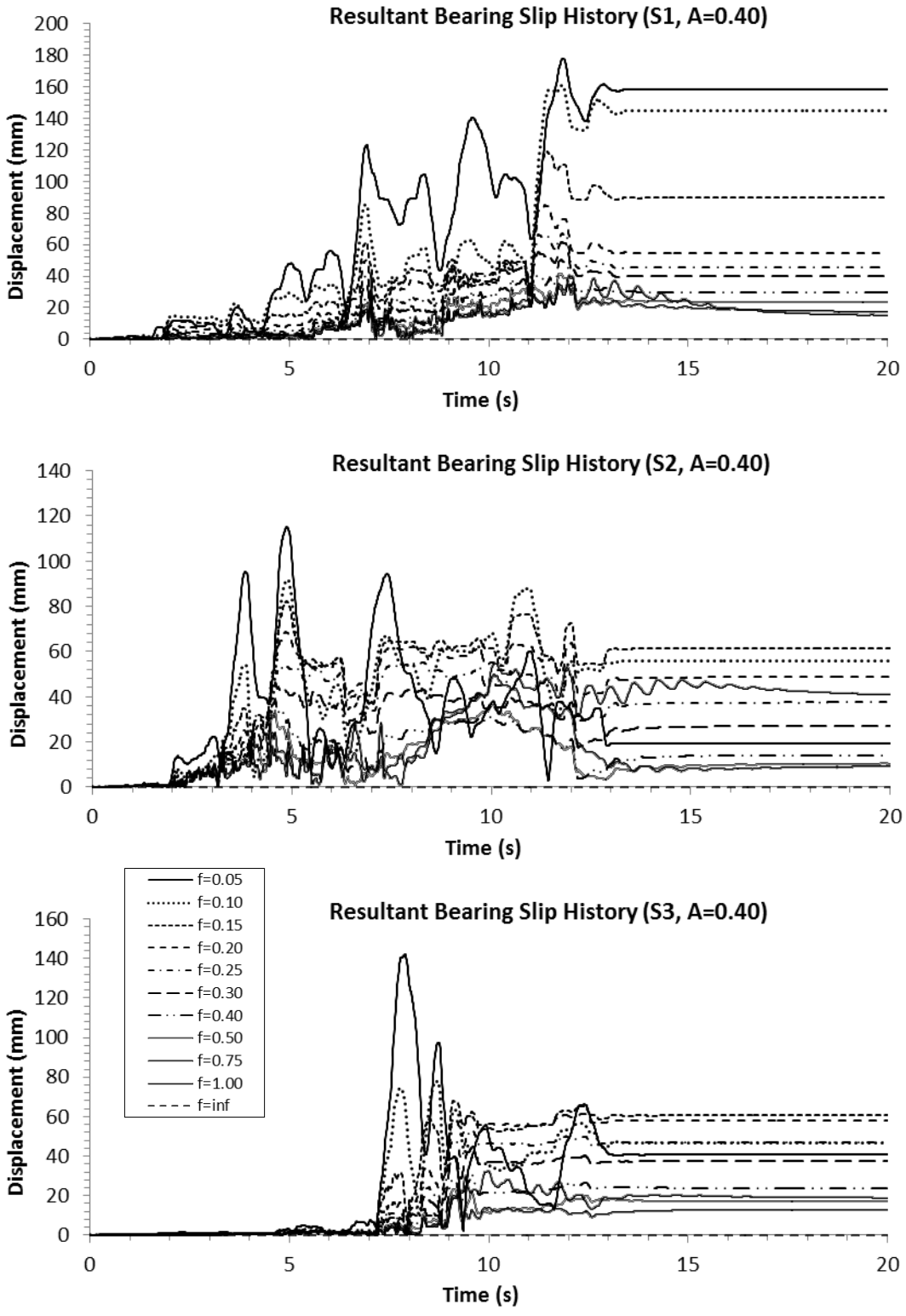


Figure 6.25: Resultant bearing slip histories for varying friction coefficients under for $A = 0.40$

### 6.5.2 EFFECT OF ACCELERATION COEFFICIENT

Maximum deck displacements relative to pier top are presented in Figure 6.26 to Figure 6.28 respectively. For friction coefficients between 0.20-0.50, maximum deck displacement and coefficient of acceleration seemed to be in approximately linear direct proportion. To further investigate the structural response, normalized resultant deck displacements with respect to the elastic displacement obtained using linear bearing elements without any friction interface are plotted on Figure 6.28.

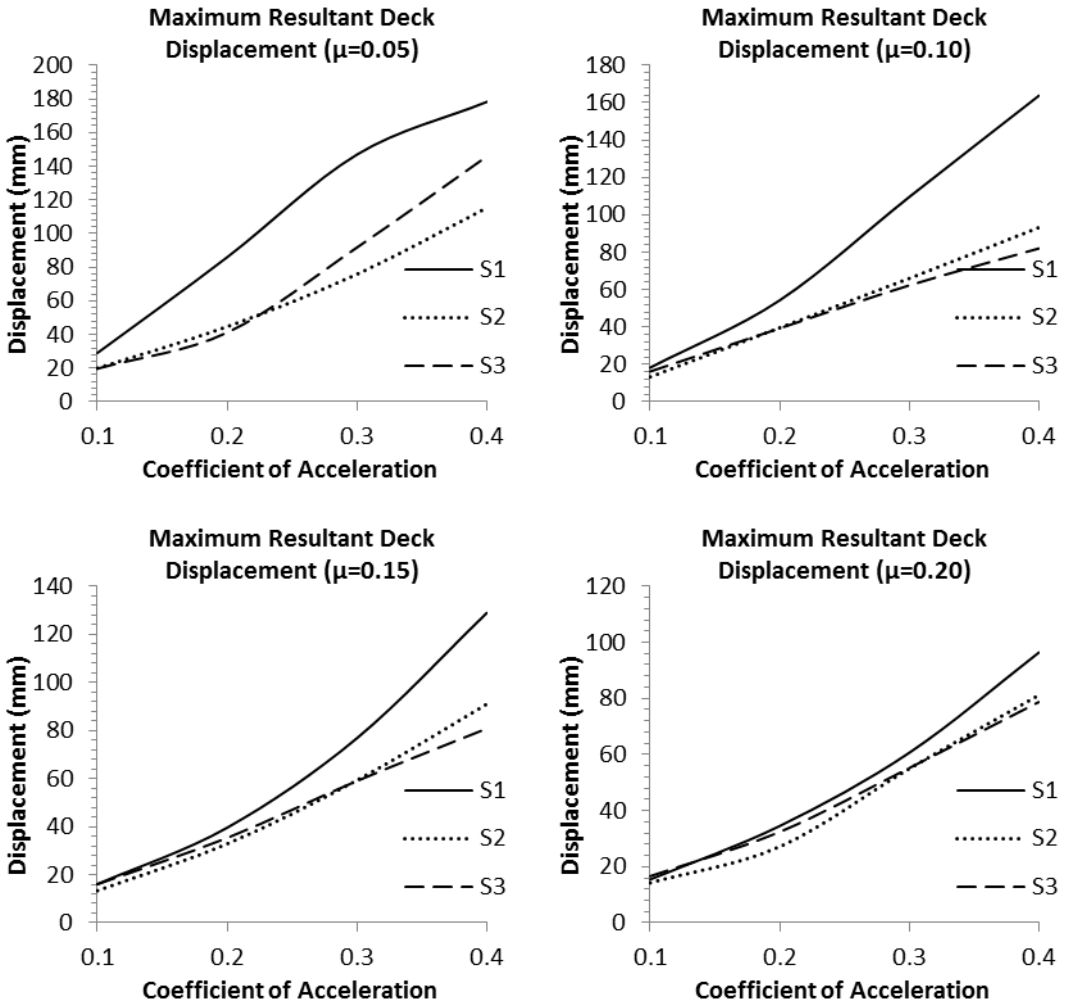


Figure 6.26: Maximum resultant deck accelerations as a function of coefficient of acceleration for various friction coefficient values – 1

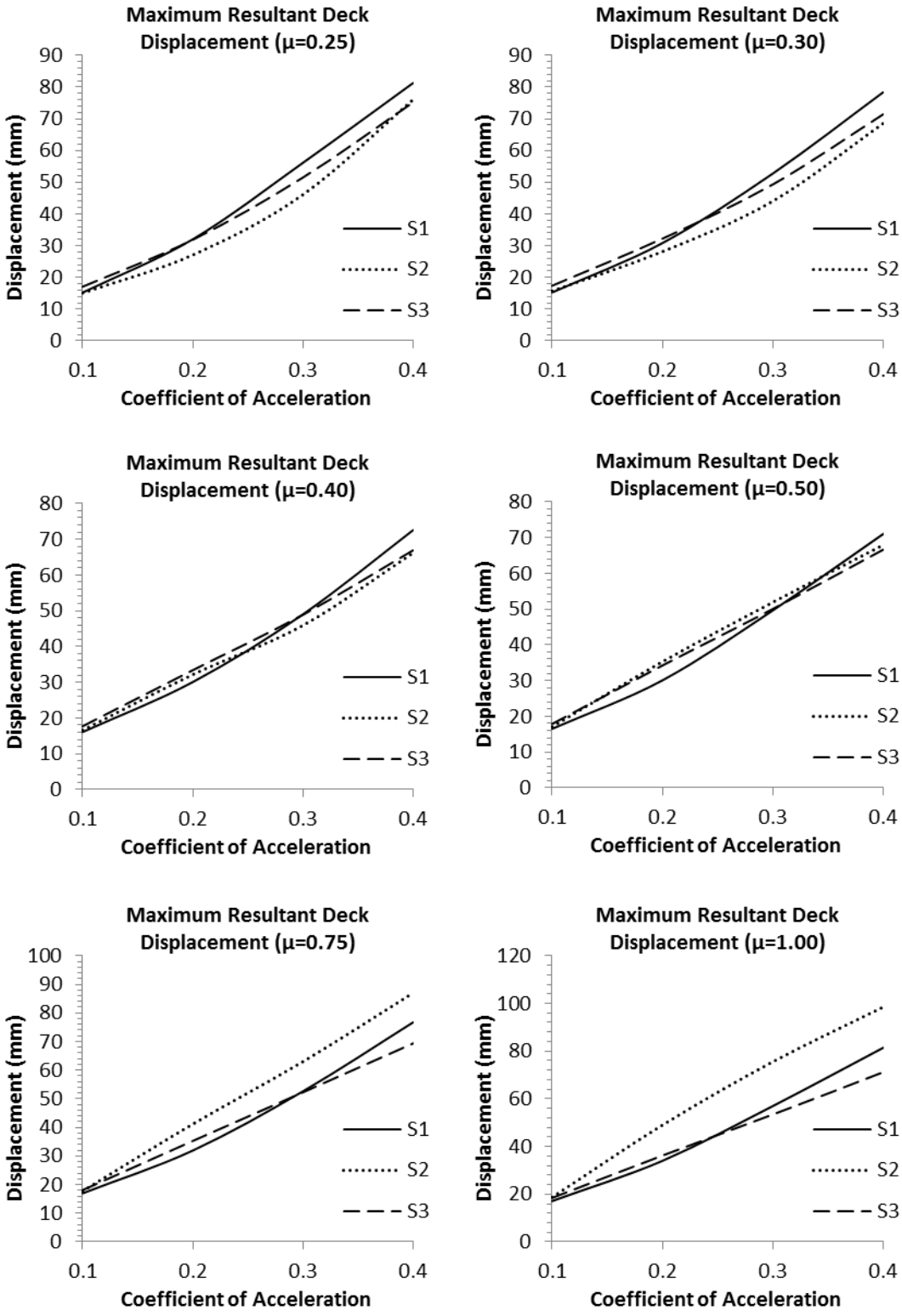


Figure 6.27: Maximum resultant deck accelerations as a function of coefficient of acceleration for various friction coefficient values – 2

For friction coefficient range 0.30-0.50, resultant relative deck displacement was nearly constant and independent of the friction coefficient (Figure 6.28).

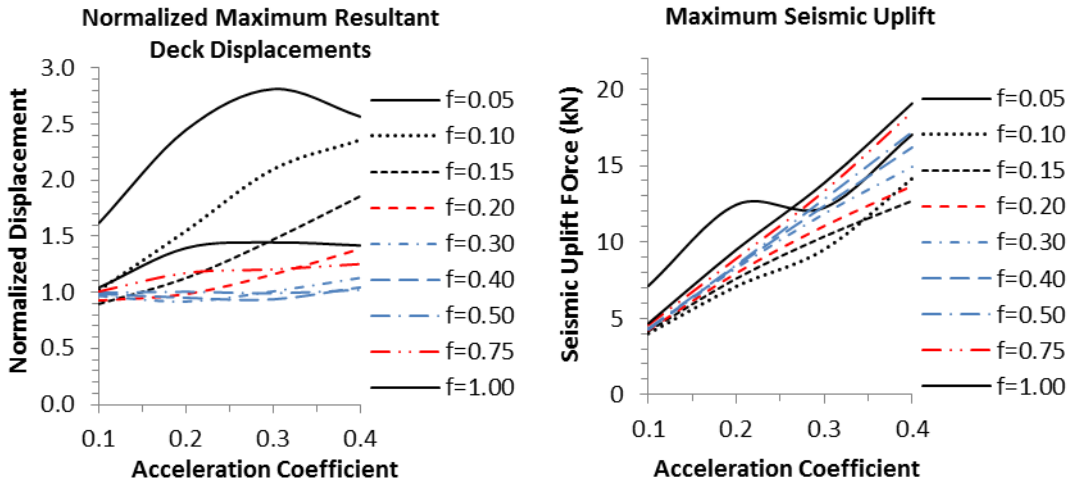


Figure 6.28: Normalized maximum resultant relative deck displacements and seismic uplift forces as a function of acceleration coefficient

An approximately linear relation also existed between seismic uplift force and acceleration coefficient for $\mu = 0.15 - 0.75$ (Figure 6.28).

### 6.5.3 EFFECT OF SKEW

Maximum longitudinal, lateral, resultant and permanent resultant deck displacements as a function of skew angle under a seismic loading of $A = 0.40$ for a friction coefficient of 0.20 are presented in Figure 6.29.

Deck displacement and uplift force histories under a seismic loading of $A = 0.40$ for friction coefficients of 0.20 and 0.50 are also presented in Figure 6.30 to Figure 6.33 for the skew angles 0 and 60°.

Results indicated that skew angle of the bridge did not have a significant effect on maximum and permanent deck displacements as well as with bearing axial forces.

This is the expected results indeed, as fundamental modes in lateral and longitudinal directions were uncoupled and fundamental frequencies were nearly the same regardless of skew angle of the bridge.

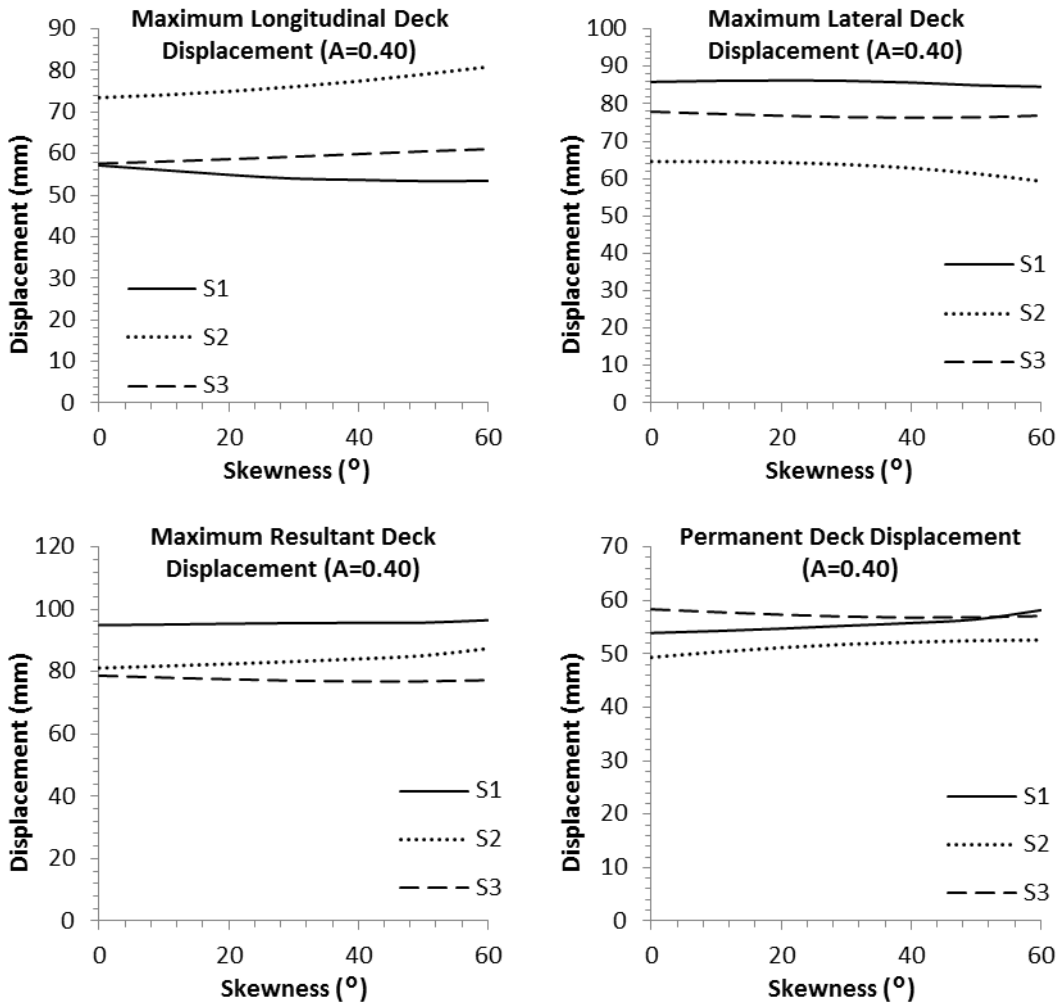


Figure 6.29: Maximum longitudinal, lateral, resultant and permanent resultant deck displacements as a function of skew angle

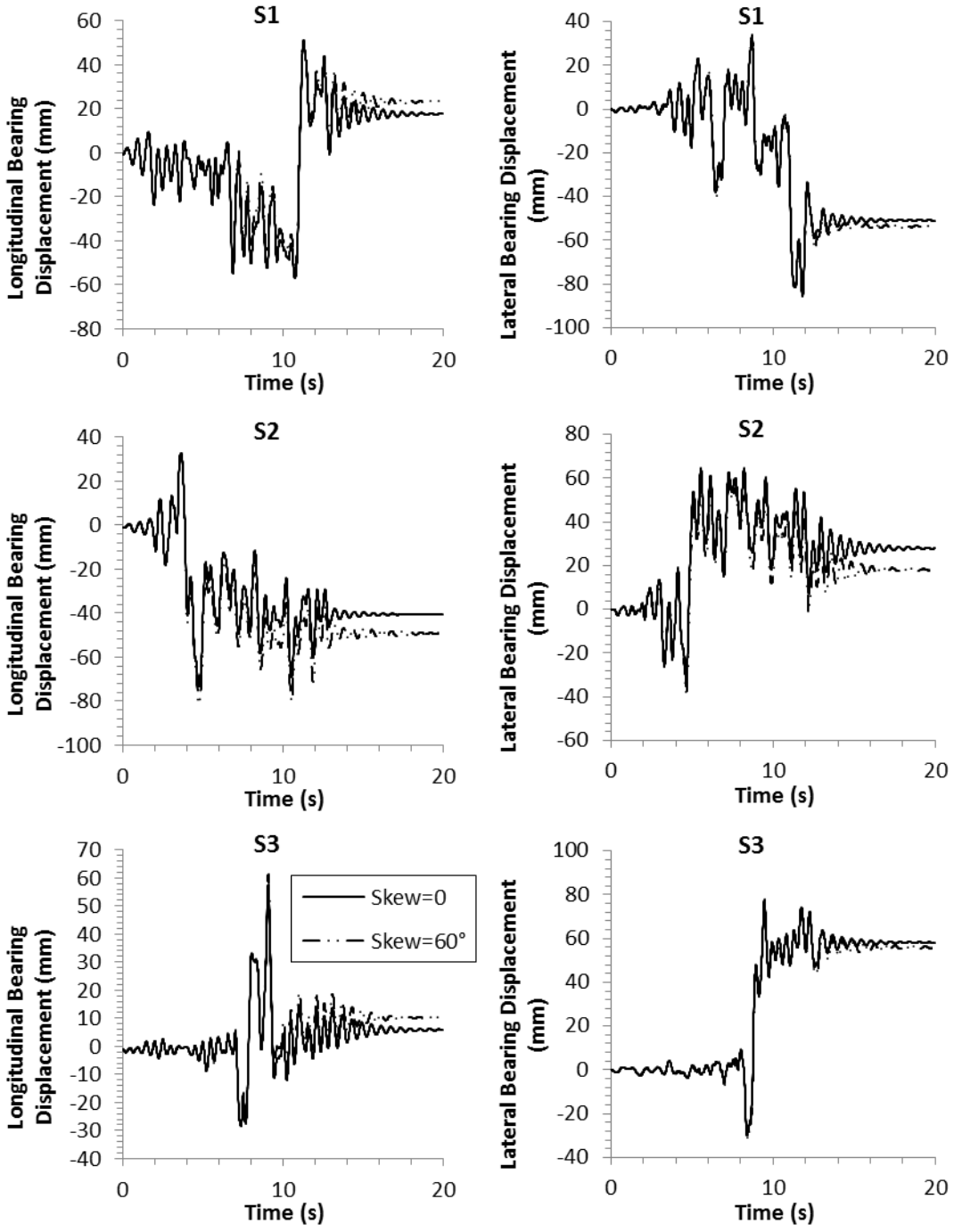


Figure 6.30: Longitudinal and lateral bearing displacement histories for $\mu = 0.20$ and $A = 0.40$

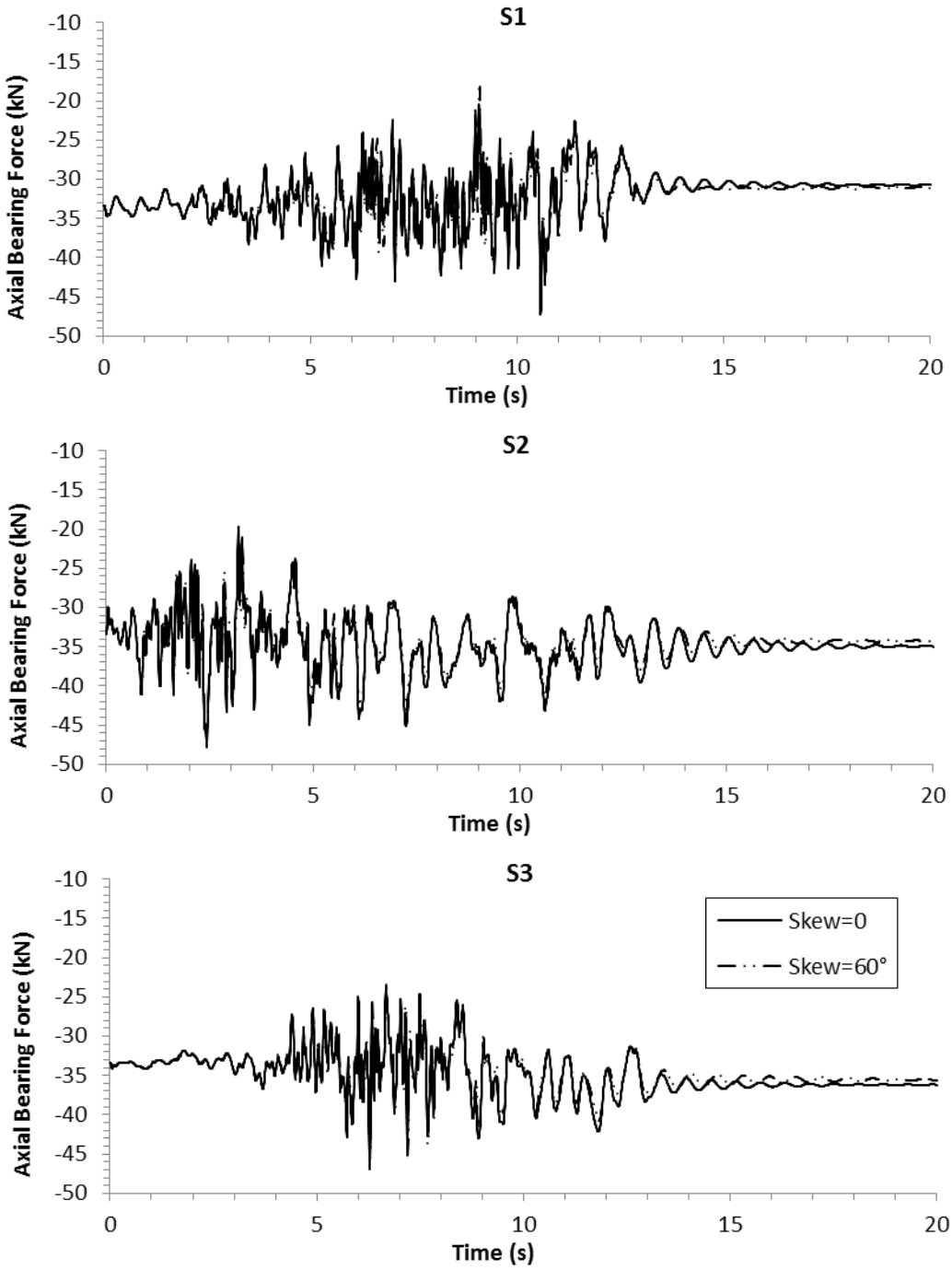


Figure 6.31: Axial bearing force history for $\mu = 0.20$ and $A = 0.40$

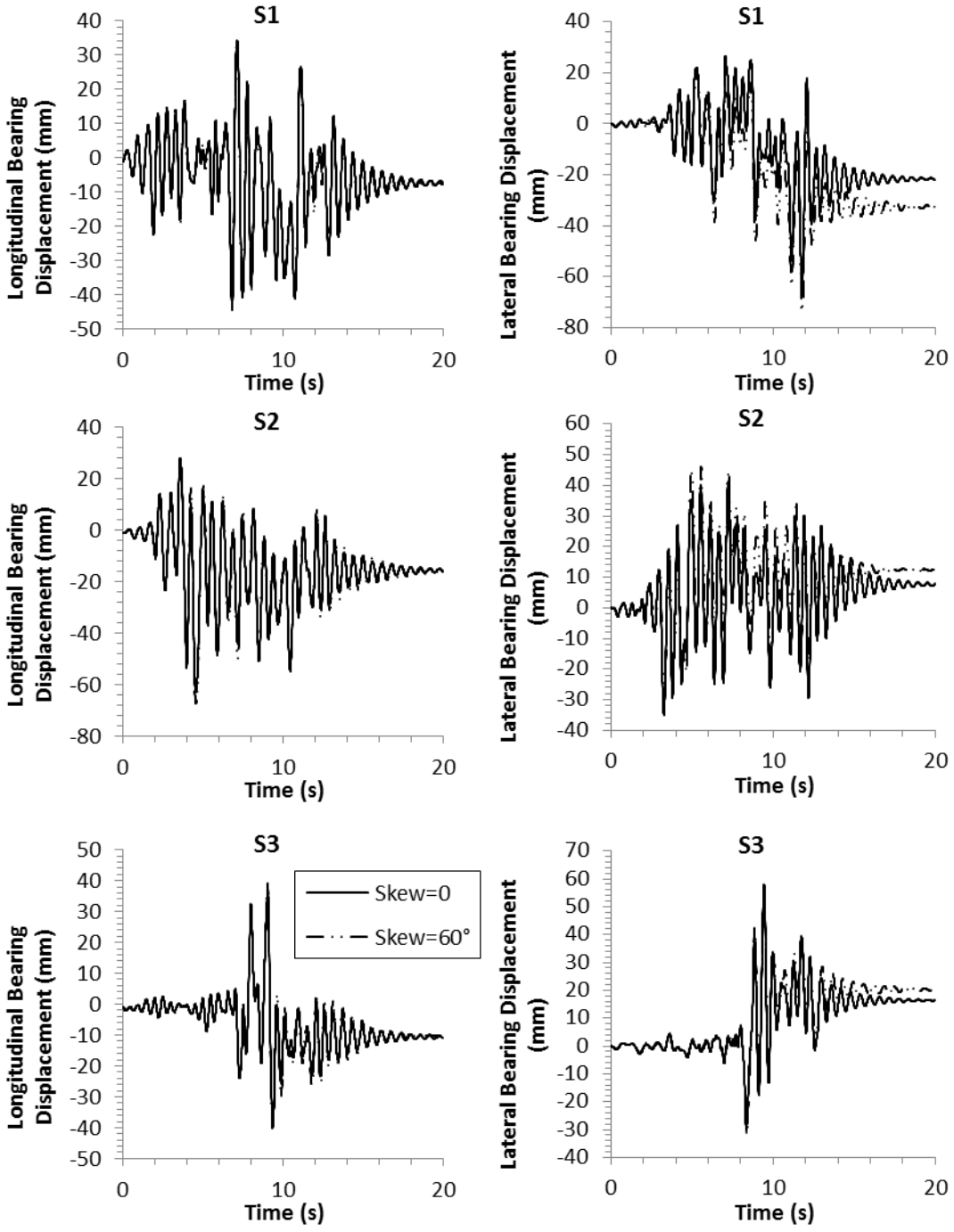


Figure 6.32: Longitudinal and lateral bearing displacement histories for $\mu = 0.50$ and $A = 0.40$

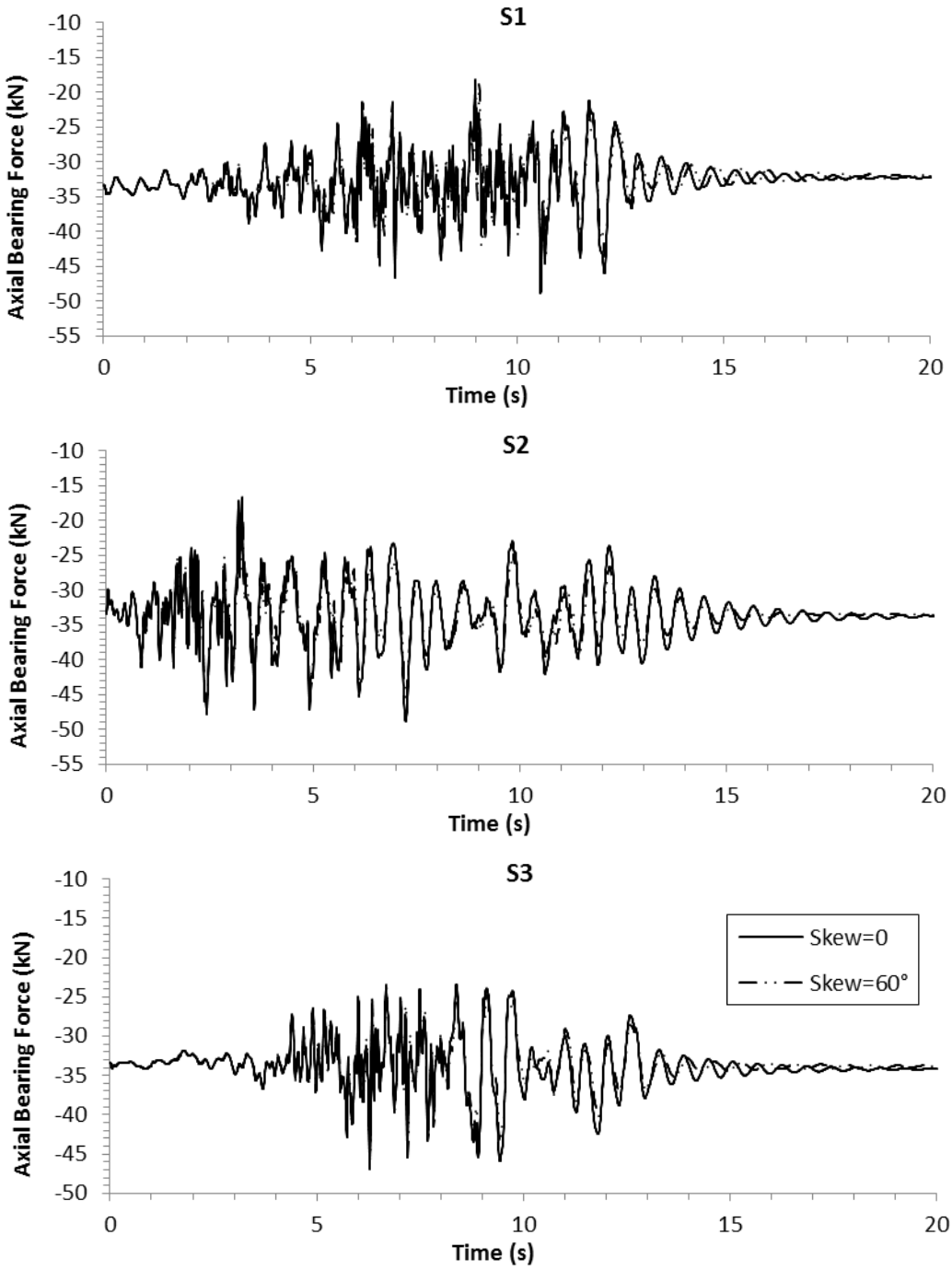


Figure 6.33: Axial bearing force history for $\mu = 0.50$ and $A = 0.40$

### 6.5.4 EFFECT OF HEIGHT TO WIDTH RATIO OF DECK

Maximum longitudinal, lateral, resultant deck displacements and seismic uplift forces are presented as a function of height-to-width ratio of deck in Figure 6.34 to Figure 6.37.

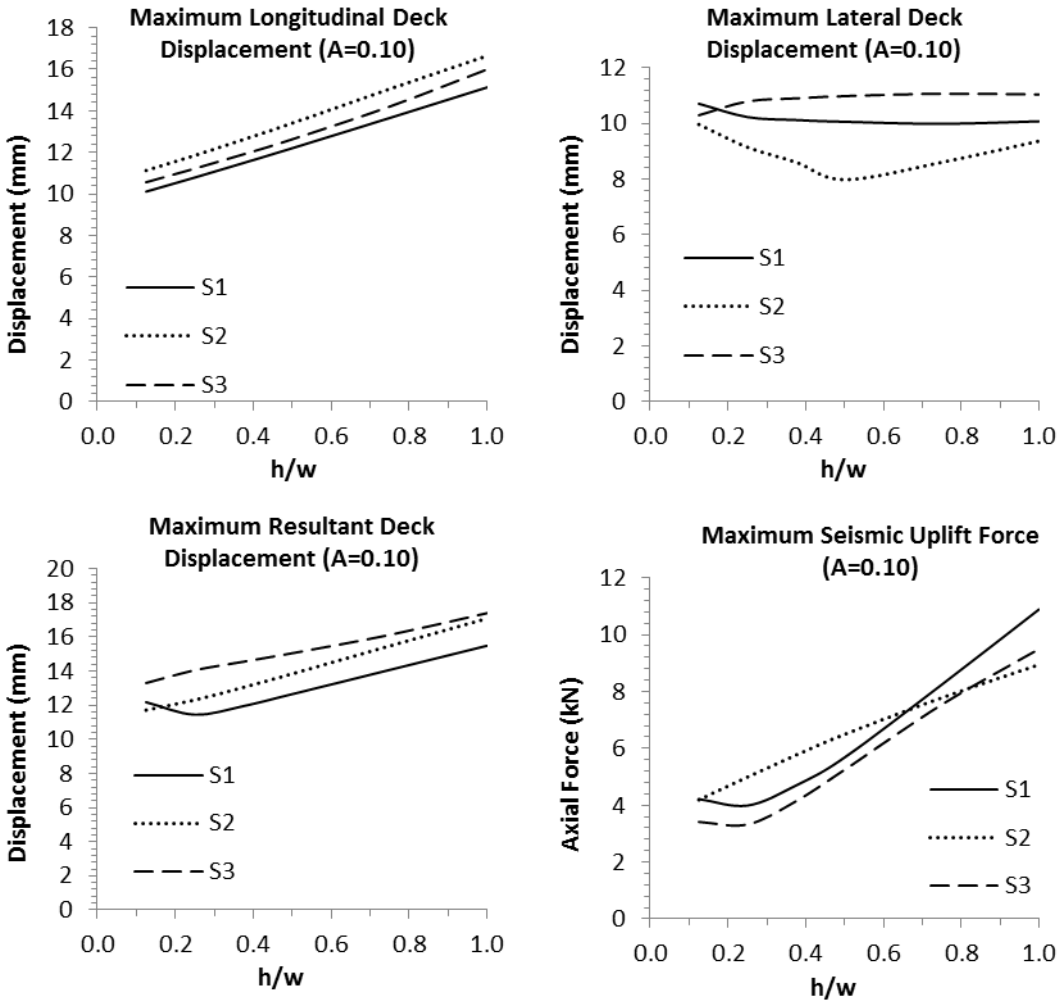


Figure 6.34: Maximum longitudinal, lateral and resultant deck displacements as a function of height-to-width ratio for $\mu = 0.20$ and $A = 0.10$

Deck displacements showed a tendency to increase when greater height-to-width deck ratios were used. However, a linear or regular relation between displacement and height-to-width deck ratio could not be observed for all loading cases.

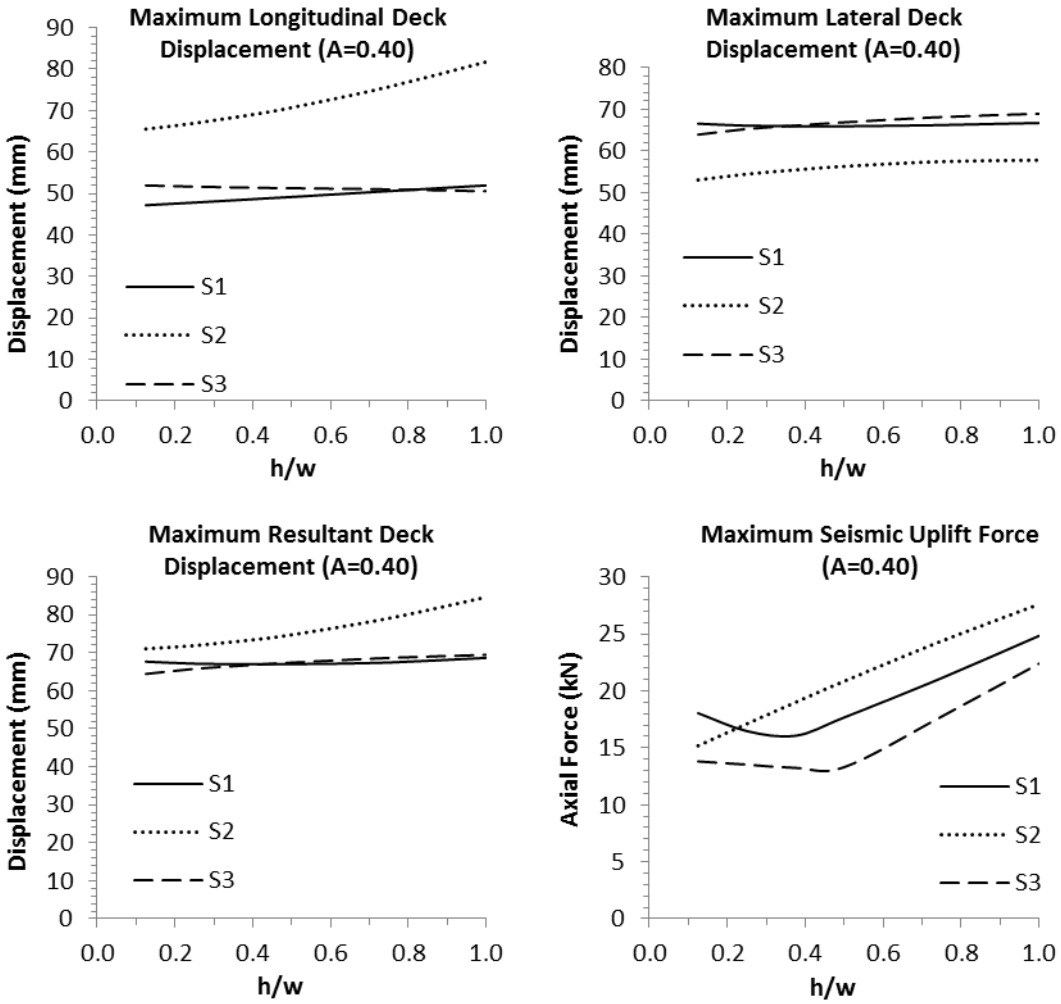


Figure 6.35: Maximum longitudinal, lateral and resultant deck displacements as a function of height-to-width ratio for $\mu = 0.20$ and $A = 0.40$

On the other hand, seismic uplift forces in bearings exhibited an approximately linear dependence to height-to-width ratio. This observation could be justified recalling Equation (2.6), where uplift force in a bearing is in direct linear proportion with height-to-width deck ratio.

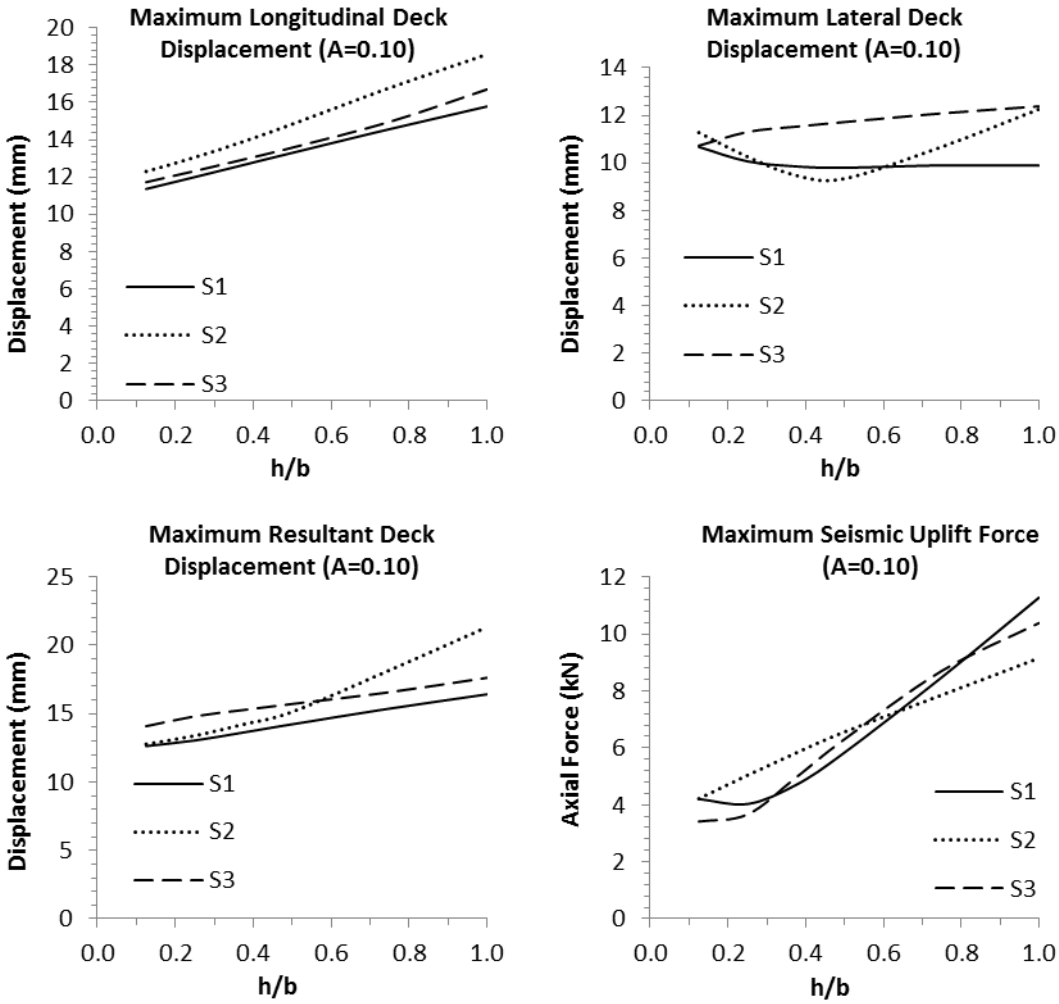


Figure 6.36: Maximum longitudinal, lateral and resultant deck displacements as a function of height-to-width ratio for $\mu = 0.50$ and $A = 0.10$

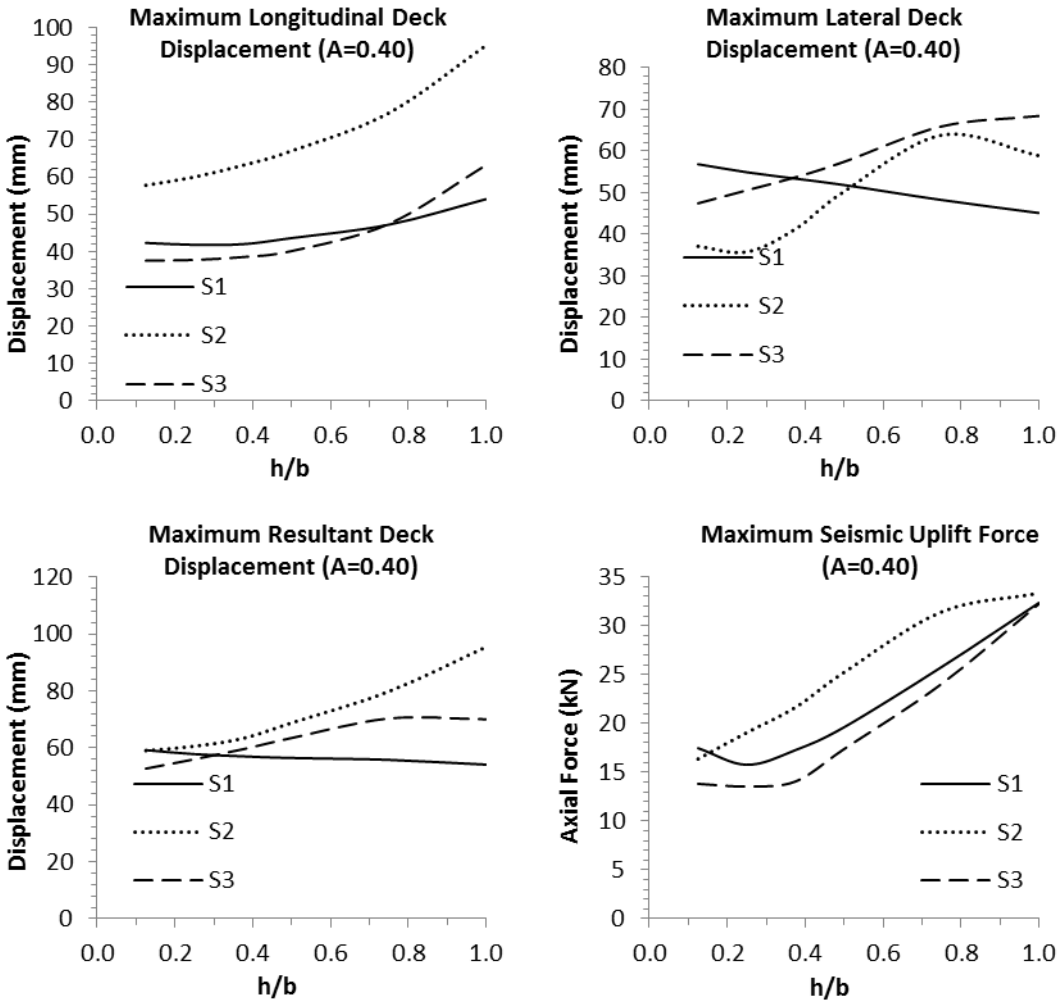


Figure 6.37: Maximum longitudinal, lateral and resultant deck displacements as a function of height-to-width ratio for $\mu = 0.50$ and $A = 0.40$

### 6.5.5 EFFECT OF FUNDAMENTAL FREQUENCY

Normalized maximum resultant deck displacements as a function of fundamental frequency is presented in Figure 6.38. Same responses are given as a function of acceleration coefficient in Figure 6.39 with seismic uplift forces in bearings.

Results indicated that normalized displacements were effected by fundamental frequency to an extent and an irregular relation exists between two. Dependence was more significant for moderate to high seismic loading ($A = 0.30 - 0.40$).

Dependence of maximum seismic uplift forces in bearings to fundamental frequency of the system was less pronounced. An approximately linear relation seemed to exist between acceleration coefficient and seismic uplift forces for the investigated values of fundamental frequency.

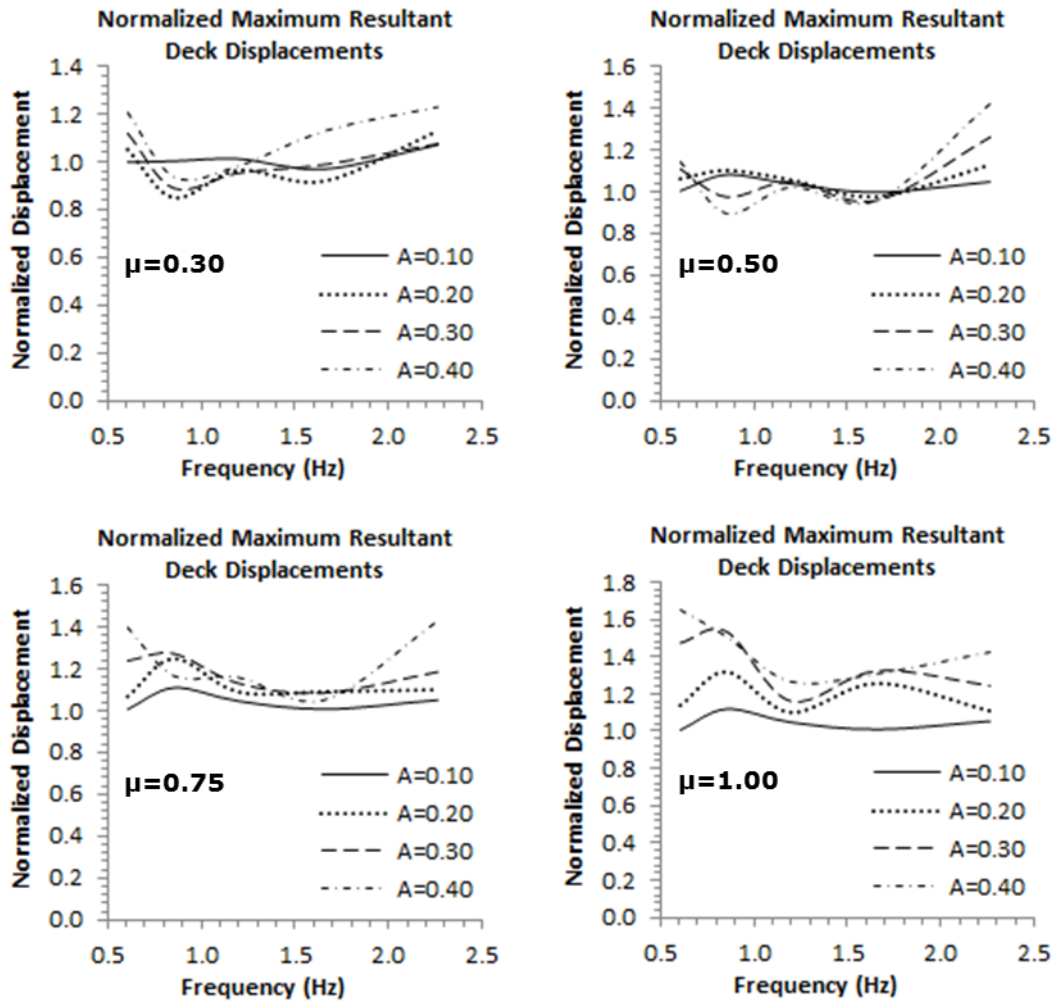


Figure 6.38: Normalized maximum deck displacements as a function of fundamental frequency

.

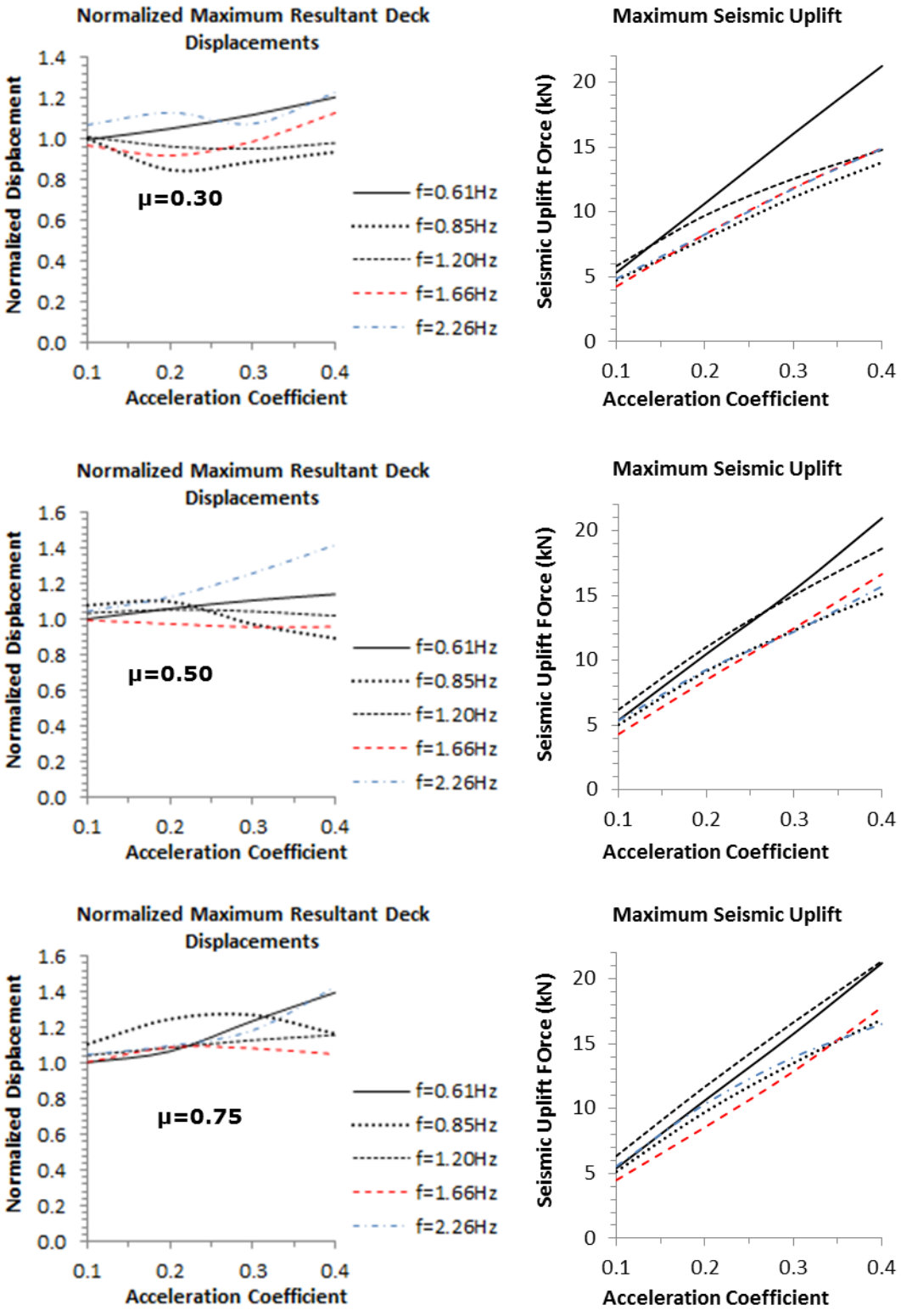


Figure 6.39: Normalized maximum deck displacements and maximum seismic uplift forces as a function of acceleration coefficient

## 6.6 EXTENDED FEA AND TRENDLINE CONSTRUCTION

Results of the parametric study pointed out to a possibility of a simple and reasonably approximate correlation between maximum resultant deck displacements normalized by the responses of corresponding bonded system and acceleration coefficient when friction of coefficient is over 0.20.

To construct such a trendline, additional FEA of 16 bridge setups using earthquake records S4 to S9 were performed to calculate maximum deck displacements normalized by the obtained responses from linear counterpart of each setup. Chosen parameters are summarized in Table 6.2.

Table 6.2: Properties of ground motion records

| Model # | Record # | $A$ | $\mu$ | t (s) | freq. (Hz) | Skew (°) | h/b |
|---|---|---|---|---|---|---|---|
| 1 | S4 | 0.1 | 0.40 | 0.836 | 1.196 | 50 | 0.25 |
| 2 | S5 | 0.1 | 1.00 | 0.836 | 1.196 | 10 | 1.00 |
| 3 | S6 | 0.1 | 0.30 | 1.648 | 0.607 | 60 | 0.75 |
| 4 | S4 | 0.2 | 0.75 | 0.603 | 1.658 | 50 | 0.25 |
| 5 | S5 | 0.2 | 0.25 | 0.442 | 2.262 | 30 | 0.50 |
| 6 | S6 | 0.2 | 0.50 | 1.171 | 0.854 | 0 | 0.50 |
| 7 | S4 | 0.3 | 0.75 | 1.648 | 0.607 | 10 | 0.25 |
| 8 | S5 | 0.3 | 0.30 | 1.171 | 0.854 | 20 | 2.00 |
| 9 | S6 | 0.3 | 0.50 | 1.648 | 0.607 | 0 | 0.75 |
| 10 | S4 | 0.4 | 0.40 | 0.603 | 1.658 | 40 | 1.50 |
| 11 | S5 | 0.4 | 0.25 | 0.836 | 1.196 | 60 | 0.75 |
| 12 | S6 | 0.4 | 1.00 | 1.171 | 0.854 | 30 | 0.25 |
| 13 | S7+S8+S9 | 0.1 | 0.40 | 1.648 | 0.607 | 0 | 0.50 |
| 14 | S7+S8+S9 | 0.2 | 0.50 | 0.442 | 2.262 | 40 | 0.25 |
| 15 | S7+S8+S9 | 0.3 | 0.30 | 0.603 | 1.658 | 20 | 0.50 |
| 16 | S7+S8+S9 | 0.4 | 0.75 | 0.442 | 2.262 | 0 | 0.25 |

Graph of calculated normalized resultant deck displacement vs acceleration coefficient is presented in Figure 6.40.

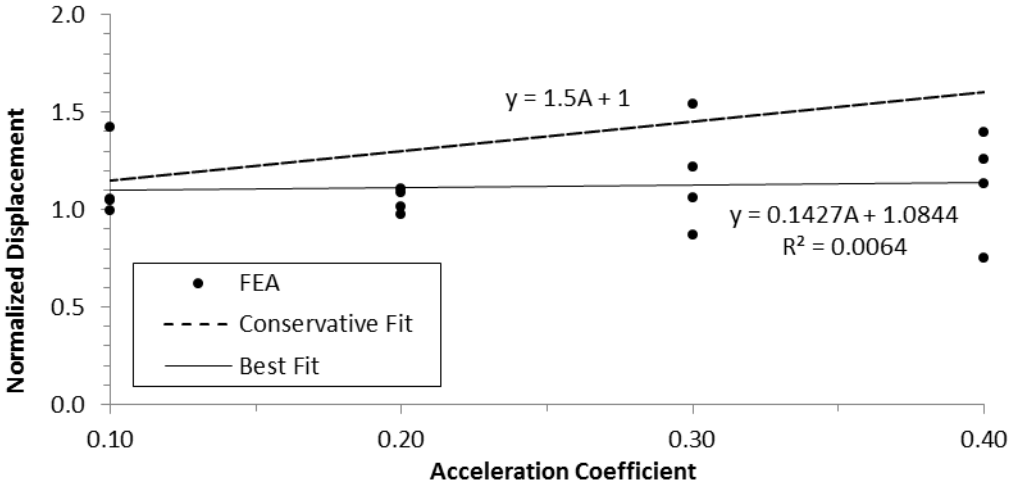


Figure 6.40: Normalized maximum deck displacements obtained from FEA of additional cases as a function of acceleration coefficient

Results indicated that, while linear regression using least squares method provided a nearly constant best fit line, use of a more conservative fitting was more suitable considering low R-squared value obtained through linear regression.

It was seen that a reasonably approximate estimation of deck displacements would be obtained using the following simple method;

- Calculate the resultant bearing displacements using linear bearing elements (simulating bonded bearings). Multiply the calculated displacement by a correction factor of:

  $C = 1.0 + 1.5A$, where A is the acceleration coefficient

Forces transferred from a bearing to substructure may also be calculated as the maximum of:

- Bonded response at the calculated unbonded displacement response, and
- $1.10D_{L,}$ where $D_L$ is the dead load action on the bearing

# CHAPTER 7

## SUMMARY AND DISCUSSIONS

In terms of their connections, elastomeric bearings can simply be grouped into two; unbonded ones that have no connection to the girders and/or piers/cap beams, and bonded bearings which are connected to both.

In Turkey, it is commonly seen that the elastomeric bearings are directly laid on the cap beams or piers having no means of connection besides friction, utilizing an unbonded setup. They are also seldom connected to the girders.

Through an experimental study backed with nonlinear time-history analyses and a parametric study, it is intended to achieve the following objectives:

- To estimate the friction coefficient between elastomeric bearings and steel girders as well as to verify the use of values suggested by the specifications in seismic design,
- To compare the results of shake tests and FEA
- To compare the seismic performance of unbonded and bonded bearings,
- To investigate the dependence of seismic displacement demands and uplift forces on bearings to following parameters:
    - Friction coefficient
    - Acceleration coefficient per AASHTO
    - Skew angle
    - Height-to-width ratio of deck
    - Fundamental frequency of the structure

First, design parameters of the bearings were calculated by cyclic shear tests and then static and cyclic friction tests were performed to explore the frictional response of bearings on steel plates.

Following determination of the shear stiffness and equivalent viscous damping ratios of the bearings, shake tests by applying harmonic loading and actual ground motion records were performed for the bridge setup with bonded bearings. After experimental data had been processed and vibration characteristics were obtained, bearings were replaced with unbonded ones and tests were repeated for the unbonded bridge setup.

Finite element models were prepared and calibrated using the results of bearing tests and harmonic shake table tests. FEA were conducted using the same ground motion records and results were compared with the experimental data.

After shake table tests were completed; deck of the bridge was pushed in the longitudinal direction to estimate the coefficient of friction between bearings and girders and to observe the static response of the bridge at low loading rates.

Last part of the thesis work consisted of a parametric study using the FEA model of the test setup and changing the examined parameters accordingly.

Investigated bridge setups are summarized on Table 7.1 and Table 7.2 with corresponding bearing properties.

Table 7.1: Explanation of test setups

| **Bridge Setup** | **Used Bearings** | **Bearing Connection** |
|---|---|---|
| Bonded | 6 x Type-1 | M12 Bolts |
| Unbonded | 2 x Type-2 (Middle) and 4 x Type-3 (Sides) | N/A |

Table 7.2: Properties of used bearings

| Bearing Type | Shape | Dimensions (mm) | # of Rubber Layers | Thick. of an Int. Rubber Layer (mm) | Thick. of an Ext. Rubber Layer (mm) | Thick. of Steel Shim Plates (mm) |
|---|---|---|---|---|---|---|
| Type-1 | Circular | $D_b = 150$ | 5 | 10 | N/A | 2 |
| Type-2 | Square | 150x150 | 4 | 8 | 4 | 2 |
| Type-3 | Square | 150x150 | 4 | 8 | 4 | (Fiber) |

Static loading test performed on the bridge yielded a friction coefficient of 0.29 between bearings and steel girders under a loading rate of approximately 20mm/min (Figure 7.1).

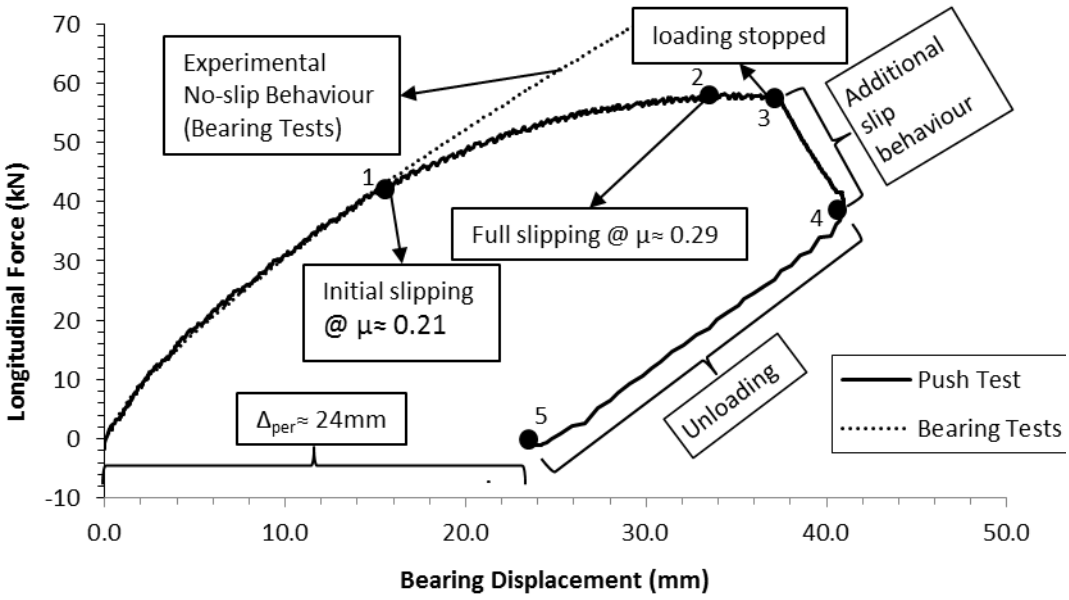


Figure 7.1: Load vs displacement graph of static loading test

Static and cyclic shear tests using four steel plates with various finishes (Figure 5.23) were performed to investigate the effect of surface finish on the friction response under various loadings speeds (5, 10, 25, 50, 100, 300 and 500mm/min).

(a) (b) (c) (d)

Figure 7.2: Steel plates with different surface finishes used in unidirectional and cyclic friction tests; (a) stainless steel, (b) slightly rusted and moderately sanded steel, (c) raw steel, (d) galvanized steel

Results indicated that (Figures 7.3 and 7.4):

- Loading rate significantly affected frictional resistance (i.e. coefficient of friction between bearings and steel plates).

- Under the same dead load measured at the bridge setup per bearing (33kN), a steady slip response was observed at long term loading rates of 10 and 25 mm/min. Both static and kinetic friction coefficients were estimated to be between 0.35-0.40, slightly higher than the common value of 0.20 provided by specifications and the range supplied in past studies (0.29-0.34).

- Faster application of loading yielded rapidly increasing shear force/compressive force ratios even exceeding unity under low compressive forces.

- Cyclic friction tests yielded identical hysteresis loops with those obtained from the bearing tests (Section 5.4) indicating zero to negligible slip on any of the steel surfaces up to 50mm lateral displacements at loading rates of 500 mm/min.

- Although the friction coefficient (between elastomeric bearings and steel surfaces) values supplied by specifications were found to be appropriate but slightly over conservative to use under long term service loads, they should not be used in seismic analysis and design unless validated test data indicate otherwise.

- Use of such coefficients in seismic design can lead to underestimation of substructural responses and overestimation of displacement demands.

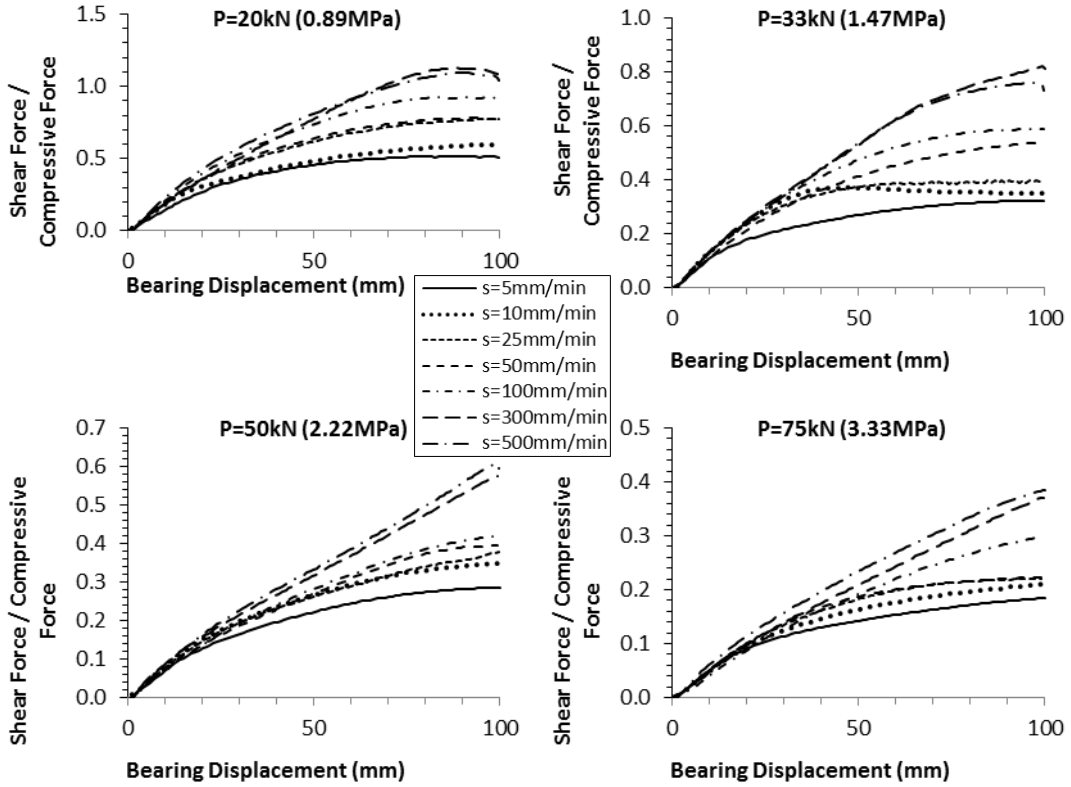


Figure 7.3: Shear force / Compressive Force vs lateral bearing displacement under varying compressive forces

Experimental studies performed both on elastomeric bearings and the bridge throughout this thesis work concluded that slip is unlikely to occur during seismic loading, at which bearings displace at very high speeds (e.g. between 1-15m/s).

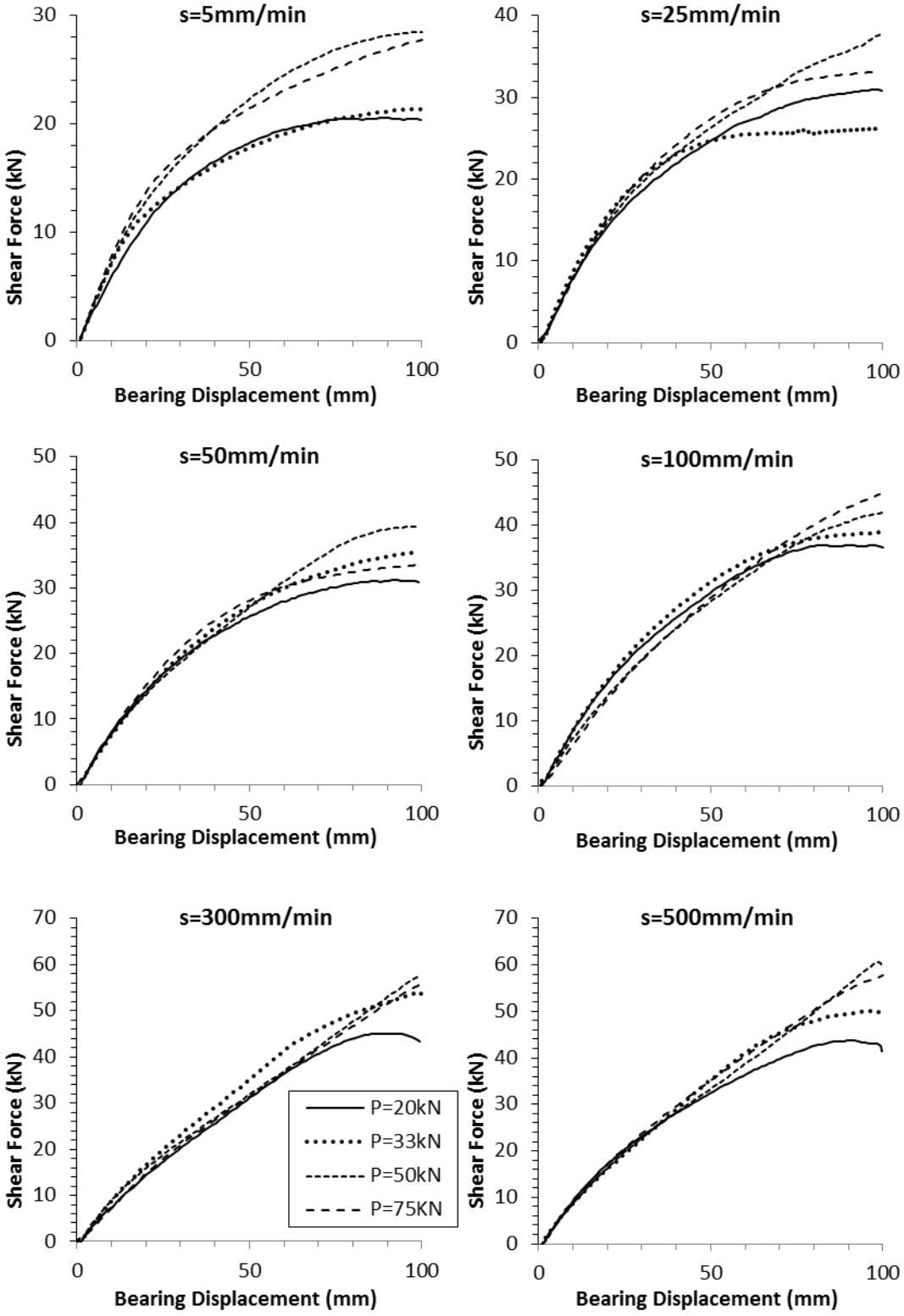


Figure 7.4: Shear force (sum of two bearings) vs lateral bearing displacement under varying loading rates

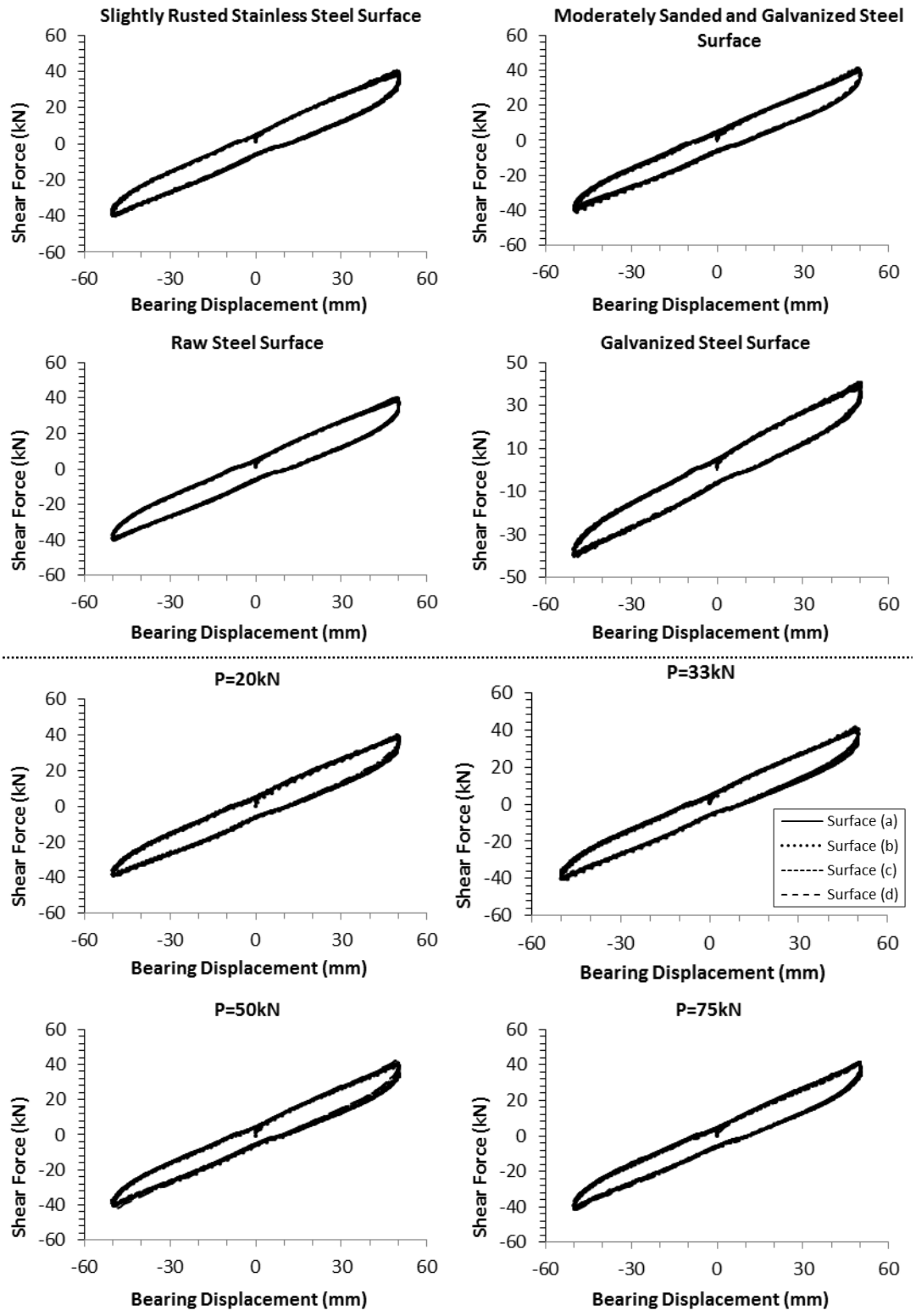


Figure 7.5: Results of cyclic friction tests

Shake test experiments and FEA results showed reasonable agreement, especially indicating better match in terms of bearing shear deformations (Figure 7.6). M1 and M4 records yielded maximum responses. No slip was measured at bearings.

FEA of the unbonded bridge setup showed that significant slip would occur in case of friction coefficients lower than 0.20 (Figure 7.7). However, actual frictional resistance of the bearings prevented slipping in shake table tests and did not require any measures to secure them vertically.

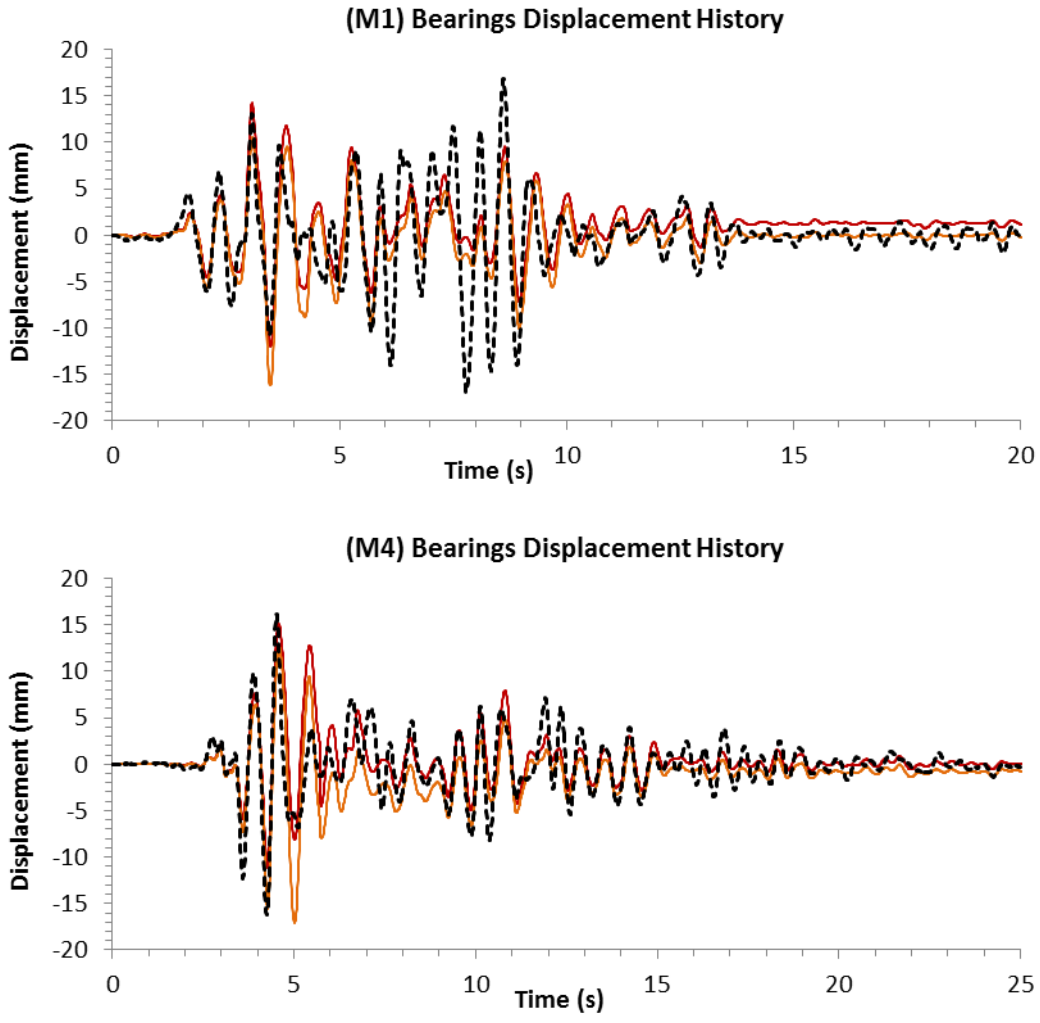


Figure 7.6: Comparison of bearing displacements obtained from shake table experiments and FEA for unbonded setup

It is also verified using a simplified formulation (Equation (5.14)) that M1 and M4 records were severe enough to initiate slipping in bearings in case of a friction coefficient equal to or lower than 0.30.

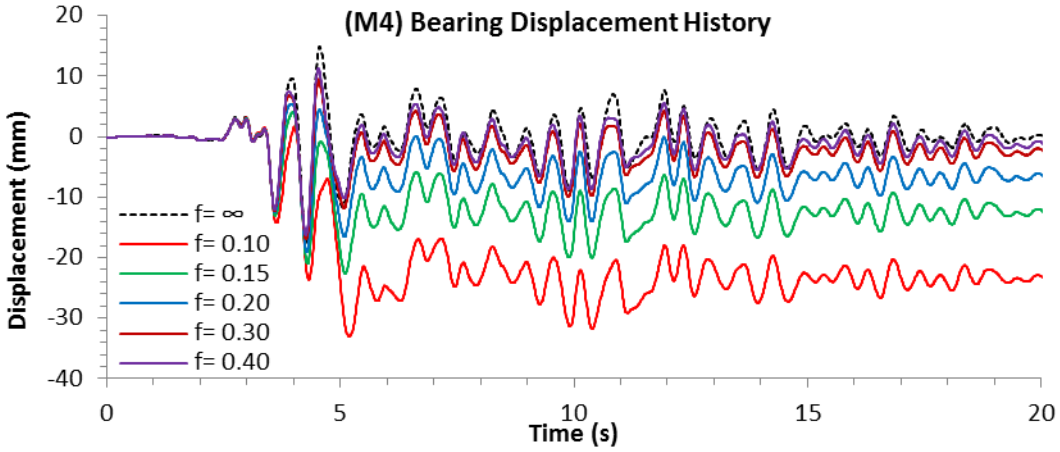


Figure 7.7: Bearing displacements for various friction coefficients under M4 ground motion record

Results of the parametric study indicated that:

- For low seismic hazard ($A = 0.10$), no significant amplification of deck displacements was observed provided that friction coefficient is greater than 0.20 (Figure 7.8).

- Below friction coefficient values of approximately 0.20, deck displacements relative to pier top increased rapidly, exceeding 2.0 times the responses of bonded solution for seismic acceleration coefficients higher than 0.10 (Figure 7.8).

- Normalized deck displacements (by the results obtained from bonded counterpart) remained between 1.17-1.25 in cases where friction coefficient is between 0.25-0.75 (Figure 7.8).

- Uplift forces on bearings were not highly dependent to friction coefficient values greater than 0.30 (Figure 7.8).

- For friction coefficient range 0.30-0.50, resultant relative deck displacement was nearly constant and independent of the friction coefficient (Figure 7.9).

- An approximately linear relation also existed between seismic uplift force and acceleration coefficient for $\mu = 0.15 - 0.75$ (Figure 7.9).

- Skewness did not have a significant effect on maximum and permanent deck displacements as well as on bearing axial forces (Figure 7.10).

- Deck displacements showed a tendency to increase when greater height-to-width deck ratios were used. However, a linear or regular relation between displacement and height-to-width deck ratio could not be observed for all loading cases (Figure 7.11).

- Seismic uplift forces in bearings exhibited an approximately linear dependence to height-to-width ratio (Figure 7.12).

- An irregular relation exists between normalized displacements and fundamental frequency. Dependence was more significant in moderate to high seismic loading conditions ($A = 0.30 - 0.40$).

- A lesser dependence of maximum seismic uplift forces in bearings to fundamental frequency was observed. An approximately linear relation seemed to exist between acceleration coefficient and seismic uplift forces for the investigated values of fundamental frequency.

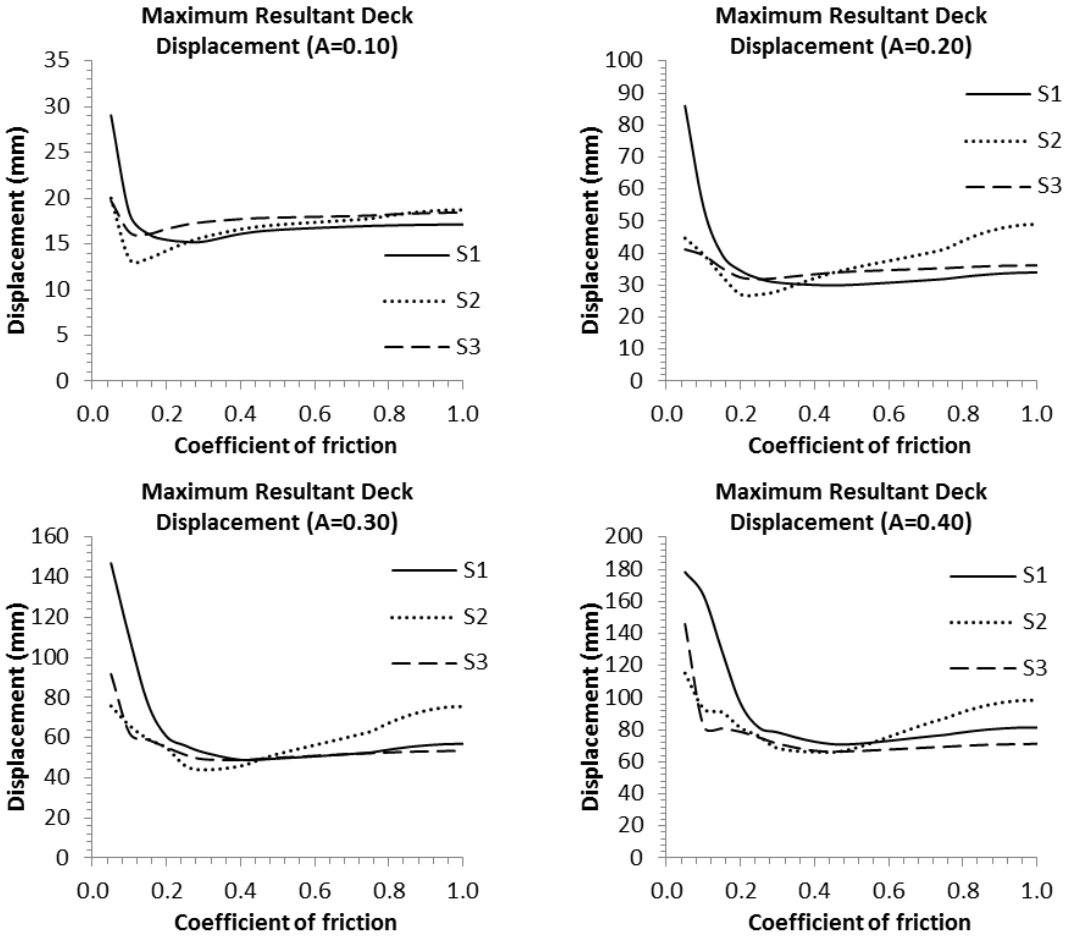


Figure 7.8: Maximum resultant deck displacements vs friction coefficient

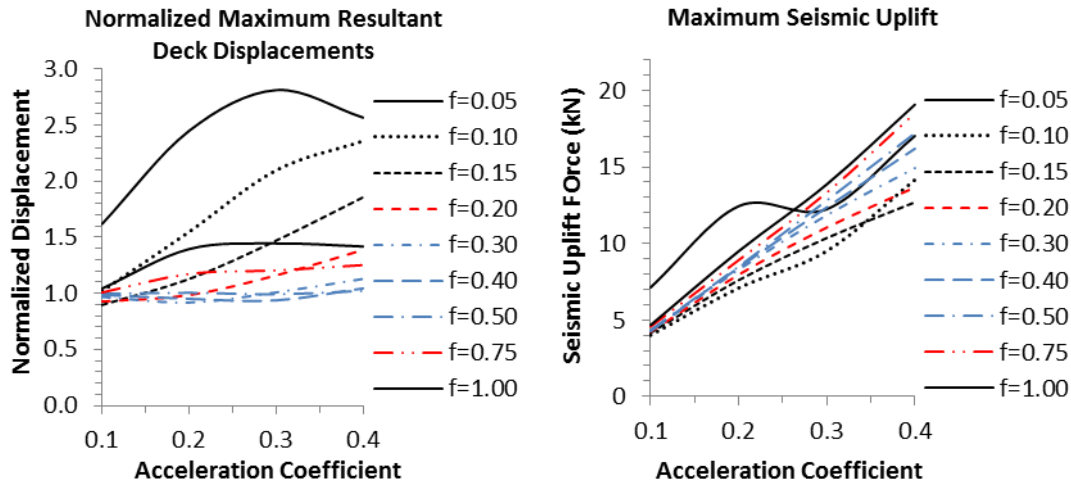


Figure 7.9: Normalized maximum resultant relative deck displacements and seismic uplift forces vs acceleration coefficient

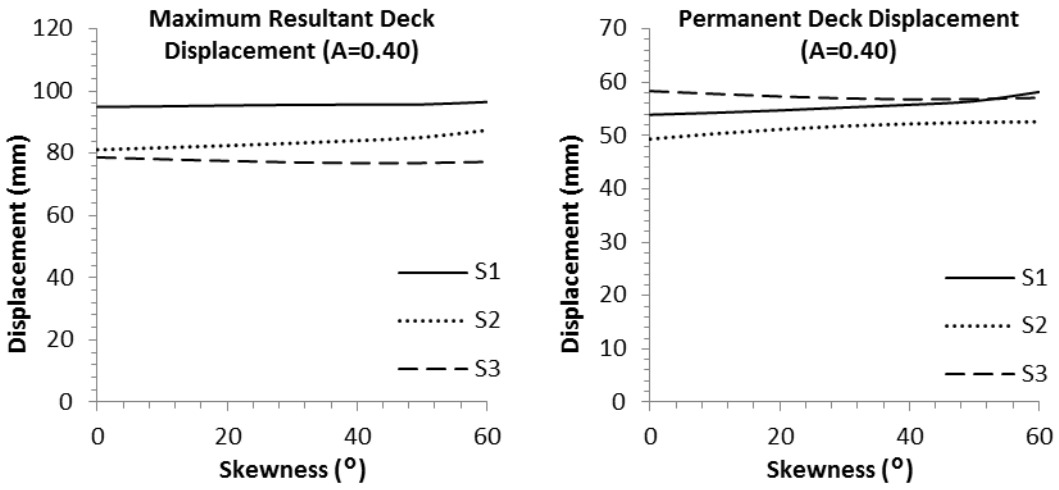


Figure 7.10: Maximum resultant and permanent deck displacements vs skew angle

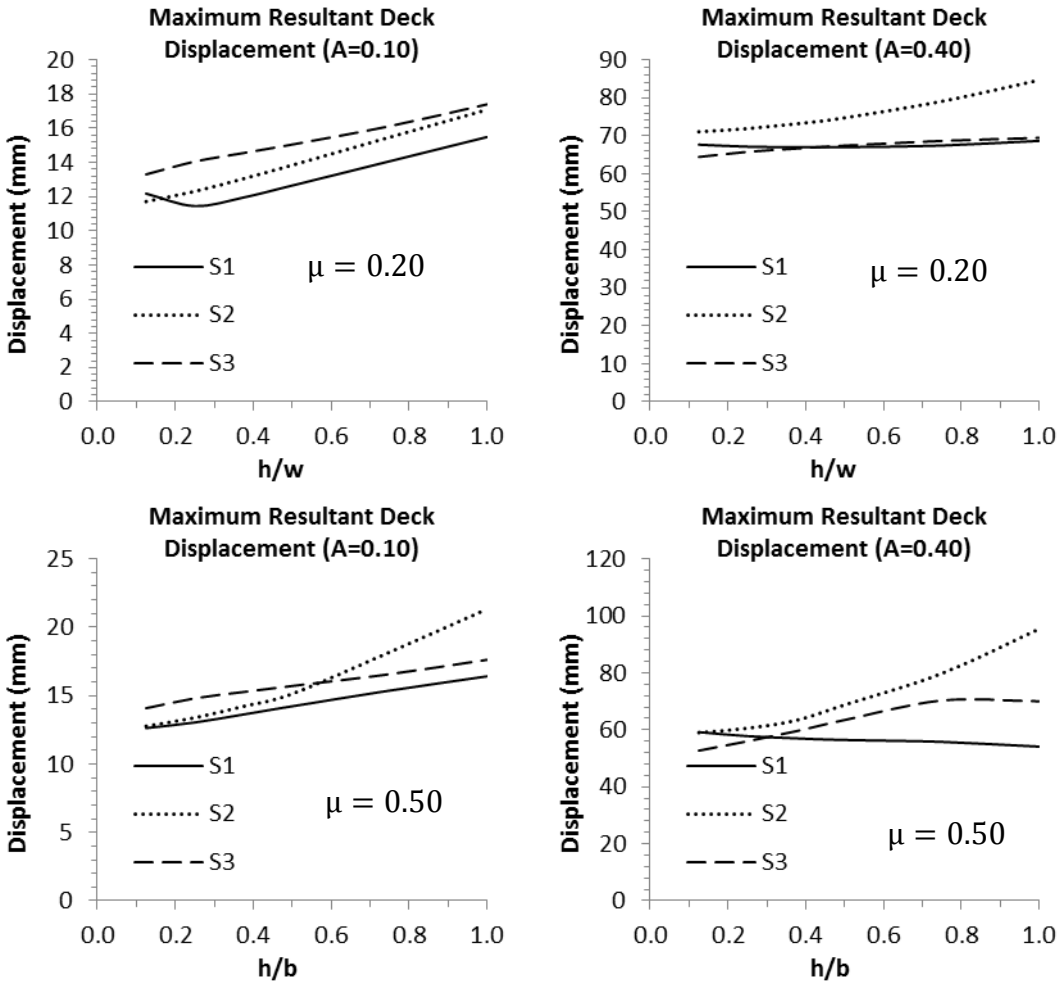


Figure 7.11: Maximum resultant deck displacements vs height-to-width ratio

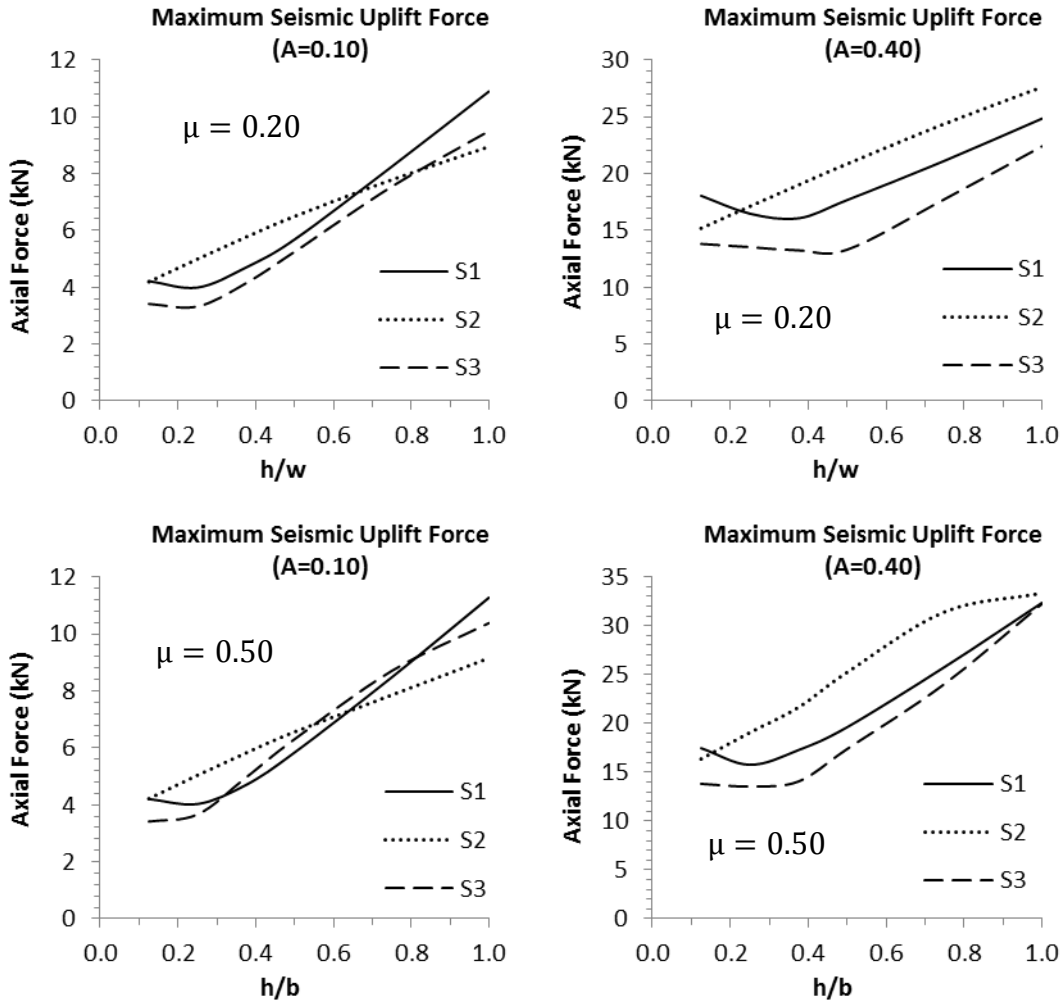


Figure 7.12: Maximum seismic uplift forces on bearings as a function of height-to-width ratio

A conservative trendline was constructed considering also the normalized maximum seismic deck displacements calculated from FEA of additional 16 bridge setups (Figure 7.13). Estimation of deck displacements could be obtained using the following simple method using the constructed trendline;

- Calculate the resultant bearing displacements using linear bearing elements (simulating bonded bearings). Multiply the calculated displacement by a correction factor of:

  $C = 1.0 + 1.5A$, where A is the acceleration coefficient

Forces transferred from a bearing to substructure may also be calculated as the maximum of:

- Bonded response at the calculated unbonded displacement response, and
- $1.10D_{L,}$ where $D_L$ is the dead load action on the bearing

However, it should be carefully noted that those results were obtained considering only a one span bridge having a certain geometry (Section 5.1) and particular range of structural parameters as follows;

- Friction coefficient range : 0.05 - 1.00
- Skewness range : 0 - 60°
- Deck height-to-width ratio range : 0.125 - 1.00
- Fundamental frequency : 0.607 - 2.262Hz
  (Fundamental period : 0.442 – 1.648s)

The results and their interpretations presented in this thesis should not be used as a generalized design guideline unless this parametric study is extended to include different bridge types with various span lengths, number of spans, widths, number of bearings, number of columns, etc.

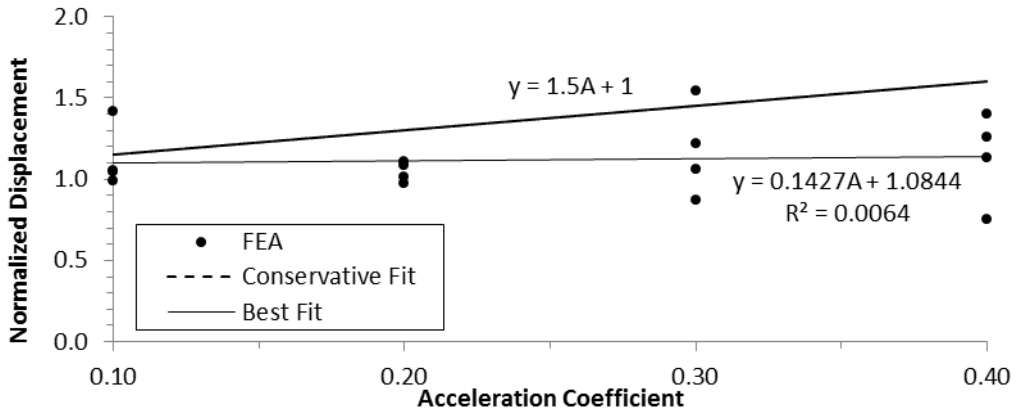


Figure 7.13: Constructed displacement trendline vs acceleration coefficient

# CHAPTER 8

# CONCLUSIONS

The suggested values of friction coefficient between bearings and steel girders per design specifications were evaluated. Dynamic and static shear behaviors of unbonded bearings were investigated through experiments.

Unidirectional and cyclic friction tests were performed on unbonded bearings at various loading rates using steel plates with various surface finishes for estimating the coefficient of friction.

An actual bridge model and a unidirectional shaking system capable of exerting actual ground motion records were constructed. Five actual ground motion records were applied and experimental data are compared with FEA results.

Static push test was performed on the experimental bridge setup to observe frictional response of the system under low loading rates.

A parametric study was performed using approximately 800 nonlinear time history analyses and 21 spectrum compatible ground motion records. The dependence of seismic displacement demands and uplift forces to friction coefficient, acceleration coefficient, skewness, height-to-width ratio of deck and fundamental frequency of the structure was investigated.

Discussions are extended to include a simplified procedure to estimate seismic displacement demands of deck and maximum bearing shear forces.

The following conclusions have been reached in this study:

1) Static friction coefficient between various steel surface finishes and elastomeric bearings were measured to be between 0.29-0.40 under very low loading rates. Obtained values are in conformity with those supplied by specifications and findings of the past studies.

2) Results indicated that coefficient of friction is highly dependent on loading rate. For moderate to high loading rates (greater than 300 mm/min), bearing slipping was not observed. Results of shake table tests also indicated that unbonded bearings were unlikely to slip under seismic loading (e.g. rates higher than 3000mm/min).

3) Results of cyclic shear tests and FEA analysis of unbonded bearings indicated that; although rolling occurred at approximately 50% shear deformation, shear behavior was almost linear up to a level of 125%. Rolling did not have a significant effect on shear stiffness and investigated unbonded bearings exhibited similar shear behavior with the bonded ones.

4) A friction coefficient of 0.20 is frequently considered for seismic design in Turkey. Use of such values can be unconservatively low for seismic analysis to determine substructure forces while significantly overestimating seismic displacement demands, and may not reflect the interaction of bearings and the structure properly during seismic loading. Such values should not be used in seismic design unless indicated otherwise by validated test data.

5) Results of the parametric study indicated that no significant amplification of deck displacements was observed provided that friction coefficient is greater than 0.20 under a low seismic loading level ($A = 0.10$).

6) Dependence of bearing uplift forces to friction coefficient was not prominent for coefficient of friction values greater than 0.30.

7) Skewness did not have a significant effect on maximum resultant deck displacements, permanent deck displacements and bearing axial forces.

8) A linear and regular relation between deck displacements and height-to-width deck ratio could not be observed. However, seismic bearing uplift forces exhibited an approximately linear and directly proportional relation with height-to-width ratio.

9) An irregular relation exists between normalized deck displacements and fundamental frequency. Dependence was more significant for moderate to high seismic loading conditions ($A = 0.30 - 0.40$). A lesser dependence of maximum seismic bearing uplift forces to fundamental frequency was observed. An approximately linear and directly proportional relation seemed to exist between acceleration coefficient and seismic uplift forces for the investigated fundamental frequency range.

10) A simple formulation defining a conservative trendline for unbonded deck displacements as a function of acceleration coefficients was presented. A simplified procedure to estimate shear forces transferred from unbonded bearings to substructure is also included. However, those presented procedures should not be used as a generalized design guideline unless this parametric study is extended to include different bridge types with various span lengths, number of spans, widths, number of bearings, number of columns, etc.

For future investigations, following studies may be included to develop a better understanding of the friction behavior of unbonded bearings and to propose a generalized seismic design guideline regarding unbonded bridge setups:

1) A smaller scale bridge with a reinforced concrete deck may be constructed and tested on shake table, to be able to induce absolute uplift on bearings and to explore frictional response of unbonded bearings on concrete.

2) Slender unbonded bearings may be used in shake table, cyclic shear and friction tests to better investigate the effect of rolling on shear response.

3) Bearings obtained from different manufacturers may be tested to compare friction responses and to observe the dependence of friction coefficient on the formulation of used rubber.

4) Parametric study performed in this thesis may be extended to include different bridge types with various span lengths, number of spans, widths, number of bearings, number of columns and superstructure types.

5) Additional spectrum compatible strong ground motion records may be included to improve the reliability and applicability of the results obtained from parametric studies.

6) Future design recommendations to be deducted from the extended parametric studies may be verified on actual case studies.

## REFERENCES


1. AASHTO (2000), “Guide Specifications for Seismic Isolation Design”, American Association of State Highway and Transportation Officials

2. AASHTO (2002), “Standard Specifications for Highway Bridges, 17th Edition”, American Association of State Highway and Transportation Officials

3. AASHTO (2007), “LRFD Bridge Design Specifications”, American Association of State Highway and Transportation Officials

4. AASHTO (2010), “LRFD Bridge Design Specifications”, American Association of State Highway and Transportation Officials

5. AASHTO (2012), “LRFD Bridge Design Specifications”, American Association of State Highway and Transportation Officials

6. ADINA R&D Inc. (2013), “ADINA Structures – Theory and Modeling Guide Volume I: ADINA Solids & Structures”, Report ARD 13-8

7. API (1993), “Recommended Practice for Planning, Designing and Constructing Fixed Offshore Platforms - Working Stress Design”, American Petroleum Institute

8. ASCE-TCLEE (1999), “Lifelines Performance, Kocaeli, Turkey Earthquake, August 17, 1999”, American Society of Civil Engineering, Technical Council on Lifeline Earthquake Engineering

9. ATC (1986), “ATC 6, Seismic Design Guidelines for Highway Bridges”, Applied Technology Council

10. ATC (1996), “ATC 32, Improved Seismic Design Criteria for California Bridges: Provisional Recommendations”, Applied Technology Council

11. Bozorgnia Y., Mahin S. A. and Brady A. G. (1998), “Vertical Response of Twelve Structures Recorded During the Northridge Earthquake”, Earthquake Spectra, Vol.14, No.3, 411-431

12. Bozorgnia Y., Niazi M. and Campbell K. W. (1996), "Relationship Between Vertical and Horizontal Response Spectra for The Northridge Earthquake", Proceedings, 11. World Conference of Earthquake Engineering, Acapulco, Mexico

13. British Standarts (2005), "BS EN 1337-3:2005 Structural Bearings: Elastomeric Bearings" (2005), Brussels

14. Buchholdt H. A., Nejad M. (2012), "Structural Dynamics for Engineers, 2nd Edition", ICE Publishing, 318 Pages

15. Buckle I., Nagarajaiah S. and Ferrell K. (2002), "Stability of Elastomeric Bearings: Experimental Study", Journal of Structural Engineering, Vol:128, No:1, 3-11

16. Button M. R., Cronin C. J. and Mayes R. L. (2002), "Effect of Vertical Motions on Seismic Response of Highway Bridges", Journal of Structural Engineering, Vol.128, 1551-1564122

17. CALTRANS (1994), "Bridge Memo to Designers", California Department of Transportation

18. CALTRANS (2006), "Seismic Design Criteria", California Department of Transportation

19. Chopra A. K. (2000), "Dynamics of Structures: Theory and Applications to Earthquake Engineering, Second Edition", Prentice Hall, 843 pages

20. Computers and Structures Inc. (2011), "CSI Analysis Reference Manual for SAP2000, ETABS, SAFE and CSI Bridge"

21. Domaniç K. A. (2008), "Effects Of Vertical Excitation On Seismic Performance Of Highway Bridges And Hold-Down Device Requirements", MS Thesis, Middle East Technical University

22. Foster B. A. D. (2011), "Base Isolation Using Stable Unbonded Fibre Reinforced Elastomeric Isolators (SU-FREI)", MS Thesis, McMaster University, Ontario

23. Hu B. and Ghali M. G. (2010), "Use of Single Pot Bearings to Reduce Uplifting on Curved Narrow Segmental Bridges", Structures Congress 2010, 32-41

24. Jakel R. (2010), "Analysis of Hyperelastic Materials with MECHANICA – Theory and Application Examples –", Presentation for the 2nd SAXIM

25. Kelly M. J. and Konstantinidis D. (2009), "Effect of Friction on Unbonded Elastomeric Bearings", Journal of Engineering Mechanics, 2009-135, 953-960

26. Kim C. W., Kawatani M., Kanbara T. and Nishimura N. (2013), "Seismic behaviour of steel monorail bridges under train load during strong earthquakes". Journal of Earthquake and Tsunami 2013; 7(2).

27. Konstantinidis D., Kelly J. M. and Makris N. (2008), "Experimental Investigation on The Seismic Response of Bridge Bearings", Technical Rep. No. EERC 2008–02, Earthquake Engineering Research Center, Univ. of California, Berkeley, Calif.

28. Liu K.Y., Chang K.C., Lu C.H. and Cheng W.C. (2008), "Seismic Performance of Skew Bridge with Friction Type Rubber Bearings", The 14th World Conference on Earthquake Engineering, October 2008

29. Mitoulis S. (2014), "Uplift of Elastomeric Bearings in Isolated Bridges Subjected to Longitudinal Seismic Excitations", Structure and Infrastructure Engineering

30. Mitoulis S., Murh A. and Ahmadi H. (2015), "Uplift of Elastomeric Bearings in Isolated Bridges – A Possible Mechanism: Effects and Remediation", Second European Conference on Earthquake Engineering and Seismology

31. Muscarella J. V. and Yura J.A. (1995), "An Experimental Study of Elastomeric Bridge Bearings with Design Recommendations", FHWA/TX-98/1304-3, The University of Austin, Texas

32. NYCDOT (2002), "Standart Specifications for Highway Bridges", New York State Department of Transportation

33. Osgooei M. P., Tait M. J. and Konstantinidis D. (2015), "Seismic Isolation of a Shear Wall Structure Using Rectangular Fiber-Reinforced Elastomeric Isolators", Journal of Structural Engineering

34. Pamuk A., Kalkan E., Ling H.I. (2005), "Structural and geotechnical impacts of surface rupture on highway structures during recent earthquakes in Turkey", Soil Dynamics and Earthquake Engineering, Vol.25, 581-589

35. Papazoglu A. J. and Elnashai A. S. (1996), "Analytical and Field Evidence of The Damaging Effect of Vertical Earthquake Ground Motion", Earthquake Engineering & Structural Dynamics, Vol.25, No.10, 1109-1137

36. Rajczyk J. and Rajczyk M. (2009), "The Methodology of the Analysis of Elastomer Bearings Properties", Manufacturing and Industrial Engineering, 2009 Issue 3, 60-32

37. Shaban N., Caner A., Yakut A., Askan A., Naghshineh A., Domaniç K. A. and Can G. (2014), "Vehicle Effects on Seismic Response of a Simple-Span Bridge During Shake Tests", Earthquake Engineering & Structural Dynamics, 44:889-905

38. Steelman J. S., Fahnestock L. A., Filipov E. T., LaFave J. M., Hajjar J. F. and Foutch D. A. (2013), "Shear and Friction Response of Nonseismic Laminated Elastomeric Bearings Subject to Seismic Demands", Journal of Bridge Engineering, Vol:18, No:7, 612-623

39. Thiele, Marko (2002), "Spectrum Compatible Accelerograms in Earthquake Engineering", Universidad de La Serena, Chile, code.google.com/resca, last visited: 14.2.2008

40. U.S. Department of Transportation (1995) "Seismic Retrofitting Manual for Highway Bridges", Federal Highway Administration

41. U.S. Department of Transportation (2012) "Steel Bridge Design Handbook: Bearing Design", FHWA-IF-12-052 - Vol. 15

42. Watari R., Hashimoto G. and Okuda H. (2013), "Mesh Coarsening Method Based on Multi-point Constraints for Large Deformation Finite Element Analysis of Almost Incompressible Hyperelastic Material", JSST 2013: International Conference on Simulation Technology

43. Yen W. P., Ghasemi H. and Cooper J. D. (2001), "Lessons Learned from Bridge Performance of the 1999 Turkish & Taiwan Earthquakes", 33rd Joint Meeting of the UJNR Panel on Wind and Seismic Effects, Tsukaba, Japan

44. Yura J., Kumar A., Yakut A., Topkaya C., Becker E. and Collingwood J. (2001), "NCHRP Report 449 - Elastomeric Bridge Bearings: Recommended Test Methods", The University of Austin, Texas

# VITA

## PERSONAL INFORMATION

Surname, Name: Domaniç, Kemal Arman

Nationality: Turkish (TC)

Date and Place of Birth: 17 December 1982, Ankara

Marital Status: Married

Phone: +90 312 225 26 78

Fax: +90 312 235 94 65

email: armandomanic@gmail.com

## EDUCATION

| Degree | Institution | Year of Graduation |
|---|---|---|
| MS | METU Civil Engineering | 2008 |
| BS | METU Civil Engineering | 2005 |
| High School | Ankara Atatürk Anadolu High School, Ankara | 2000 |

## WORK EXPERIENCE

| Year | Place | Enrollment |
|---|---|---|
| 2005-Present | Yüksel Domaniç Müh. | Sanat Yapıları Proje Mühendisi |

## FOREIGN LANGUAGES

Advanced English

## PUBLICATIONS

1. Bayraktar A., Altunışık C. A., Sevim B., Türker T., Domaniç A. and Taş Y., "Vibration Characteristics of Kömürhan Highway Bridge Constructed with Balanced Cantilever Method", Journal of Performance of Constructed Facilities, 23(2), April 2009

2. Karakaplan A., Caner A., Kurç Ö., Domaniç A. and Lüleç A., "Yapı Çözümlemesinde Yeni Bir Devir: Yapım Aşaması", İMO Teknik Dergi 2009, 4905-4917, 2009

3. Altunışık C. A., Bayraktar A., Sevim B., Adanur S. and Domaniç A., "Construction Stage Analysis of Kömürhan Highway Bridge Using Time Dependent Material Properties", 36(2), September 2010

4. Shaban N., Caner A., Yakut A., Askan A., Karimzadeh N., Domaniç A. and Can G., "Vehicle Effects on Seismic Response of a Simple-Span Bridge During Shake Tests", Earthquake Engineering and Structural Dynamics, 44(6), 889-905, May 2015

## HOBBIES

Computer Programming, Music, Motorcycles, Team Sports, Wood Working